POST-TRANSCRIPTIONAL REGULATION OF LYSOSOMAL FUNCTION BY THE LYSINE DEACYLASE SIRTUIN 1

A Dissertation

Presented to the Faculty of the Graduate School

of Cornell University

In Partial Fulfillment of the Requirements for the Degree of

Doctor of Philosophy

by

Arash Latifkar

August 2020

POST-TRANSCRIPTIONAL REGULATION OF LYSOSOMAL FUNCTION BY THE LYSINE DEACYLASE SIRTUIN 1

Arash Latifkar, Ph. D.

Cornell University 2020

Spread of tumor cells from their primary sites to vital distant organs and tissues, i.e. metastasis, is the most devastating stage of cancer development. Metastatic tumors grow rapidly, and they rarely respond to therapeutic interventions. Thus, a better understanding of how aggressive cancer cells get into the circulation and colonize the secondary site is essential for blocking metastasis.

In Chapter 2, I describe the role of a lysine deacylase in regulating the ability of breast cancer cells to secrete factors that promote their aggressiveness. Specifically, I will discuss the mechanism by which, breast cancer cells can take advantage of SIRT1 downregulation to promote secretion of nanometer sized vesicles, known as exosomes, as well as protein hydrolases capable of degrading the extracellular matrix. The secretion of these factors results in the ability of other cancer cells in microenvironment to become more invasive. I also show that SIRT1 is in fact regulating the activity of an organelle called lysosomes by influencing the expression of a subunit (i.e. ATP6V1A) of the machinery responsible for lysosomal acidification.

In Chapter 3, I found that SIRT1 is modulating the RNA stability of the ATP6V1A transcript through deacetylating IGF2BP2, an RNA binding protein that binds to the 3'-untranslated region (UTR) of this transcript. Mechanistically, acetylation of IGF2BP2, under conditions where SIRT1 is downregulated, results in recruitment of the

exonuclease XRN2, which promotes the degradation of the ATP6V1A mRNA. I also show that knocking down IGF2BP2 or XRN2 can reverse the effect of SIRT1 downregulation on the cellular secretome.

In the final chapter, I will discuss the implication of my findings in cancer and other biological contexts as well as describing outstanding questions that have emerged from my dissertation.

BIOGRAPHICAL SKETCH

Arash Latifkar was born and raised in Kerman, a beautiful and ancient city in the south-east of Iran. After elementary school, following the footsteps of his siblings, he was admitted into the National Development of Exceptional Talents education system, where a great emphasis was put on natural sciences and mathematics. Arash's interest in chemistry began in his freshman year at high school, when he learned enough English to be able to read his mother's college textbooks, notably *Organic Chemistry* by Morrison & Boyd and later on *Organic Chemistry* by John E. McMurry. As a high school junior, Arash participated in the National Chemistry Olympiad and was awarded the silver medal. Holding this strong enthusiasm towards chemistry, he went to pursue chemistry as his major in Tehran at Sharif University of Technology, where his mother got her degree in Chemical Engineering. In college, he worked as an undergraduate research assistant in the Laboratory of Natural Product Synthesis under the supervision of Prof. Firouz Matloubi Moghaddam, who taught him the art of organic synthesis as well as introducing him to experimental research. Towards the end of his college, Arash became fascinated with chemistry of life, i.e. biology, and he decided to go to graduate school to study chemical biology at Cornell University, where he joined the laboratories of Professor Richard Cerione and Professor Hening Lin. There, he switched his research focus from organic synthesis to cell biology, investigating the biogenesis of extracellular vesicles in aggressive breast cancer. Although the transition from chemistry to biology was not easy, Arash enjoyed every minute spent in learning and exploring within the biological realm. This was made possible only due to the family-like and encouraging atmosphere that always existed in his mentors and colleagues. After graduation, he plans to start his post-doctoral training under the

mentorship of Prof. David Bartel and Prof. David Sabatini at Massachusetts Institute of Technology, where he will study molecular pathways that regulate RNA metabolism in physiology and disease.

Dedicated to my parents and the mentors
who provide the opportunity to create
ourselves.

ACKNOWLEDGMENTS

I am immensely grateful to my parents, who encouraged and supported me at all stages of my life. They have been instrumental in recognizing my interest in science and providing me with the necessary tools to pursue it as career goal. Their love, encouragement, and sacrifice have always been the cornerstone for overcoming any difficulties in my life.

I am forever grateful to my sister, Azadeh Latifkar, for her unwavering support and for her passion in art, which has been a source of enlightenment in our family. I am also thankful to my brother, Amin Latifkar, who has backed me up in all of my decisions and for being an amazing source of encouragement.

I can't thank enough my chemistry teacher in middle school, Reza Nekouamal, for sparking my interest in chemistry through his innovative and animated teaching style. My high school years had been one of the most formative periods of my life. I feel extremely fortunate to have made long-standing friendships with an extremely talented and caring group of people, in no particular order: Amin Ghafourian, Pooya Rashidi, Ali Tabibzadeh, Arian Hakak, Hamidreza Khajoie, Milad Nadernejad. I specifically thank Hamidreza Rashidi and Abolhassan Arjmand for their amazing friendship and our transformative conversations on intersection of chemistry and biology. Although distance has separated us, our memories together still warms my heart.

I would also like to acknowledge the chemistry faculty at Sharif University of Technology: Prof. Ali Pourjavadi who let me to audit his organic chemistry course during freshman year; Prof. Mohammadreza Saidi for his encouragement and belief in me; Prof. Hamidreza Kalhor for his exciting courses in biochemistry; and Prof. Matloubi Moghaddam for his endless support.

I considered myself extremely lucky to be trained under the excellent

mentorship of Prof. Richard Cerione and Prof. Hening Lin. I deeply appreciate their guidance, patience, and support for my non-linear research trajectory. Rick Cerione is a virtuoso scientist and his level of care for his trainees is universally unmatched. Rick is also a great narrator, and I have learnt a lot about history of science from his anecdotes. I would like to also thank Prof. Brian Crane, my committee member, for his thoughtful advice as well as Prof. Maurine Linder and Prof. Claudia Fischbach for their continuous support of developing young scientists. In the same light, I am eternally grateful to Prof. Marc Antonyak who has mentored me throughout my graduate work, and has always pushed me to be a better scientist.

For my time at Cornell University, I could not have wished for more remarkable colleagues and friends, with whom I had the pleasure to grow and learn countless wonderful things. I particularly cherish the company of Julio Sanchez, Fangyu Wang, Michael Lukey, Kristin Wilson, Xiaoyu Zhang, Irma Fernandez, Valentina Pinoba, Tatsiana Kosciuk, Yang Gao, Stella Li, Bridget Kreger, Kathy Rojas, Kai Su Greene, Wen-Hsuan Chang, Thuy-Tien Nguyen, Makoto Endo, Shawn Milano, Bill Kat, Sekar Ramachandran, Elena Panizza, James Mullman, Yun Ha Hur, Oriana Teran, and Jenny Guo. I am also thankful to the three talented Cornell undergraduate students who work with me during my graduate work: Amrit Hingorani, Amdiel Clement, and Eric Johansen. I am extremely proud of their dedication and I am confident that a very bright future lies ahead of of them.

Last but foremost, I am grateful beyond words to my life partner, Negar Khojasteh, for her unconditional love and support as well as all the late nights she kept me company in the laboratory. I am specially indebted to her intelligent acumen and always look up to her persevering character.

TABLE OF CONTENTS

“Not all those who wander are lost…”

- J.R.R. Tolkien

CHAPTER 1

Introduction

Overview

Cells, ranging from single-cell organisms to those that make-up the human body, communicate with their environment to promote a number of different biological effects. Perhaps one of the best examples of this involves the ability of cells to secrete soluble factors, such as growth factors, cytokines, and extracellular matrix proteins. In each of these cases, highly-conserved cellular machinery is responsible for trafficking specific soluble factors to the cell surface, where they are released into the extracellular space. The secreted molecules can then interact with their corresponding receptors expressed on the surfaces of target cells and activate them, promoting intracellular signaling events that can mediate a variety of cellular process, such as cell growth, survival, and migration.

The ability of cells to use soluble factors to mediate intercellular communication can be divided into three major types, based on the target cell, as well as the distance that these factors travel to mediate their effects (**Figure 1.1**); (i) endocrine signaling, (ii) paracrine signaling, and (iii) autocrine signaling. Endocrine signaling involves soluble factors that are transported through the circulatory system, and ultimately act on cells that are located some distance from the site where they were produced. On the other hand, paracrine signaling involves soluble factors produced by one type of cell that then influence another cell type located within the local environment. Autocrine signaling is similar to paracrine signaling, except the donor cell (i.e. the cell generating the soluble factor) and the recipient, or target cell, are the same cell type. In the following sections, I will describe the various mechanisms used by cells for autocrine and paracrine signaling, and other modes of

Figure 1.1 Types of Extracellular Signaling
Depending on the distance that signaling molecules travel, extracellular signaling can classified into three types: (A) Endocrine Signaling, (B) Paracrine Signaling, and (C) Autocrine Signaling

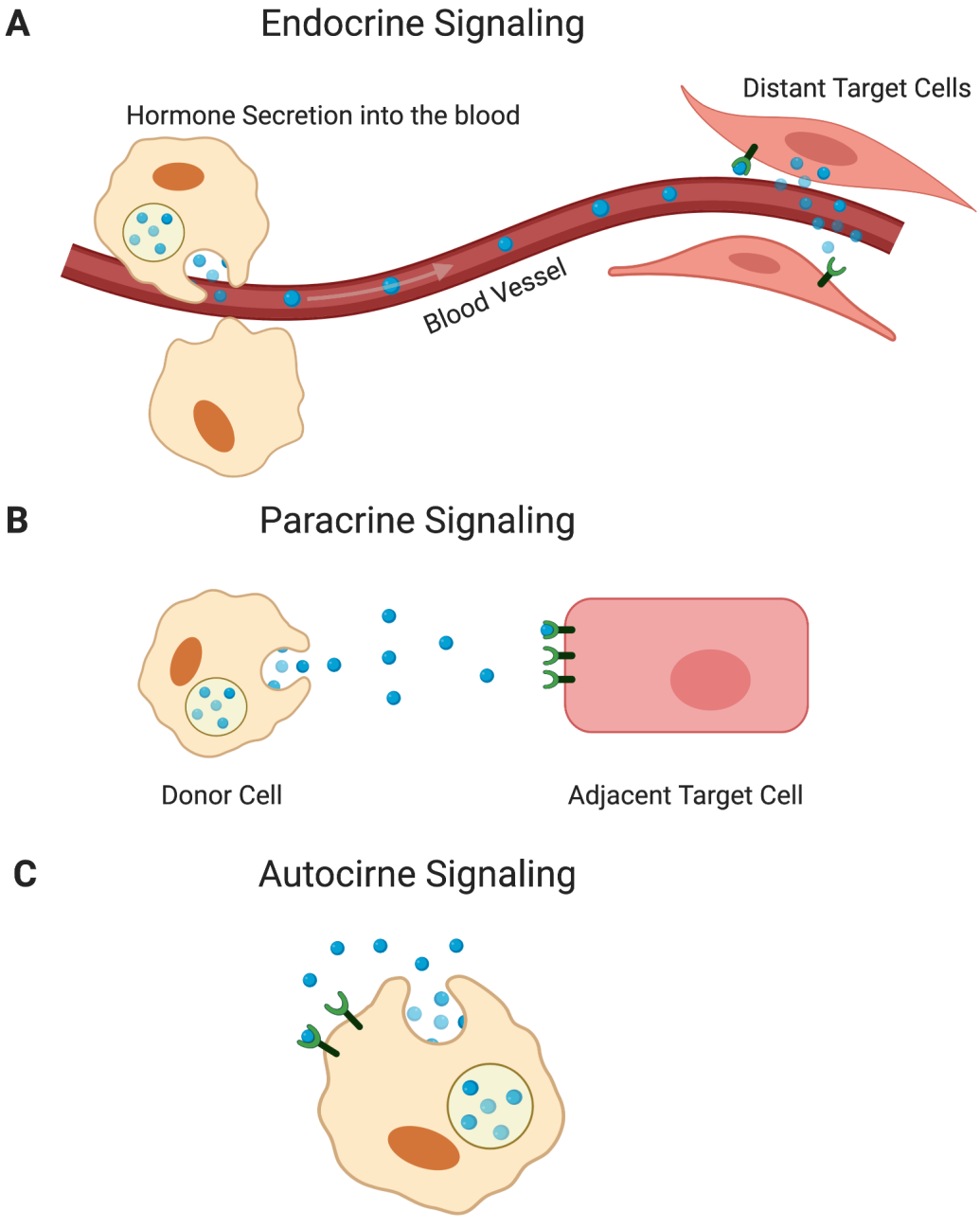
A
Endocrine Signaling
Hormone Secretion into the blood
Distant Target Cells
Blood Vessel
B
Paracrine Signaling
Donor Cell
Adjacent Target Cell
C
Autocirne Signaling

intercellular communication. I will then focus on two important aspects of my thesis research, extracellular vesicles and the sirtuin family of proteins.

Endocrine Signaling

Hormones are among the primary forms of signaling molecules that mediate endocrine signaling. They are synthesized in specialized secretory organs, such as the pancreas and adrenal glands, and are released into the blood stream. The production of insulin by the pancreas was the first endocrine signaling event that was discovered in 1922, and it was based on even earlier observations that showed dogs, whose pancreases had been removed, became severely diabetic[1]. Elegant biochemical work carried-out by Fredrick Banting and J.J.R Macleod resulted in the successful isolation of insulin from pancreases. It was subsequently demonstrated that this purified insulin, when injected into diabetic patients, could lower their blood sugar level and even prevent them from dying[2]. For this work Banting and Macleod were jointly awarded the Nobel Prize in Physiology and Medicine in 1923. Extensive research over the next century has elucidated the molecular mechanism behind their findings, i.e. the pathway by which insulin signaling maintains glucose homeostasis.

The insulin signaling pathway is initiated by absorption of glucose in the beta-cells of the pancreas, where it stimulates the uptake of calcium and subsequent secretion of insulin from dense-core vesicles. Insulin then enters into the blood stream and travels throughout the body, before it interacts with insulin receptors expressed on muscle and fat cells. The binding of insulin to its receptor triggers intracellular signaling events that results in the uptake of glucose from the blood[3]. Failure of beta-cells in the pancreas to produce sufficient amounts of insulin, or an insufficient response of target cells to insulin stimulation, are two of the most common causes of diabetes.

Paracrine Signaling

The growth factor signaling paradigm is a particularly well-studied example of paracrine signaling. Growth factors are extracellular polypeptides that are secreted by certain cell types, and they passively diffuse throughout the local environment. These growth factors then bind to specific types of receptors expressed in neighboring cells and induce their activation to promote cell growth, survival, and migration. Rita Levi-Montalcini and Stanley Cohen isolated and characterized the first growth factor, referred to as nerve growth factor (NGF)[4]. Specifically, they discovered that co-culturing sensory and sympathetic ganglia derived from chicken embryos with fragments of mouse sarcoma resulted in the formation of nerve fibers[5]. This effect was even more pronounced when the chicken cells were treated with snake venom, which Cohen later used as a source to purify NGF[6,7]. During these studies, it was also shown that mouse salivary glands produced significant amounts of NGF[8]. However, administration of extracts isolated from these glands to mice led to significant side effects, such as the premature opening of eyelids and tooth eruption[9], which were not observed when NGF purified from snake venom was used. This then led Cohen to identify the component in salivary gland extracts that were responsible for mediating these side effects. His efforts resulted in the discovery of another growth factor that promotes several important paracrine signal pathways, referred to as epidermal growth factor (EGF)[10]. The isolation and characterization of NGF and EGF earned Levi-Montalcini and Cohen the Nobel Prize in Physiology or Medicine in 1986.

Since paracrine signaling acts locally and does not require a circulatory system to mediate its effects at distant sites, this form of intercellular communication can also be carried-out by lower organisms (i.e. single-cell organisms). One prominent example of this is quorum sensing[11] in bacterial communication, which was discovered while studies investigating the behavior of the bioluminescent gram-

negative bacteria *Vibrio fisheri* were being performed. A tight coupling between cell density and light emission was reported in cultures of these bacteria[12]. The molecular bases for this phenomenon was discovered and involved the ability of *V. fisheri* to secrete auto-inducer hormones, such as homoserine lactone derivatives, when it is actively growing. These hormones then directly bind the transcription factor LuxR, which is expressed in other nearby bacteria, and induce the expression of genes that produce bioluminescence.

Autocrine Signaling

In autocrine signaling, secretion of a soluble factor by a cell is accompanied by expression of the receptor for this ligand by the same cell, a process that is referred to as the secrete-and-sense motif[13]. Autocrine signaling has been extensively studied in the context of malignant transformation, where cancer cells tend to both secrete and respond to the same secreted growth factors to promote transformed phenotypes, such as the ability to grow under nutrient-limiting conditions (i.e. growth in low serum), and to survive serum starvation[14]. A good example of autocrine signaling in cancer involves the pathway stimulated by transforming growth factor (TGF), which was isolated from the conditioned medium from murine fibroblasts that had been transformed through their infection with the Moloney Sarcoma Virus. These cells secrete sarcoma growth factor (SGF), which then binds the epidermal growth factor receptor (EGFR) on the same cell and activates signaling pathways that promote their growth[15].

Bifunctional Secretory Molecules

It is possible for some signaling pathways to distinguish between being activated with paracrine versus autocrine ligands. Even in the presence of identical

receptors and their ligands, cells can behave differently depending on whether or not the ligand and receptor are expressed in the same cell. This phenomenon has been demonstrated by Maheshwari *et. al*[16]*., when they were comparing the paracrine versus autocrine stimulation of the EGFR. Specifically, they showed that* activation of EGF receptor by exogenous EGF, which was present in the cell culture medium (i.e. a paracrine ligand), resulted in the scattered or random migration of epithelial cells. Conversely, when these cells were engineered to produce a protease-cleavable transmembrane form of EGF on the plasma membrane (i.e. an autocrine ligand), the subsequent EGFR activation that occurred led to directional cell migration, as well as an increased ability of these cells to form gland-like structure[16].

Pathways of Protein Secretion in Eukaryotes

From a historical point of view, protein secretion can be broadly classified into two main types: (i) conventional and (ii) unconventional secretion systems. Most secretory proteins go through a well-defined, i.e. conventional, pathway that was first described by George Palade's laboratory[17,18], and involves the endoplasmic reticulum (ER) and Golgi complex. The unconventional secretory mechanisms bypass the ER and Golgi and result in the delivery of proteins to the plasma membrane, and their subsequent release into the extracellular space.

Conventional Protein Secretion

Initially, there were several lines of evidence suggesting that secreted proteins resided in the ER before being released from the cell[19–21], but the intermediate steps in this process were not known. Some light was shed on this question when Jamieson *et. al.*[17,18] investigated protein biosynthesis in exocrine pancreas cells, a type of highly specialized cell that is dedicated to the formation and secretion of proteins.

Specifically, they supplemented their cell growth media with a radiolabeled form of lysine, and performed pulse-chase experiments to follow its incorporation in newly synthesized proteins, and their subsequent trafficking. Using various molecular and biochemical approaches, including cell fractionation, autoradiography, and electron microscopy, they showed that the digestive enzymes of the pancreas were synthesized in the ER and trafficked to the Golgi complex, before ending up in zymogen granules prior to being secreted[22]. At the time these experiments were being performed, mammalian functional genomic screens were not available. Thus, the molecular components of this conventional secretory pathway had to be elucidated using *S. cerevisiae*.

Using the power of yeast genetics, in the late 1970s, Schekman and colleagues devised a strategy which resulted in the identification of 23 different proteins that were critical for the proper secretion of proteins, referred to as secretory or *sec* proteins[23,24]. Because retention of secretory proteins in yeast increased their mass and density, they used this as a read-out to identify mutant yeast strains that were defective in their ability to form and secrete proteins. Analysis of these yeast strains also led to the identification of membrane-bound secretory vesicles that functioned to transport proteins from the ER to the plasma membrane (**Figure 1.2**). For this work, Schekman, together with James Rothman and Thomas Sudof, was awarded the Nobel Prize in Physiology and Medicine in 2013.

Analysis of the proteins that are secreted through the conventional secretory pathway has revealed that most contain a signal peptide[25] which promotes their insertion into the ER membrane. Signal peptides are 16-30 amino acids-long N-terminal sequences that typically have the following characteristics: (i) an *n-region* which consists of hydrophilic and usually positive charged amino acids, (ii) a central homophobic *h-region* of 5-15 residues, and (iii) a *c-region* that contains the cleavage

site for enzymes that digest this peptide from the rest of the protein[26]. A Majority of polypeptides with a signal sequence are detected by the signal recognition particle (SRP), as they are emerging from the ribosome. This complex is then captured by the SRP receptor and inserted in the ER membrane[27].

Unconventional Protein Secretion

Research over the past two decades has shown that not all secreted proteins are released from cells via an ER-Golgi complex-dependent mechanism. In fact, a group of proteins that lack the canonical signal peptide that target proteins to the ER membrane, referred to as leaderless proteins, are released from cells using unconventional protein secretion[28] (UPS) pathways (**Figure 1.2**). These mechanisms involve the coordinated actions of three distinct sets of machinery[29]; Type I, or pore-mediated translocation secretion; Type II, or ABC transporter-mediated secretion; Type III, or autophagosome/endosome based secretion. With a few exceptions (see below), UPS is induced by cellular stresses, possibly as an alternative strategy to secrete proteins when the classical secretory pathway is impaired[30]. Despite having a signal peptide, some proteins, under stress conditions, can also bypass the Golgi complex on their way to the plasma membrane. This process is known as the Type IV UPS, or Golgi-bypass, pathway[29].

In the following sections, the mechanisms underlying the secretion of leaderless proteins will be highlighted.

Figure 1.2 Protein Secretion Pathways

The conventional secretion pathway (left) transports proteins containing signal peptide from the ER-Golgi to the cell surface. Type I-III unconventional protein secretion pathway (middle) acts on leaderless proteins without passing through ER-Golgi. In Type IV (right), some proteins, despite containing signal peptides, can reach the plasma membrane by bypassing the Golgi complex. Figure *reprinted with permission from Company of Biologists*[28].

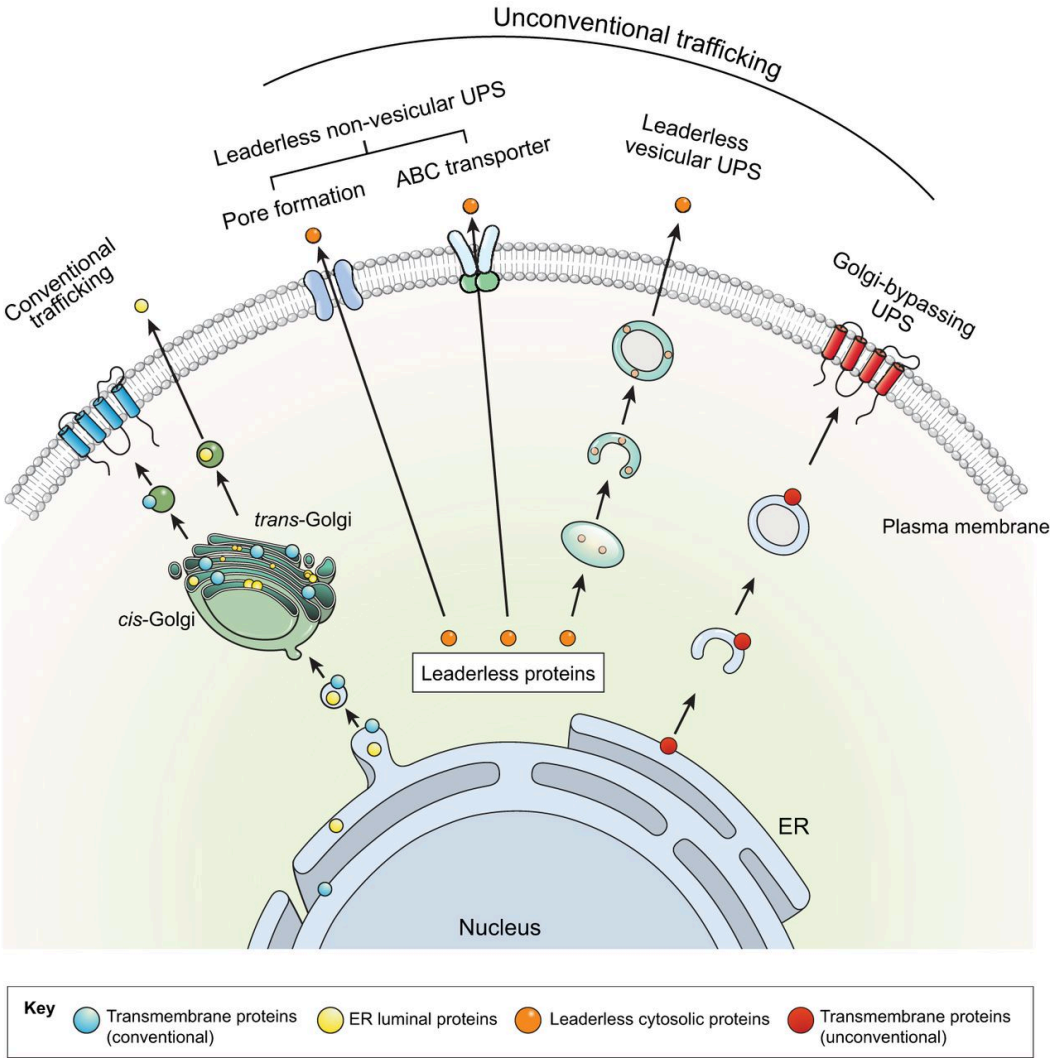
Unconventional trafficking
Leaderless non-vesicular UPS
Pore formation
ABC transporter
Leaderless vesicular UPS
Conventional trafficking
Golgi-bypassing UPS
Plasma membrane
trans-Golgi
cis-Golgi
Leaderless proteins
ER
Nucleus
Key
Transmembrane proteins (conventional)
ER luminal proteins
Leaderless cytosolic proteins
Transmembrane proteins (unconventional)

Type I UPS

Fibroblast growth factor 2 (FGF2) and HIV trans-activator of transcription (TAT) are two examples of proteins that are released from cells by the Type I UPS pathway. These proteins are also unique examples of UPS, because their secretion is not stimulated by cellular stress, but rather occurs in response to other forms of extracellular stimuli. Both FGF2[31,32] and TAT[33,34] form self-made lipid pores that facilitates their constitutive translocation across the plasma membrane and into the extracellular space. Interestingly, when FGF2 was engineered to contain a secretory signal peptide, which caused it to undergo conventional secretion, its biological activity was found to be significantly diminished. Wegehingel *et. al.* suggested that the reason for this was that certain post-translational modifications that occurred to FGF2 during the time it spend in the Golgi, such as O-linked chondroitin, reduced its activity[35], providing a rationale for why certain proteins may be released from cells by an UPS mechanism.

Type I secretion is most often induced by cellular stresses, such as inflammation. For example, extracellular ATP, released from activated innate immune cells, was shown to promote the secretion of the protein cross-linking enzyme, transglutaminase 2 (TGM2), by activating the Purinergic receptor P2X7[36]. P2X7R is a cell surface ATP-gated channel[37] that, upon binding ATP, forms an “open channel” that allows proteins to be released from cells. TGM2, in fact, has been suggested to be secreted through these pores[36]. P2X7R is also reported to be important for the secretion of the pro-inflammatory cytokine interleukin (IL)-1β as well[38]. In this scenario, the inflammation-induced cleavage of IL-1β by caspase 1 results in IL-1β release[39]. Interestingly, mice lacking both copies of P2X7 exhibit reduced severity in models of acute inflammatory joint or lung disease, presumably due to their inability to properly secrete the mature, pro-inflammatory, form of IL-1β[40–42].

Type II UPS

Although Type II UPS was initially reported more than 30 years ago[43], it is the least understood type of secretion. What is currently known regarding this form of secretion is that certain acylated proteins work together with ATP-binding cassette (ABC) transporters to promote their release from cells[29]. For example, the mating pheromone of *S. cerevisiae*, known as alpha-factor, was the first protein that was discovered to be secreted by such a mechanism[43]. ABC transporters are localized to the cell surface, where they use the energy generated from ATP hydrolysis to translocate substrates across the plasma membrane[44] through a poorly understood mechanism. A more recent example of Type II UPS is the translocation of hydrophilic acylated surface protein B (HASPB) across the plasma membrane. During *Leishmaniasis* pathogenesis, HASPB is essential for parasite transmission to the host, as well as for the establishment of parasites within host macrophages[45,46]. The N-terminus of HASPB contains a SH4 domain that is commonly found in the Src family of tyrosine kinases. Dual acylation (myristylation and palmitoylation) of this domain is responsible for the ability of HASPB to associate with the plasma membrane and its subsequent secretion[45].

Type III UPS

The Type III UPS pathway involves the packaging of leaderless cargo into membrane bound organelles for their delivery into the extracellular space. Autophagosomes and endosomes are two organelles that are typically involved in delivering cargo to the lysosome for degradation. However, under certain circumstances that will be described later in Chapter 2, these organelles can also give rise to secretory vesicles. In contrast to Type I and Type II UPS, where proteins are directly translocated across the plasma membrane and released as soluble proteins,

in Type III UPS, proteins are first captured in the lumen of intracellular vesicles and trafficked to the cell surface. At this point they fuse with the plasma membrane and are released as components of vesicles.

Autophagy is best known for its role in promoting the transport of macromolecules, and other organelles, to the lysosome for degradation. This process contributes heavily to cellular catabolism and nutrient recycling[47]. Several cytokines and inflammatory proteins are known to use components of the autophagy machinery for their secretion. For example, in addition to the Type I UPS-dependent mechanism of IL-1β secretion described earlier, serum starvation of HEK-293T cells has been reported to promote the export of IL-1β in a manner that is dependent on Atg5[48], a key protein involved in the synthesis of autophagosome membranes[49].

Another organelle that can significantly contribute to the cellular secretome are endosomes. Endosomes are formed when cells internalize material from their surfaces as a result of the inward budding of the plasma membrane, a process known as endocytosis. Endosomes are typically involved in the sorting and delivery of cargo to lysosomes for degradation[50]. Similar to autophagosomes, endosomes can also be used to secrete both soluble and membrane bound cargo. One of the important aspects of endosomal protein secretion is protein quality control (PQC), which has been implicated in the promotion of a variety of neurodegenerative diseases, such as Alzheimer's, Parkinson's, and Huntington's diseases[51–53]. Overloading of proteasomes with misfolded proteins has been shown to result in their endosomal-mediated secretion. This pathway, also known as misfolding-associated protein secretion (MAPS), involves the recognition of misfolded proteins that have been ubiquitinated, and their translocation into the lumen of Rab9-positive endosomes[54]. Fusion of these endosomes with the plasma membrane results in the secretion of misfolded proteins. It has been hypothesized that MAPS can contribute to cell-to-cell

transmission of aggregation-prone polypeptides, thereby promoting the progression of neurodegeneration. For example, β-amyloid (Aβ) plaques, which are a hallmark of Alzheimer's disease, has been reported to spread between neurons and induce cytotoxicity in recipient cells[55]. Another important function of endosomal-mediated secretion is the ability of multivesicular bodies (MVBs), also known as multivesicular endosomes, to secrete their vesicular content. This aspect of Type III UPS is highly relevant to my research and will be revisited again below.

Extracellular vesicles as another unconventional form of secretion

While the active release of soluble factors, such as growth factors and cytokines, has been extensively studied over the past century, the secretion of extracellular vesicles (EVs) has only more recently been recognized as an important form of intercellular communication.

It has been hypothesized that the secretion of EVs is one of the key evolutionary events that led to the formation of the endomembrane system in eukaryote cells[56]. Electron microscopy images of the surfaces of bacteria show that bacteria can secrete vesicles by the direct outward budding of their plasma membrane (**Figure 1.3A**), also known as outer-membrane vesicles (OMVs)[57]. Functionally, the secretion of OMVs by bacteria promotes their survival[58] and induces changes in their environment[59]. Thus, when early bacteria were engulfed by archaea to form a hybrid organism, the bacterium continued to release OMVs and, for the first time, gave rise to vesicles that were present within the archaea. What followed was billions of years of evolution that eventually led to the formation of the endomembrane trafficking process, as we know it today in eukaryotes[56]. Interestingly, mitochondria, which is

Figure 1.3 Extracellular Vesicles in Bacteria (A) Electron microscopy image of *Escherichia coli* of producing outer-membrane vesicles (annotated as g in the figure). *Image reprinted with permission from John Wiley and Sons*[57]. **(B)** Electron microscopy image of a mitochondria forming mitochondrial derived vesicles[60].

A

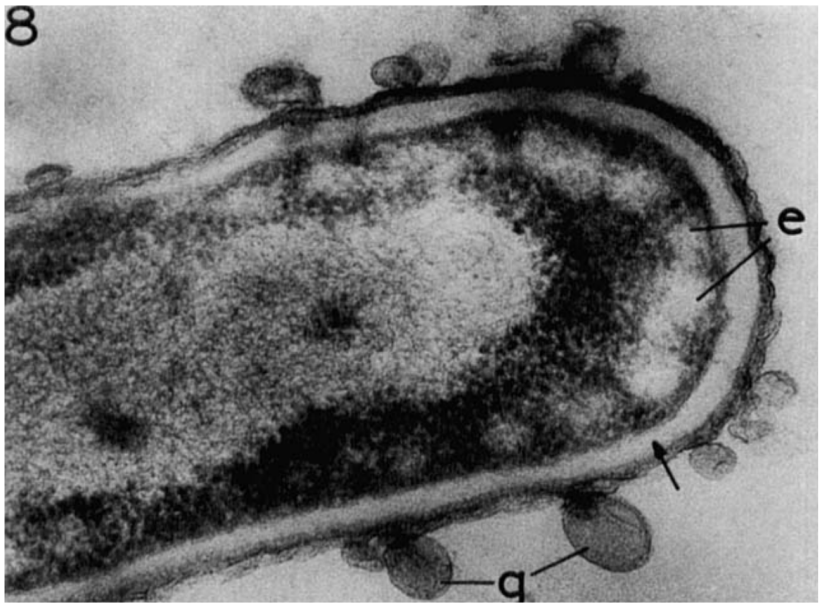

B

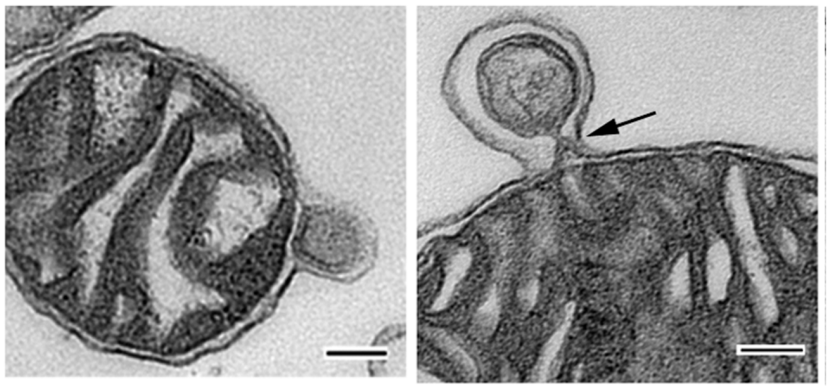

also considered to be derived from endosymbiont bacteria, similarly form outer-membrane vesicles[60] (**Figure 1.3B**, known as mitochondrial derived vesicles (MDV)).

Analogous to the formation of OMVs in bacterial cells, eukaryotic cells can form vesicles through direct budding of the plasma membrane[61]. The EVs generated through this mechanism, as well as through the endosomal pathway, which was described earlier as a Type III UPS, have been highly conserved in diverse organisms and contribute to a variety of physiological processes. In the next section, our current understanding of EV biogenesis in mammalian cells, and how they contribute to the progression of diseases, such as cancer, will be discussed.

Secretion of EVs in Mammalian Cells

Stahl and colleagues carried out one of the earliest studies that showed the secretion of EVs by mammalian cells[62]. While studying the trafficking of the cell surface transferrin receptor (TfR) in maturing reticulocytes, they found that TfRs were present on ~50 nm sized vesicles that were being released into the extracellular space by viable cells (**Figure 1.4**). Subsequent research carried-out over the next several decades in this area of biology has now revealed that virtually all cell types are capable of secreting multiple distinct sub-populations of vesicles. The prevalence of this process has prompted researchers to revisit various physiological and pathological processes, such as cancer and development, and examine the roles played by EVs in these different contexts. The findings from these studies has led to an appreciation of EVs as a major form of intercellular communication. However, despite these advances in our understanding of EV biology, the mechanisms by which cells regulate their production, i.e. EV biogenesis, and their heterogeneity have received significantly less attention.

Figure 1.4 Exocytosis of an MVB containing transferrin receptor on smaller luminal vesicles. Electron microscopy image of an MVB undergoing exocytosis in unfixed rat reticulocyte cell that had been incubated with gold labeled transferrin (bar, 200 nm). *Image reprinted with permission from Rockefeller University Press*[62]*.*

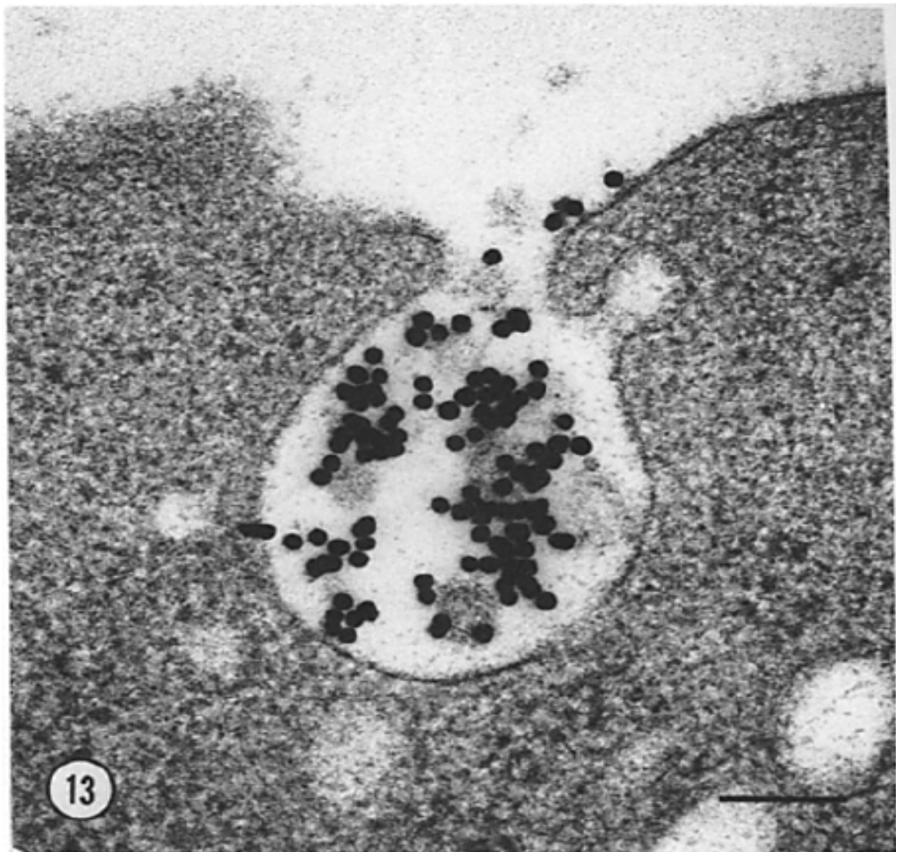
13

Most investigators in the field divide EVs into two broad sub-families, based on their size and the mechanism responsible for their generation. One major sub-family of EVs is comprised of vesicles that range in size from 200 nm to 1–2 μm in diameter, and are generated at a result of the outward budding and fission of the plasma membrane. This class of EVs is most commonly referred to as microvesicles (MVs) (**Figure 1.5A**), although the earlier literature also referred to them as shedding vesicles, ectosomes and, when shown to contain transforming and/or oncogenic cargo, oncosomes. The other major sub-family of EVs is made up of vesicles that range in size from 30 to 150 nm in diameter, and are formed as intraluminal vesicles within endosomal multivesicular bodies (MVBs) released from cells upon the fusion of MVBs with the plasma membrane. At this point the vesicles are referred to as exosomes (**Figure 1.5B**).

In order to have functional outcomes, both MVs and exosomes have to dock onto their target cells, at which point they can stimulate signaling events that originate at the plasma membrane, or are internalized by the cells[63]. In the first scenario, the proteins present on the EV surface engage and activate receptors on the plasma membranes of recipient cells, and initiate specific signaling pathways. For example, we and others have shown that extracellular matrix proteins, such as laminin and fibronectin, are highly expressed along the surfaces of MVs and/or exosomes derived from a variety of cell types ranging from embryonic stem-cells to highly aggressive forms of brain and breast cancer cells. These extracellular matrix proteins bind to their corresponding receptors expressed on recipient cells and activate intracellular signaling proteins that mediate physiological processes, i.e. by promoting the maintenance of the stem cell phenotype and implantation[65], as well as pathological processes, like cancer cell growth, survival, invasion[66,67].

Figure 1.5 Two major classes of extracellular vesicles: MVs and Exosomes
(A) MV formation is initiated by the outward budding of the plasma membrane at lipid raft-like domains. The MV is then loaded with various cargo, before it is shed into the extracellular space. The size of MVs ranges from 200 to 2000 nm. (B) Exosomes represent the second major class of EVs. They are derived as MVBs containing ILVs are routed to the cell surface. The MVB then fuses with the plasma membrane and releases its contents. The ILVs that are released are referred to as exosomes. This class of EVs is typically 50–120 nm in diameter. *Figure and legend reprinted with permission from Portland Press*[64]*.*

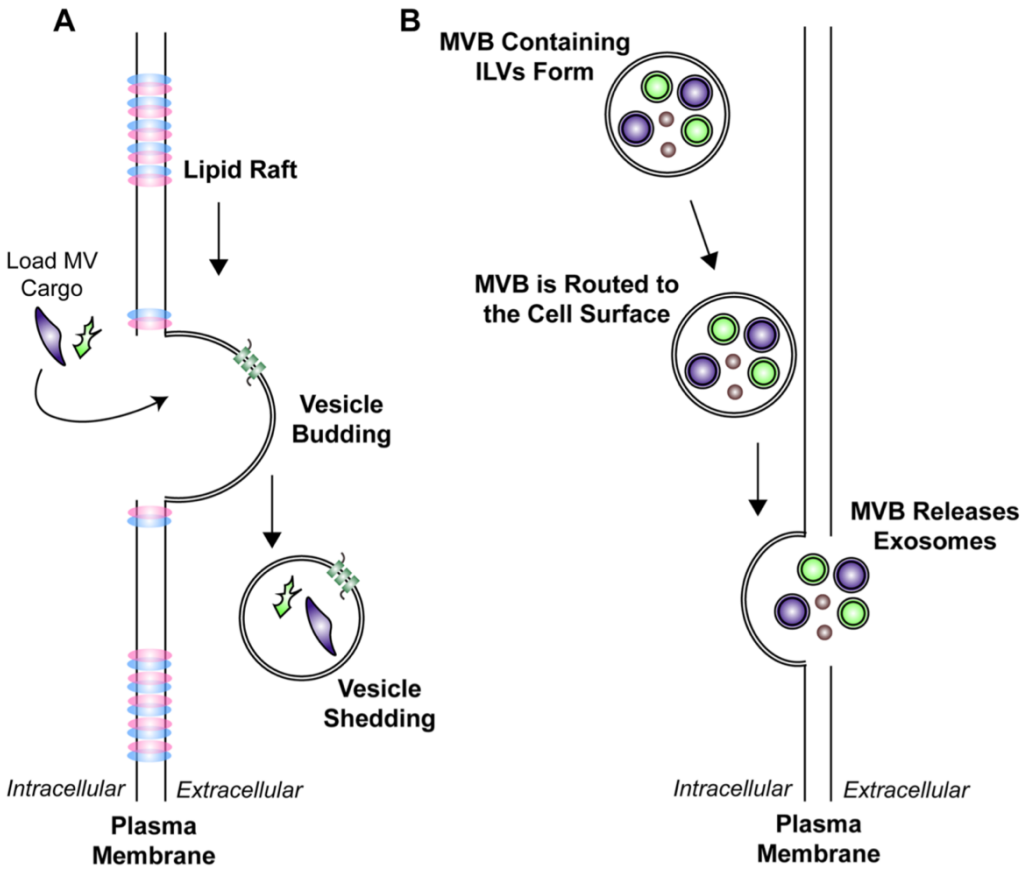
A
Lipid Raft
Load MV
Cargo
Vesicle
Budding
Vesicle
Shedding
Intracellular
Extracellular
Plasma
Membrane
B
MVB Containing
ILVs Form
MVB is Routed to
the Cell Surface
MVB Releases
Exosomes
Intracellular
Extracellular
Plasma
Membrane

EVs can also transfer their contents to recipient cells via direct fusion with the plasma membrane of the recipient cells, or undergo endocytosis. In the latter case, EVs release their contents to the cytosol via fusion with the limiting membrane of the endosome that contains them. This uptake mechanism is particularly useful for cargos that require the cytosolic machineries of recipient cells. A case in point is the study by Skog *et. al.,* where they demonstrated that EVs secreted by glioblastoma cells contained RNA transcripts that can be translated into functional proteins in recipient cells to promote their growth[68].

The following section is devoted to our current understanding of the roles played by EVs in different aspects of cancer progression.

EVs and Tumor Development

In contrast to the classical view that malignant lesions are formed due to the accumulation of aberrant genetic events, i.e. mutations, cancer is becoming increasingly well-recognized as an "ecological disease". In this paradigm, the communication of cancer cells with the other cells within its local environment, known as the tumor microenvironment (TME), plays a critical role in tumor development. Intriguingly, cancer cells typically secrete more EVs than their non-transformed counter parts[69]. The secretion of MVs and exosomes, which contain unique cargo, by cancer cells serve as satellites of intercellular communication that can mediate processes that promote several aspects of malignant transformation. For example, cancer cell-derived EVs have been shown to increase the growth, invasive activity, and drug resistance of other cancer cells[70–72]. However, these EVs can also be transferred to normal cell types that make-up the TME, and alter their behavior in ways that further support tumor growth. For example, exosomes derived from the human PC3 prostate cancer cell line have been shown to induce the differentiation of

fibroblasts into myofibroblasts. This effect is due to the large amount of TGFβ that is associated with exosomes, and its ability to stimulate SMAD3 activity in the recipient cells. SMAD signaling promotes the differentiation of fibroblasts into myofibroblasts, as indicated by the up-regulation of α-smooth muscle actin expression[73]. The presence of myofibroblast cells in the TME of solid tumors has been shown to increase tumor growth and invasive activity [74,75]. Thus, PC3 cells injected into mice can enhance their own growth by interacting with components of the TME using exosomes.

One of the earliest indications suggesting that EVs play an important role in cancer biology came from work performed in our group, when Marc Antonyak *et. al.* discovered that MVs derived from the triple-negative MDA-MB-231 breast cancer cell line can induce several of the characteristics of a transformed cell in normal (non-transformed) fibroblasts and mammary epithelial cells, including the ability to form colonies in soft agar and grow under nutrient-limiting conditions[67]. Subsequently, Qiyu Feng, while a postdoc in Professor Richard Cerione's laboratory, showed that MVs from breast cancer lines contain a unique form of vascular endothelial growth factor (VEGF) that can potently activate the VEGF receptor on endothelial cells and promote angiogenesis, a critical step in tumor progression[76]. A common therapeutic strategy to target tumor angiogenesis has been the administration of monoclonal antibodies, such as Avastin®, that bind and inactivate soluble forms of VEGF[77]. Although these approaches have worked well in the *in vitro* setting, and in animal models, they have largely failed in the clinics. Interestingly, Feng *et. al.* also showed that the unique form of VEGF that associated with the MVs from cancer cells was insensitive to the inhibitory actions of Avastin®, thereby providing a plausible explanation for why Avastin has not been effective as an anti-angiogenesis therapy[78].

The other major class of EVs, namely exosomes, have been shown to promote many of the same processes as MVs. However, exosomes are unique in their ability to facilitate the spread of tumors to other locations in the body. In advanced/aggressive stages of most types of cancer, tumor cells acquire the ability to break free from their local environment, enter and travel through the bloodstream, and ultimately exit the blood stream at a distinct site and colonize it[79]. This process, which is also known as metastasis, is responsible for ~90% of cancer related deaths, thus understanding the mechanisms of metastatic spread is vital. In a series of investigations, David Lyden and his colleagues at Weill Cornell discovered exosomes produced by cancer cells play a critical role in promoting the formation of the pre-metastatic niche, which involves future sites of metastasis to change in ways that make them more receptive for the arrival of cancer cells that are circulating in the bloodstream of cancer patients[80,81]. In one study, Hoshino *et. al.* showed that exosomes play an important role in determining where metastasis occurs[80], a phenomenon that is known as organotropism. Specifically, they found that specific combinations of integrins present on the exosome surface are responsible for targeting them to specific organs long before the arrival of cancer cells. Integrins are a class of cell-surface receptors that bind specifically to different types of extracellular matrix proteins, and are best known for their roles in mediating the physical attachment of cells to their environment. The specificity of ligand binding by integrins is achieved by the dimerization of different integrin subunits[82]. In the context of metastasis, Hoshino et al showed that the integrins expressed on exosomes derived from cancer cells allowed them to accumulate in specific organs. The uptake of exosomes by cells within these secondary sites promoted changes, such as the production of growth factors or the formation of a highly fibrotic environment, which collectively result in the environment becoming more receptive to circulating tumor

cells (**Figure 1.6A**). For example, in brain metastasis, Rodriguez *et. al.* have recently shown that exosomes containing cell migration-inducing and hyaluronan-binding protein (CEMIP) are taken up by brain endothelial and microglial cells. This phenomenon can then give rise to upregulation of pro-inflammatory cytokines that promote brain vasculature remodeling and metastasis[83].

One of the most promising therapeutic approaches to target tumor progression is immunotherapy, where the immune system is reactivated to detect and eliminate cancer cells. A common way to achieve this is to block immunosuppressive ligands, such as PD-L1, that are expressed on the surfaces of tumor cells. Recently, exosomes have been implicated in promoting the ability of cancer cells to evade the immune system. Specifically, Chen *et. al.* have shown that melanoma cancer cells secrete exosomes that express PD-L1 on their surfaces[84]. Exposure of CD8-positive T-cells to these exosomes reduced their proliferation, cytokine production, and induced cytotoxicity. (**Figure 1.6B)**. More recently, Poggio *et. al.* found that a significant portion of the PD-L1 expressed in cancer cells, is present on the exosomes released by the cells, and this form of PD-L1 is resistant to anti-PD-L1 antibodies that are being used in the clinics[85]. Thus, it appears that at least some forms of cancer can generate exosomes that can shield the cancer cells from surveilling immune cells, inactivating them before than can ever reach the tumor.

Despite the many studies that have suggested a role for EVs in tumor progression, the molecular mechanisms that regulate their formation and release are still not well understood. Determining these mechanisms is crucial for the development of novel therapeutic strategies that take aim at inhibiting the production of EVs by cancer cells. The next two sections of this overview will describe what is currently known regarding how MVs and exosomes are formed.

Figure 1.6 Exosomes in Tumor Development
(A) Exosomes carrying specific integrins are generated by cancer cells at primary tumor sites and travel through the bloodstream. Once in the secondary site, they promote formation of a pre-metastatic niche that is receptive for colonization of metastatic tumors. (B) Cancer cells can secrete exosomes that have PD-L1 on their surface. Binding of exosomal PD-L1 to PD-1 receptors on T cells results in T cell exhaustion and allows cancer cells to evade the immune system.

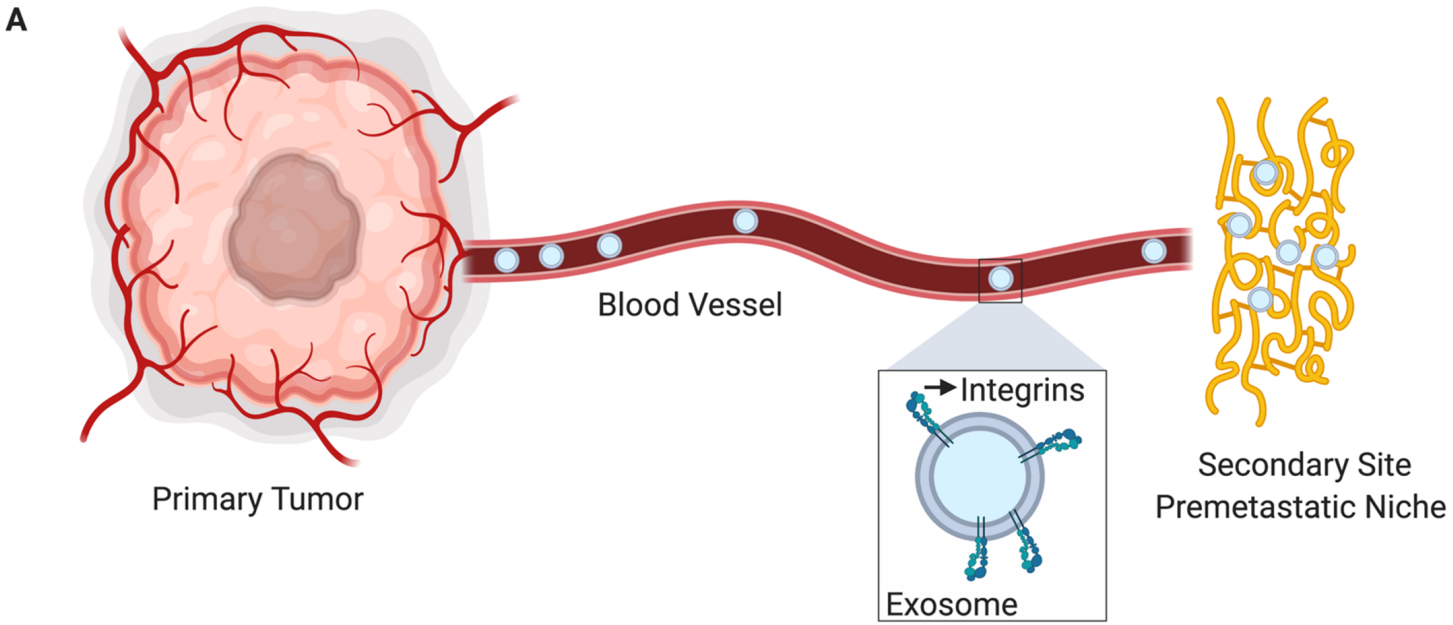
A
Blood Vessel
Primary Tumor
Integrins
Exosome
Secondary Site
Premetastatic Niche

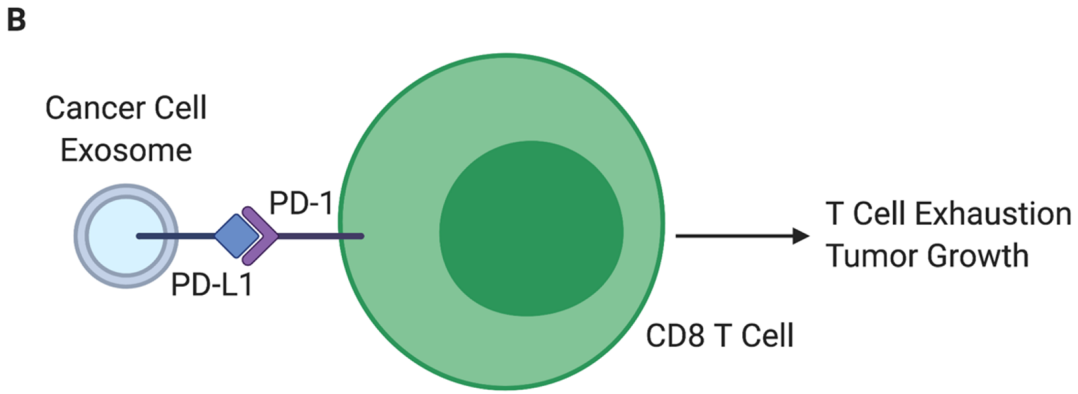
B
Cancer Cell
Exosome
PD-1
PD-L1
CD8 T Cell
T Cell Exhaustion
Tumor Growth

The Biogenesis of Microvesicles

One of the initial demonstrations of cells generating MVs was conducted using highly aggressive brain tumor cells. Due to their relatively large size (200 nm-2000 nm), MVs can be visualized using scanning electron microscopy[86], as well as by conventional immunofluorescent microscopy, when immunostaining the cells for proteins known to expressed in MVs, such as the small GTPase ARF6. Studies from the Rak and Breakefield laboratories have shown that glioblastoma cells ectopically expressing an oncogenic form of the EGF receptor, EGFRvIII, produced significantly more MVs, compared to their control counterparts[87,88]. Consistent with these findings, it was later observed that treating HeLa cervical carcinoma cells with EGF resulted in an increase in the formation and release of MVs[86]. These studies provided some of the initial suggestions that the biogenesis of MVs can be regulated by growth factor-mediated signaling pathways.

In a follow-up study, Bo Li, while a graduate student in the Cerione laboratory, discovered the molecular basis for how activation of the EGFR promoted MV production. Specifically, he showed that treating HeLa cells with EGF increased the activation of a member of the Rho family of small GTPases, specifically RhoA. Interestingly, knocking-down RhoA expression using siRNA in HeLa cells completely blocked EGF-stimulated MV production, while the ectopic expression of an activated form of RhoA in these same cells strongly promoted MV formation. Interestingly, ectopically expressing an activated form of the highly related family member RhoC in these same cells failed to increase MV formation or release, suggesting that this process is highly regulated. Li then went on to delineate the rest of the signaling pathway that functions downstream of RhoA to promote MV biogenesis and found that it involved the sequential activation of Rho-associated, coiled-coil containing protein kinase (ROCK) and LIM kinase. LIMK kinase then phosphorylates the actin

severing enzyme cofilin and inhibits it, resulting in the accumulation of actin filaments and the promotion of the actin-cytoskeletal rearrangements that are needed for MVs to bud from the surfaces of cells[89]. More recently, it has been suggested, by Nagar *et. al.,* that scission of nascent MVs is also dependent on actin polymerization[90]. Thus, actin polymerization is required for budding as well as the ultimate release of MVs from the surfaces of cancer cells.

Another important regulator of MV biogenesis is ADP-ribosylation factor 6 (ARF6) signaling. In a seminal study, Clancy *et. al.* identified the molecular components of this pathway. They specifically showed that ARF6 stimulated the phospholipase D (PLD)-mediated activation of extracellular signal-regulated kinase (ERK), which in turn, increases myosin light chain kinase activity and the phosphorylation of myosin. This modification of myosin leads to the activation of contractile machinery that promotes MV budding at the cell surface [91].

The Biogenesis of Exosomes

The endomembrane system is responsible for the transport of various macromolecules, such as lipids and proteins, to different locations in the cell. The part of this system that deals with trafficking molecules associated with the plasma membrane to intracellular locations is called the endocytic pathway. This process begins with endocytosis, which involves the inward budding of small portions of the plasma membrane. Through the actions of a family of small GTPases, referred to as dynamins, the newly formed invaginations are pinched off into the cytosol, at which point they are called endosomes[50]. The newly formed endosomes then undergo several maturation steps until their contents are either recycled back to plasma membrane, or eventually fuse with lysosomes at which point the contents are degraded. Although the recycling and degradation of proteins are key processes

carried-out by the endocytic pathway, decades of research have shown that this pathway is far more complicated than originally thought. In fact, maturing endosomes are now known to undergo several rounds of invagination to form smaller vesicles called intraluminal vesicles (ILVs) that are contained within the larger multivesicular bodies[50]. Formation of ILVs serves two important purposes: (i) it allows for effective inactivation of signals originating from receptors that are located on the limiting membranes of the endosomes , (ii) it provides the cell with an opportunity to employ endosomes for capturing cytosolic material that would otherwise not be able to be trafficked to lysosomes for degradation.

In the mid 1980's, two different research groups tracked the fate of the transferrin receptor by performing immunoelectron microscopy on rat reticulocytes at different timepoints during their maturation. They observed that the transferrin receptor lifetime on the cell surface was approximately 15 minutes, before it was internalized by endocytosis. Within an hour, the receptor could be detected on the surfaces of ILVs in a subset of maturing endosomes, which are also known as multivesicular bodies (MVBs). At this point, it was expected that these MVBs would be trafficked to the lysosome for degradation. Surprisingly, however, the authors noted that many of the MVBs containing the transferrin receptor were directed to the plasma membrane. They even captured images of MVBs fusing with the plasma membrane and ILVs containing the transferrin receptors were being released into the extracellular environment[92,93]. These vesicles are what are now referred to as exosomes. The findings from these two seminal studies revealed, for the first time, that lysosomes are not the only destination for MVBs, but some of MVBs can also be trafficked to the cell membrane. However, the details regarding which MVBs are routed to the cell surface, versus lysosomes, is not clear. One potential interesting clue as to how this may occur, has to do with emerging evidence that suggests

exosome formation and release is tightly coupled to lysosomal function. For example, inhibiting lysosomal acidification by treating cells with Chloroquine or Bafilomycin consistently results in increased exosome release[94].

Because exosomes are derived from the endocytic pathway, their biogenesis is influenced by mechanisms that control MVB maturation and trafficking. Endosomal sorting complexes required for transport (ESCRTs) are a family of proteins that work together to sort membrane-associated proteins to nascent ILVs on the limiting membrane of MVBs[50] (**Figure 1.7**). Many proteins that are known to be sorted to ILVs in an ESCRT-dependent manner are also often found as exosomal cargo. These proteins, however, include only a modest fraction of the total content of exosomes. In fact, these vesicles have also been shown to contain numerous cytosolic/nuclear proteins, RNA transcripts, as well as DNA, which are not sorted by ESCRTs. Recent studies are beginning to shed some light on additional mechanisms by which these cargos can be incorporated into ILVs, and eventually end up in exosomes. One such mechanism is to capture cytosolic cargo at the limiting membrane of the endosome, through a process known as endosomal microautophagy. In this context, the coordinated actions of ESCRT I and III, as well as that of the chaperone HSC70, results in the recognition of cytosolic proteins that contain the pentapeptide KFERQ sequence, and their sorting into ILVs as they are being formed[95]. Components of autophagy can also contribute to the diversity of exosomal cargo[96]. For example, Leidal *et. al.* have recently described that specific MVBs use microtubule-associated proteins 1A/1B light chain 3B (LC3), which is involved in substrate selection in autophagy, to sort RNA-binding proteins (RBPs) into ILVs, and ultimately exosomes.

Figure 1.7 Cargo Sorting at the Limiting Membrane of MVBs.
ESCRT machinery responsible for sorting of ubiquitinated membrane proteins into the lumen of nascent ILVs. After the invagination on the MVB limiting membrane, the plasma membrane orientation of proteins is retained on surface of the ILVs.

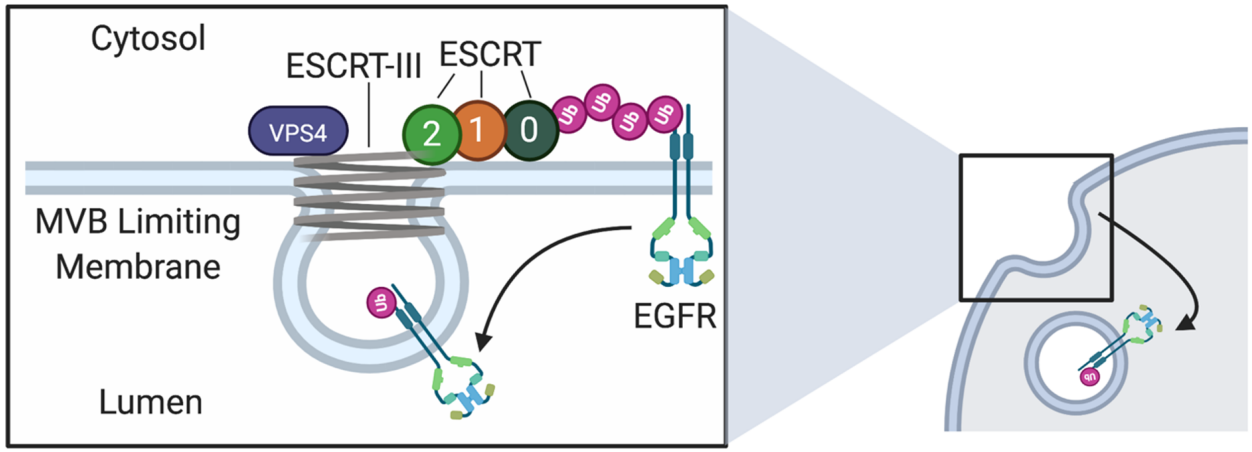
Cytosol
ESCRT-III
ESCRT
VPS4
2
1
0
Ub
Ub
Ub
Ub
MVB Limiting
Membrane
EGFR
Lumen
Ub

They also found that this particular pathway is responsible for sorting of small nucleolar RNAs (snoRNAs) in exosomes[97].

As discussed previously, cancer cells typically form and release significantly more exosomes, compared to their normal cellular counterparts. These exosomes have also been shown to contain a unique sub-set of cargo, which is often responsible for their ability to promote several different cancer-related phenotypes[72]. Thus, exosomes are garnering a great deal of attention from the cancer and cell biology communities, as well as from the pharmaceutical industry. However, the signaling pathways that influence the production of exosomes and the cargo they contain remain poorly understood. Dr. Xiaoyu Zhang, a former graduate student in Professor Hening Lin's laboratory, discovered a previously unappreciated relationship between class III lysine deacylases, referred to as Sirtuins, and exosome biogenesis. Specifically, he showed that one member of this family, namely Sirtuin 6 (SIRT6), had the ability to regulate the sorting of ribosomal proteins into exosomes generated by cells[98]. This study also helped lay the groundwork for the research that will be presented in Chapters 2 and 3 of this thesis.

Sirtuins as NAD^+ Dependent Lysine Deacylating Enzymes

Sirtuins are the only lysine decylases that require NAD^+ for their enzymatic activity[99]. In contrast to many enzymatic reactions that use NAD^+ as an electron acceptor, the deacylase activity of sirtuins breaks down NAD^+ (**Figure 1.8A**). One of the byproduct of this reaction is nicotinamide (NAM), which is usually converted to nicotinamide mononucleotide (NMN), and ultimately NAD^+, in the NAD salvage pathway (**Figure 1.8B**). All sirtuins have a conserved catalytic core, which consists of a zinc binding domain, as well as a Rossmann fold that is responsible for binding NAD^+. Based on phylogenic analysis, sirtuins can be divided into four classes:

Figure 1.8 Sirtuins are NAD-consuming lysine deacylases.

(A) Overall lysine deacylation reaction catalyzed by sirtuins. (B) NAD^+ Salvage pathway that recycles nicotinamide for NAD^+ biosynthesis. NAM: nicotinamide, NMN: nicotinamide mononucleotide, NAMPT: nicotinamide phosphoribosyltransferase, NMNAT: Nicotinamide-nucleotide adenylyltransferase.

A

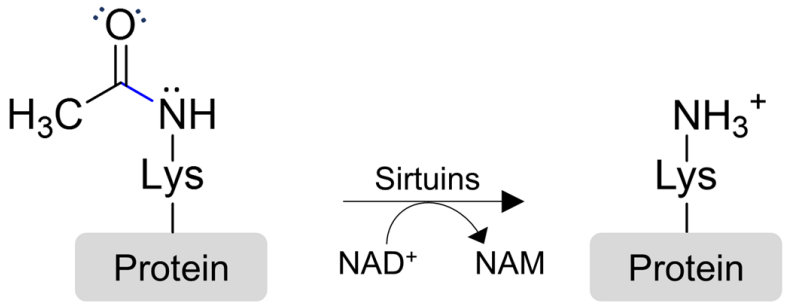

B

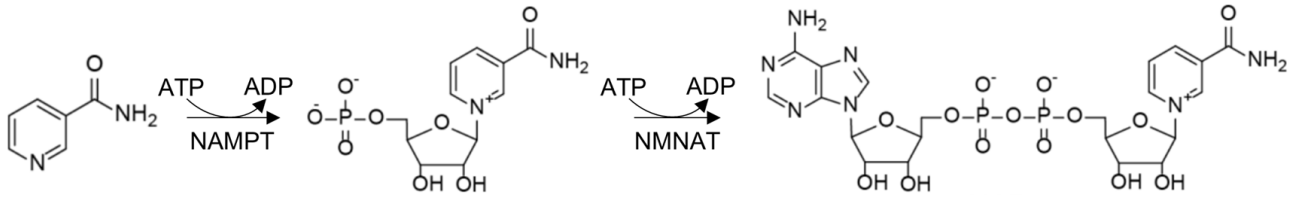

NAM **NMN** **NAD+**

SIRT1-SIRT3 in class I, SIRT4 in class II, SIRT5 in class III, and SIRT6 and SIRT7 in class IV[100]. SIRT1-SIRT3 are the only members of this family of enzymes that have robust deacetylation activity *in vitro*[99], and the enzymatic activity of SIRT4 and SIRT7 is still unclear. Elegant biochemical experiments have shown that SIRT5 prefers negatively charged acyl groups[99], such as succinyl and malonyl. SIRT6, on the other hand, is better at hydrolyzing long-chain fatty acyl groups, such as myristoyl[101,102]. Although, SIRT1-SIRT3 can also hydrolyze long-chain fatty acyl groups *in vitro*, the biological substrates of this activity are only known for SIRT2[103,104] and SIRT6[98,101,105]. Because of the hydrophobic nature of long-chain fatty acyl groups and their association with the lipid membrane, the defatty acylation activity of SIRT2 and SIRT6 can significantly impact the membrane trafficking of their substrates. Most recently, *Kosciuk et. al.* have characterized the lysine myrisotylation-demyristoylation cycle of ARF6 that is catalyzed by N-myristoyltransferase (NMT) and SIRT2[104]. Specifically, they have found that the myristoylation of lysine 3 of ARF6 by NMT is critical for its membrane association during its GTPase cycle. However, in order for ARF6 to encounter its guanine exchange factors (GEFs), that can facilitate the exchange of hydrolyzed GTP, i.e. GDP, to GTP, myristylation at lysine 3 has to be removed by SIRT2. This coordinated actions of NMT and SIRT2 ensures proper activation and recycling of ARF6 during each endocytic event.

Biological Functions of Lysine Deacetylation by SIRT1

Historically, NAD^+ dependent lysine deacetylation was first discovered in SIR2, the yeast homologue of SIRT1[100]. The first indication that Sir2 has lysine deacetylase activity came from findings[106,107] showing: (i) silencing of the silent-mating type cassette resulted in enhanced acetylation of a lysine residue in the N-terminal domains of histones H3 and H4, and (ii) overexpression of Sir2 in yeast results in a

strong reduction in the acetylation levels of histones. Based on these observations, Imai *et. al.* carried out a series of biochemical experiments with purified SIR2 and acetylated peptides to demonstrate that SIR2 was directly responsible for deacetylating substrates in an NAD^+-dependent manner[100].

SIRT1 is not only the founding member of the sirtuin family, but it is also the most studied. It is important for development, i.e. loss of SIRT1 often causes embryonic lethality, with only 20% of mice lacking both copies of SIRT1 being able to reach maturity[108]. Over the last two decades, SIRT1, and its homologues in other organisms, have been extensively studied in the context of various physiological conditions and diseases.

SIRT1 and Lifespan. Sirtuins gained a lot of attention in 1999, when it was reported that overexpression of Sir2 extended yeast lifespan[109]. This effect has now also been seen in various other organisms, such as *Caenorhabditis elegans*[110], *Drosophila melanogaster*[111], and mice[112]. The exact mechanism by which SIRT1 prolongs lifespan is still unclear. While whole-body overexpression of SIRT1 in mice fails to promote lifespan[113], tissue-specific overexpression of SIRT1 appears to be more effective. For example, brain-specific overexpression of SIRT1 has been shown to promote longevity, possibly by promoting the deacetylation of the transcription factor NKs homeobox 1 (NKX2-1). In the hypothalamic brain regions, deacetylated NKX2-1 upregulates the transcription of Oregon type 2 receptor (Ox2r), which is hypothesized to enhance neuronal activity that maintains skeletal muscle mitochondrial morphology and function, physical activity, body temperature, and oxygen consumption during aging[112].

Since overexpression of SIRT1 is currently not a viable option for extending the lifespan of humans, pharmacological and dietary strategies have been proposed

to enhance SIRT1 activity[114]. One such strategy is based on the observation that calorie restriction (CR) upregulates SIRT1 expression[115] and increases NAD^+ levels[116]. Interestingly, CR has been implicated in extension of lifespan as well. However, the mechanistic basis for this effect is not understood and may not be solely due to increasing SIRT1 activity.

SIRT1 and Circadian Clock. Circadian clocks are innate biological timing mechanisms that allow for the coordination of physiological processes with daily environmental cycles. A vast array of cellular processes, including metabolic reactions, follow rhythmic patterns that are set by the circadian cycle[117]. Disruption of these cycles can have detrimental effects on the overall fitness of the organism. For example, mutation of molecular components of the circadian clock (see below) in mice significantly alters glucose tolerance and insulin secretion by pancreatic islets, and can lead to the onset of diabetes[118].

The circadian rhythm typically consists of transcriptional feedback loops to control gene expression. One of the earliest described circadian oscillators involves the negative feedback loop of Period (PER) and cryptochrome (CRY) towards the transcriptional activator complex CLOCK/BMAL1. Interestingly, CLOCK is known to have acetyl transferase activity, and can promote the acetylation of histones, thereby inducing the transcription of PER and CRY. This process can be inhibited when CLOCK catalyzes the acetylation of its own partner BMAL1, which then promotes the recruitment of CRY1 to the transcriptional complex and inactivates it[119]. It is thought that subsequent SIRT1-mediated deacetylation of histones is necessary to revert the chromatin back to its repressive state. SIRT1 also catalyzes the deacetylation of other circadian components, such as BMAL1, and resets them for the next round of the circadian cycle[120,121]. As a result, the deacetylase activity of SIRT1 facilitates timely

inactivation and re-initiation of the circadian rhythm. The regulation of circadian rhythm by SIRT1 has two intriguing implications: (i) because SIRT1 activity is NAD^+ dependent, this pathway couples the metabolic state of the cell to the circadian clock, (ii) the systematic SIRT1 deacetylation is induced at a specific phase corresponding to the activation of the cellular catabolism/fasting[122]. This coincidence suggests that SIRT1 activity might also influence the catabolic processes. In the conlcuding chapter, I shall revisit this hypothesis in light of my dissertation studies.

SIRT1 and Tumor Development. The role of SIRT1 in cancer progression is multi-faceted and context dependent. Some studies have suggested that SIRT1 acts as a tumor suppressor and limits cancer cell growth [123,124]. For example, in breast cancer, downregulation of SIRT1 expression is correlated with tumor expansion[125] and metastatic spread[126]. However, in other types of cancer, SIRT1 has been shown to have the opposite effect and promote cancer progression[127]. A case in point is the negative regulation of SIRT1 activity that is imparted through its interaction with Deleted in Breast Cancer 1 (DBC1) [128,129]. Inhibition of SIRT1 by DBC1 results in hyperacetylation of the SIRT1 substrate, p53, and upregulation of its transcriptional and apoptotic activities. However, when DBC1 is mutated or deleted, which frequently occurs in breast cancer, SIRT1 is able to deacetylate p53 and reduce its transcriptional activity, thus preventing the induction of cell death. Consistent with this idea, SIRT1 deficient mice have been reported to have increased rates of radiation-induce death, compared to wild-type mice[108].

Thus, understanding how SIRT1 functions in different contexts to influence various aspects of the transformed phenotype remains an important are of investigation and it is the subject of my dissertation. In the following Chapter, I will describe how aggressive breast cancer cells with reduced expression of the lysine

deacylase SIRT1 produces a secretome that markedly increases their aggressiveness and potential for metastatic spread. In Chapter 3, I will outline the molecular components of this phenotype and discuss an underappreciated role of SIRT1 in RNA biology.

REFERENCES

1. Williams MJ. J. J. R. Macleod: the co-discoverer of insulin. *Proc R Coll Physicians Edinb*. 1993;**23**:1-125

2. Banting FG, Best CH, Collip JB, Cambell WR, Fletcher AA, Macleod JJR NE. The effect produced on diabetes by extractions of pancreas. *Trans Assoc Am Physicians*. 1922;**37**:337-347

3. Haeusler RA, McGraw TE, Accili D. Metabolic signalling: Biochemical and cellular properties of insulin receptor signalling. *Nat Rev Mol Cell Biol*. 2018;**19**:31-44.

4. Levi-Montalcini R. The nerve growth factor 35 years later. *Science.* 1997;**273:**384-392

5. Levi-Montalcini R, Meyer H, Hamburger V. In Vitro experiments on the effects of mouse sarcomas 180 and 37 on the spinal and sympathetic ganglia of the chick embryo. *Cancer Res*. 1954;**14**:49-57

6. Levi-Montalcini R, Cohen S. in Vitro and in vivo effects of a nerve growth-stimulating agent isolated from snake venom. *Proc Natl Acad Sci*. 1956;**42**:695-699

7. Cohen SN. Purification and metabolic effects of a nerve growth-promoting protein from snake venom. *J Biol Chem*. 1959;**234**:1129-1137.

8. Cohen S. Purification of a nerve-growth promoting protein from the mouse salivary gland and its neuro-cytotoxic antiserum. *Proc Natl Acad Sci*. 1960;**46**:302-311

9. Cohen SN. Isolation of a mouse submaxillary gland protein accelerating incisor eruption and eyelid opening in the new-born animal. *J Biol Chem*. 1962;**237**:1555-1562.

10. Cohen S. Origins of growth factors: NGF and EGF. *Ann N Y Acad Sci*. 2004;**1038**:98-102

11. Miller MB, Bassler BL. Quorum sensing in bacteria. *Annu Rev Microbiol*. 2001;**55**:165-199

12. Nealson KH, Hastings JW. Bacterial bioluminescence: Its control and ecological significance. *Microbiol Rev*. 1979;**43**:496-518

13. Youk H, Lim WA. Secreting and sensing the same molecule allows cells to achieve versatile social behaviors. *Science.* 2014;**343**:1242782

14. Sporn MB, Todaro GJ. Autocrine secretion and malignant transformation of cells. *N Engl J Med*. 1980;**303**:878-880

15. De Larco JE, Todaro GJ. Growth factors from murine sarcoma virus-transformed cells. *Proc Natl Acad Sci U S A*. 1978;**75**:4001-4005.

16. Maheshwari G, Steven Wiley H, Lauffenburger DA. Autocrine epidermal growth factor signaling stimulates directionally persistent mammary epithelial cell migration. *J Cell Biol*. 2001;**155**:1123-1128.

17. Jamieson JD, Palade GE. Intracellular transport of secretory proteins in the pancreatic exocrine cell. II. Transport to condensing vacuoles and zymogen granules. *J Cell Biol*. 1967;**34**:597-615.

18. Jamieson JD, Palade GE. Intracellular transport of secretory proteins in the pancreatic exocrine cell. I. Role of the peripheral elements of the Golgi complex. *J Cell Biol*. 1967;**34**:577-596.

19. Siekevitz P, Palade GE. A cytochemical study on the pancreas of the guinea pig. II. Functional variations in the enzymatic activity of microsomes. *J Biophys Biochem Cytol*. 1958;**4**:309-318.

20. Siekevitz P, Palade GE. A cytochemical study on the pancreas of the guinea pig. I. Isolation and enzymatic activities of cell fractions. *J Biophys Biochem Cytol*. 1958;**4**:203-218.

21. Siekevitz P, Palade GE. A cyto-chemical study on the pancreas of the guinea pig. III. In vivo incorporation of leucine-1-C14 into the proteins of cell fractions. *J Biophys Biochem Cytol*. 1958;**4**:557-566.

22. Palade GE. Intracellular aspects of the process of protein synthesis. *Science.* 1975;**189**:347-358.

23. Novick P, Schekman R. Secretion and cell-surface growth are blocked in a temperature-sensitive mutant of Saccharomyces cerevisiae. *Proc Natl Acad Sci*. 1979;**76**:1858-1862.

24. Novick P, Field C, Schekman R. Identification of 23 complementation groups required for post-translational events in the yeast secretory pathway. *Cell*. 1980;**21**:205-215.

25. Rapoport TA, Blobel G. Protein translocation across and integration into membrane. *Crit Rev Biochem Mol Biol*. 1986;**20**:73-137.

26. Nothwehr SF, Gordon JI. Targeting of proteins into the eukaryotic secretory pathway: Signal peptide structure/function relationships. *BioEssays*. 1990;**12**:479-484

27. Hegde RS, Bernstein HD. The surprising complexity of signal sequences. *Trends Biochem Sci*. 2006;**31**:563-571

28. Rabouille C, Malhotra V, Nickel W. Diversity in unconventional protein secretion. *J Cell Sci*. 2012;**125**:5251-5255

29. Kim J, Gee HY, Lee MG. Unconventional protein secretion - new insights into the pathogenesis and therapeutic targets of human diseases. *J Cell Sci*. 2018;**131**: jcs213686

30. Giuliani F, Grieve A, Rabouille C. Unconventional secretion: A stress on GRASP. *Curr Opin Cell Biol*. 2011;**23**:498-504.

31. Steringer JP, Müller HM, Nickel W. Unconventional secretion of fibroblast growth factor 2 - A novel type of protein translocation across membranes? *J Mol Biol*. 2015;**427**:1202-1210

32. La Venuta G, Zeitler M, Steringer JP, Müller HM, Nickel W. The startling properties of fibroblast growth factor 2: How to exit mammalian cells without a signal peptide at hand. *J Biol Chem*. 2015;**290**:27015-27020

33. Debaisieux S, Rayne F, Yezid H, Beaumelle B. The ins and outs of HIV-1 Tat. *Traffic*. 2012;**13**:355-363

34. Zeitler M, Steringer JP, Möller HM, Mayer MP, Nickel W. HIV-Tat protein forms phosphoinositide-dependent membrane pores implicated in unconventional protein secretion. *J Biol Chem*. 2015;**290**:21976-21984

35. Wegehingel S, Zehe C, Nickel W. Rerouting of fibroblast growth factor 2 to the classical secretory pathway results in post-translational modifications that block binding to heparan sulfate proteoglycans. *FEBS Lett*. 2008;**582**:2387-2392

36. Adamczyk M, Griffiths R, Dewitt S, Knäuper V, Aeschlimann D. P2X7 receptor activation regulates rapid unconventional export of transglutaminase-2. *J Cell Sci*. 2015;**128**:4615-4628.

37. Savio LEB, Mello P de A, da Silva CG, Coutinho-Silva R. The P2X7 receptor in inflammatory diseases: Angel or demon? *Front Pharmacol*. 2018;**9**:52

38. Pelegrin P, Barroso-Gutierrez C, Surprenant A. P2X7 receptor differentially couples to distinct release pathways for IL-1β in mouse macrophage. *J Immunol*. 2008;**180**:7147-7157

39. Mariathasan S, Weiss DS, Newton K, et al. Cryopyrin activates the inflammasome in response to toxins and ATP. *Nature*. 2006;**440**:228-232

40. Lucattelli M, Cicko S, Müller T, et al. P2X7 receptor signaling in the pathogenesis of smoke-induced lung inflammation and emphysema. *atsjournals.org*. 2011;**44**:423-429

41. Bartlett R, Stokes L, Sluyter R. The P2X7 receptor channel: recent developments and the use of P2X7 antagonists in models of disease. Pharmacol Rev. 2014;**66**:638-675

42. Wicks JR, Audoly L, Gabel McCurdy CA, et al. Absence of the P2X7 receptor alters leukocyte function and attenuates an inflammatory response. *J Immunol.* 2002;**168**:6436-6445

43. McGrath JP, Varshavsky A. The yeast STE6 gene encodes a homologue of the mammalian multidrug resistance P-glycoprotein. *Nature*. 1989;**340**:400-404.

44. Hollenstein K, Dawson RJ, Locher KP. Structure and mechanism of ABC transporter proteins. *Curr Opin Struct Biol*. 2007;**17**:412-418

45. Denny PW, Gokool S, Russell DG, Field MC, Smith DF. Acylation-dependent protein export in Leishmania. *J Biol Chem*. 2000;**275**:11017-11025

46. Stegmayer C, Kehlenbach A, Tournaviti S, et al. Direct transport across the plasma membrane of mammalian cells of Leishmania HASPB as revealed by a CHO export mutant. *J Cell Sci*. 2005;**118**:517-527

47. He L, Zhang J, Zhao J, et al. Autophagy: The last defense against cellular nutritional stress. *Adv Nutr*. 2018;**9**:493-504

48. Zhang M, Kenny SJ, Ge L, Xu K, Schekman R. Translocation of interleukin-1β into a vesicle intermediate in autophagy-mediated secretion. *Elife*. 2015;**4**:e11205

49. Levine B, Kroemer G. Biological functions of autophagy genes: A disease perspective. *Cell*. 2019;**176**:11-42

50. Huotari J, Helenius A. Endosome maturation. *EMBO J*. 2011;**30**:3481-3500.

51. Hetz C, Mollereau B. Disturbance of endoplasmic reticulum proteostasis in neurodegenerative diseases. *Nat Rev Neurosci*. 2014;**15**:233-249.

52. Ryno LM, Wiseman RL, Kelly JW. Targeting unfolded protein response signaling pathways to ameliorate protein misfolding diseases. *Curr Opin Chem Biol*. 2013;**17**:346-352

53. Knowles TPJ, Vendruscolo M, Dobson CM. The amyloid state and its association with protein misfolding diseases. *Nat Rev Mol Cell Biol*. 2014;**15**:384-396

54. Lee JG, Takahama S, Zhang G, Tomarev SI, Ye Y. Unconventional secretion of misfolded proteins promotes adaptation to proteasome dysfunction in mammalian cells. *Nat Cell Biol*. 2016;**18**:765-776.

55. Nath S, Agholme L, Kurudenkandy FR, Granseth B, Marcusson J, Hallbeck M. Spreading of neurodegenerative pathology via neuron-to-neuron transmission of β-amyloid. *J Neurosci*. 2012;**32**:8767-8777

56. Gould SB, Garg SG, Martin WF. Bacterial vesicle secretion and the evolutionary origin of the eukaryotic endomembrane system. *Trends*

Microbiol. 2016;**24**:525-534.

57. Schwechheimer C, Kuehn MJ. Outer-membrane vesicles from Gram-negative bacteria: Biogenesis and functions. *Nat Rev Microbiol*. 2015;**13**:605-619

58. Manning AJ, Kuehn MJ. Contribution of bacterial outer membrane vesicles to innate bacterial defense. *BMC Microbiol*. 2011;**11**:258

59. Ellis TN, Kuehn MJ. Virulence and immunomodulatory roles of bacterial outer membrane vesicles. *Microbiol Mol Biol Rev*. 2010;**74**:81-94

60. Sugiura A, McLelland G, Fon EA, McBride HM. A new pathway for mitochondrial quality control: mitochondrial-derived vesicles. *EMBO J*. 2014;**33**:2142-2156.

61. Raposo G, Stoorvogel W. Extracellular vesicles: Exosomes, microvesicles, and friends. *J Cell Biol*. 2013;**200**:373-383

62. Harding C, Heuser J, Stahl P. Receptor-mediated endocytosis of transferrin and recycling of the transferrin receptor in rat reticulocytes. *J Cell Biol*. 1983;**97**:329-339.

63. French KC, Antonyak MA, Cerione RA. Extracellular vesicle docking at the cellular port: Extracellular vesicle binding and uptake. *Semin Cell Dev Biol*. 2017;**67**:48-55

64. Latifkar A, Cerione RA, Antonyak MA. Probing the mechanisms of extracellular vesicle biogenesis and function in cancer. *Biochem Soc Trans.* 2018;**46**:1137-1146

65. Desrochers LM, Bordeleau F, Reinhart-King CA, Cerione RA, Antonyak MA. Microvesicles provide a mechanism for intercellular communication by embryonic stem cells during embryo implantation. *Nat Commun*. 2016;**7**:11958

66. Chanda D, Otoupalova E, Hough KP, et al. Fibronectin on the surface of extracellular vesicles mediates fibroblast invasion. *Am J Respir Cell Mol Biol*. 2019;**60**:279-288

67. Antonyak MA, Li B, Boroughs LK, et al. Cancer cell-derived microvesicles induce transformation by transferring tissue transglutaminase and fibronectin to recipient cells. *Proc Natl Acad Sci*. 2011;**108**:4852-4857

68. Skog J, Würdinger T, van Rijn S, et al. Glioblastoma microvesicles transport RNA and proteins that promote tumour growth and provide diagnostic biomarkers. *Nat Cell Biol*. 2008;**10**:1470-1476

69. Xu R, Rai A, Chen M, Suwakulsiri W, Greening DW, Simpson RJ. Extracellular vesicles in cancer — implications for future improvements in cancer care. *Nat Rev Clin Oncol*. 2018;**15**:617-638

70. Soung YH, Nguyen T, Cao H, Lee J, Chung J. Emerging roles of exosomes in cancer invasion and metastasis. *BMB Rep*. 2016;**49**:18-25

71. O'Neill CP, Gilligan KE, Dwyer RM. Role of extracellular vesicles (EVs) in cell stress response and resistance to cancer therapy. *Cancers (Basel)*. 2019;**11**:2

72. Kalluri R. The biology and function of exosomes in cancer. *J Clin Invest*. 2016;**126**:1208-1215

73. Webber J, Steadman R, Mason MD, Tabi Z, Clayton A. Cancer exosomes trigger fibroblast to myofibroblast differentiation. *Cancer Res*. 2010;**70**:9621-9630

74. Akira Orimo, Piyush B. Gupta, Dennis C. Sgroi, et al. Stromal fibroblasts present in invasive human breast carcinomas promote tumor growth and angiogenesis through elevated SDF-1/CXCL12 secretion. *Cell*. 2005;**6**:335-348.

75. Olumi AF, Grossfeld GD, Hayward SW, Carroll PR, Tlsty TD, Cunha GR. Carcinoma-associated fibroblasts direct tumor progression of initiated human prostatic epithelium. *Cancer Res*. 1999;**59**:5002-5011

76. Feng Q, Zhang C, Lum D, et al. A class of extracellular vesicles from breast cancer cells activates VEGF receptors and tumour angiogenesis. *Nat Commun*. 2017;**8**:14450

77. Muller YA. CY. CHW. LB. CBC. LHB. de VAM. VEGF and the Fab fragment of a humanized neutralizing antibody: crystal structure of the complex at 2.4 A resolution and mutational analysis of the interface. *Structure*. 1998;**6**:1153-1167

78. Mortimer J, Zonder H, Pal SK. Lessons learned from Avastin. *Cancer Control*. 2012;**19**:309-3016

79. Varki A, Varki NM, Borsig L. Molecular basis of metastasis. *N Engl J Med*. 2009;**360**:1678-1680

80. Hoshino A, Costa-Silva B, Shen T-L, et al. Tumour exosome integrins determine organotropic metastasis. *Nature*. 2015;**527**:329-335

81. Costa-Silva B, Aiello NM, Ocean AJ, et al. Pancreatic cancer exosomes initiate pre-metastatic niche formation in the liver. *Nat Cell Biol*. 2015;**17**:1-7

82. Humphries JD., Byron A, Humphries MJ. Integrin ligands at a glance. *J Cell Sci*. 2006;**119**:3901-3903.

83. Rodrigues G, Hoshino A, Kenific CM, et al. Tumour exosomal CEMIP protein promotes cancer cell colonization in brain metastasis. *Nat Cell Biol*. 2019;**21**:1403-1412

84. Chen G, Huang AC, Zhang W, et al. Exosomal PD-L1 contributes to immunosuppression and is associated with anti-PD-1 response. *Nature*. 2018;**560**:382-386

85. Poggio M, Hu T, Pai CC, et al. Suppression of Exosomal PD-L1 Induces Systemic Anti-tumor Immunity and Memory. *Cell*. 2019;**177**:414-427

86. Antonyak MA, Li B, Boroughs LK, et al. Cancer cell-derived microvesicles induce transformation by transferring tissue transglutaminase and fibronectin to recipient cells. *Proc Natl Acad Sci*. 2011;**108**:4852-4857

87. Skog J, Würdinger T, van Rijn S, et al. Glioblastoma microvesicles transport RNA and proteins that promote tumour growth and provide diagnostic biomarkers. *Nat Cell Biol*. 2008;**10**:1470-1476

88. Al-Nedawi K, Meehan B, Micallef J, et al. Intercellular transfer of the oncogenic receptor EGFRvIII by microvesicles derived from tumour cells. *Nat Cell Biol*. 2008;**10**:619-624

89. Li B, Antonyak MA, Zhang J, Cerione RA. RhoA triggers a specific signaling pathway that generates transforming microvesicles in cancer cells. *Oncogene*. 2012;**31**:4740-4749

90. Nager AR, Goldstein JS, Herranz-Pérez V, et al. An actin network dispatches ciliary GPCRs into extracellular vesicles to modulate signaling. *Cell*. 2017;**168**:252-263

91. Muralidharan-Chari V, Clancy J, Plou C, et al. ARF6-regulated shedding of tumor cell-derived plasma membrane microvesicles. *Curr Biol*. 2009;**19**:1875-1885

92. Harding C, Heuser J, Stahl P. Receptor-mediated endocytosis of transferrin and recycling of the transferrin receptor in rat reticulocytes. *J Cell Biol*. 1983;**97**:329-339

93. Pan BT, Teng K, Wu C, Adam M, Johnstone RM. Electron microscopic evidence for externalization of the transferrin receptor in vesicular form in sheep reticulocytes. *J Cell Biol*. 1985;**101**:942-948

94. Miao Y, Li G, Zhang X, Xu H, Abraham SN. A TRP channel senses lysosome neutralization by pathogens to trigger their expulsion. *Cell*. 2015;**161**:1306-1319

95. Sahu R, Kaushik S, Clement CC, et al. Microautophagy of cytosolic proteins by late endosomes. *Dev Cell*. 2011;**20**:131-139

96. Gudbergsson JM, Johnsen KB. Exosomes and autophagy: rekindling the vesicular waste hypothesis. *J Cell Commun Signal*. 2019;**13**:443-450

97. Leidal AM, Huang HH, Marsh T, et al. The LC3-conjugation machinery specifies the loading of RNA-binding proteins into extracellular vesicles. *Nat*

Cell Biol. 2020;**22**:187-199

98. Zhang X, Khan S, Jiang H, et al. Identifying the functional contribution of the defatty-acylase activity of SIRT6. *Nat Chem Biol*. 2016;**12**:614-620

99. Jing H, Lin H. Sirtuins in epigenetic regulation. *Chem Rev*. 2015;**115**:2350-2375

100. Imai SI, Armstrong CM, Kaeberlein M, Guarente L. Transcriptional silencing and longevity protein Sir2 is an NAD-dependent histone deacetylase. *Nature*. 2000;**403**:795-800

101. Jiang H, Khan S, Wang Y, et al. SIRT6 regulates TNF-α secretion through hydrolysis of long-chain fatty acyl lysine. *Nature*. 2013;**496**:110-113

102. Feldman JL, Baeza J, Denu JM. Activation of the protein deacetylase SIRT6 by long-chain fatty acids and widespread deacylation by mammalian sirtuins. *J Biol Chem*. 2013;**288**:31350-31356

103. Jing H, Zhang X, Wisner SA, et al. SIRT2 and lysine fatty acylation regulate the transforming activity of K-Ras4a. *Elife*. 2017;**6**:e32436

104. Kosciuk T, Price IR, Zhang X, et al. NMT1 and NMT2 are lysine myristoyltransferases regulating the ARF6 GTPase cycle. *Nat Commun*. 2020;**11**:1

105. Zhang X, Spiegelman NA, Nelson OD, Jing H, Lin H. SIRT6 regulates Ras-related protein R-Ras2 by lysine defatty-acylation. *Elife*. 2017;**6**:e25158

106. Braunstein M, Rose AB, Holmes SG, David Allis C, Broach JR. Transcriptional silencing in yeast is associated with reduced nucleosome acetylation. *Genes Dev*. 1993;**7**:592-604

107. Braunstein M, Sobel RE, Allis CD, Turner BM, Broach JR. Efficient transcriptional silencing in Saccharomyces cerevisiae requires a heterochromatin histone acetylation pattern. *Mol Cell Biol*. 1996;**16**:4349-4356

108. Cheng HL, Mostoslavsky R, Saito S, et al. Developmental defects and p53 hyperacetylation in Sir2 homolog (SIRT1)-deficient mice. *Proc Natl Acad Sci*. 2003;**100**:10794-10799

109. Kaeberlein M, McVey M, Guarente L. The SIR2/3/4 complex and SIR2 alone promote longevity in Saccharomyces cerevisiae by two different mechanisms. *Genes Dev*. 1999;**13**:2570-2580

110. Tissenbaum HA, Guarente L. Increased dosage of a sir-2 gene extends lifespan in Caenorhabditis elegans. *Nature*. 2001;**410**:227-230

111. Rogina B, Helfand SL. Sir2 mediates longevity in the fly through a pathway related to calorie restriction. *Proc Natl Acad Sci*. 2004;**101**:15998-16003

112. Satoh A, Brace CS, Rensing N, et al. Sirt1 extends life span and delays aging in mice through the regulation of Nk2 Homeobox 1 in the DMH and LH. *Cell Metab*. 2013;**18**:416-430

113. Herranz D, Muñoz-Martin M, Cañamero M, et al. Sirt1 improves healthy ageing and protects from metabolic syndrome-associated cancer. *Nat Commun*. 2010;**1**:1

114. Grabowska W, Sikora E, Bielak-Zmijewska A. Sirtuins, a promising target in slowing down the ageing process. *Biogerontology*. 2017;**18**:447-476

115. Civitarese A, Carling S, Heilbronn L, et al. Calorie restriction increases muscle mitochondrial biogenesis in healthy humans. *PLoS Med*. 2007;**4**:e76.

116. Chen D, Bruno J, Easlon E, et al. Tissue-specific regulation of SIRT1 by calorie restriction. *Genes Dev*. 2008;**22**:1753-1757

117. Patke A, Young MW, Axelrod S. Molecular mechanisms and physiological importance of circadian rhythms. *Nat Rev Mol Cell Biol*. 2020;**21**:67-84

118. Marcheva B, Ramsey KM, Buhr ED, et al. Disruption of the clock components CLOCK and BMAL1 leads to hypoinsulinaemia and diabetes. *Nature*. 2010;**466**:627-631

119. Takahashi JS. Transcriptional architecture of the mammalian circadian clock. *Nat Rev Genet*. 2017;**18**:164-179

120. Asher G, Gatfield D, Stratmann M, et al. SIRT1 Regulates circadian clock gene expression through PER2 deacetylation. *Cell*. 2008;**134**:317-328

121. Nakahata Y, Kaluzova M, Grimaldi B, et al. The NAD^+-dependent deacetylase SIRT1 modulates CLOCK-mediated chromatin remodeling and circadian control. *Cell*. 2008;**134**:329-340

122. Challet E. Circadian clocks, food intake, and metabolism. *Prog Mol Biol Transl Sci*. 2013;**119**:105-135

123. Wang RH, Sengupta K, Li C, et al. Impaired DNA damage response, genome instability, and tumorigenesis in SIRT1 mutant mice. *Cancer Cell*. 2008;**14**:312-323

124. Oberdoerffer P, Michan S, McVay M, et al. SIRT1 redistribution on chromatin Promotes Genomic Stability but Alters Gene Expression during Aging. *Cell*. 2008;**135**:907-918

125. Wang RH, Zheng Y, Kim HS, et al. Interplay among BRCA1, SIRT1, and Survivin during BRCA1-associated tumorigenesis. *Mol Cell*. 2008;**32**:11-20

126. Simic P, Williams E, Bell E, Gong J, Bonkowski M, Guarente L. SIRT1 suppresses the epithelial-to-mesenchymal transition in cancer metastasis and organ fibrosis. *Cell Rep*. 2013;**3**:1175-1186

127. Luo J, Nikolaev AY, Imai S ichiro, et al. Negative control of p53 by Sir2α promotes cell survival under stress. *Cell*. 2001;**107**:137-148

128. Kim J-E, Chen J, Lou Z. DBC1 is a negative regulator of SIRT1. *Nature*. 2008;**451**:583-586

129. Zhao W, Kruse JP, Tang Y, Jung SY, Qin J, Gu W. Negative regulation of the deacetylase SIRT1 by DBC1. *Nature*. 2008;**451**:587-590

CHAPTER 2

[1]Loss of Sirtuin 1 Alters the Secretome of Breast Cancer Cells by Impairing Lysosomal Integrity

The NAD+-dependent deacetylase Sirtuin 1 (SIRT1) is downregulated in triple-negative breast cancer. To determine the mechanistic basis by which reduced SIRT1 expression influences processes related to certain aggressive cancers, we examined the consequences of depleting breast cancer cells of SIRT1. We discovered that reducing SIRT1 levels decreased the expression of one particular subunit of the vacuolar-type H+ ATPase (V-ATPase), which is responsible for proper lysosomal acidification and protein degradation. This impairment in lysosomal function caused a reduction in the number of multi-vesicular bodies (MVBs) targeted for lysosomal degradation and resulted in larger MVBs prior to their fusing with the plasma membrane to release their contents. Collectively, these findings help explain how reduced SIRT1 expression, by disrupting lysosomal function and generating a secretome comprising exosomes with unique cargo and soluble hydrolases that degrade the extracellular matrix, can promote processes that increase breast-cancer-cell survival and invasion.

[1] Currently in press as a cover article by Arash Latifkar, Lu Ling, Amrit Hingorani, Eric Johansen, Amdiel Clement, Xiaoyu Zhang, John Hartman, Claudia Fischbach, Hening Lin, Richard A. Cerione, and Marc A. Antonyak in *Developmental Cell*.

Introduction

Sirtuins are NAD^+-dependent deacetylases that play important roles in a number of physiological processes and diseases[1].This family of enzymes consists of 7 members, many of which differ in their location and function[2]. One of the most extensively studied members of the family is Sirtuin 1 (SIRT1), largely because its ectopic expression in yeast and mammals results in lifespan extension[3,4]. However, SIRT1 has been suggested to play multiple and, in some cases, contradictory roles in cancer[1]. Some studies[5,6] suggest that SIRT1 potentiates cancer phenotypes, while others indicate that SIRT1 functions as a tumor suppressor, such as in highly aggressive breast cancers, where decreased SIRT1 expression is correlated with tumor expansion and metastatic spread[7–9]. Given these findings, we were interested in probing how reduced SIRT1 expression enhances cellular phenotypes that underlie breast cancer progression. As described below, this led us to uncover a connection between SIRT1 and lysosomal function. Deregulation of this process results in the generation of a secretome with unique components, including exosomes and resident lysosomal hydrolases, that promote cell survival and invasive activity.

Exosomes are a type of non-classical secretory vesicle referred to as extracellular vesicles (EVs)[10]. They are attracting a good deal of attention because they contain various proteins, RNA transcripts, and microRNAs and impact a wide range of diseases, including cancer. Exosomes can be distinguished from the other major type of EV and microvesicles (MVs) based on their size and biogenesis. MVs range from 0.2 to 2.0 μm in diameter and directly bud off from the plasma membrane, whereas, exosomes are ~30–150 nm in diameter and are contained within multi-vesicular bodies (MVBs). The fusion of MVBs with the plasma membrane results in the release of their exosome content into the extracellular space.

Both types of EVs generated by cancer cells can engage and transfer cargo to neighboring cancer cells, stimulating their growth and survival. However, EVs from cancer cells can also affect normal cells, conferring upon them several characteristics of cancer cells, including the ability to exhibit anchorage-independent growth[11,12]. EVs derived from highly aggressive cancer cells also promote chemotherapy resistance[13,14], tumor angiogenesis[15], and metabolic reprogramming[16]. Exosomes, in particular, have been implicated in the formation of the pre-metastatic niche and enhancing organ-specific metastasis[17,18]. It has been suggested that lysosomal function can impact exosome biogenesis by altering the fate of MVBs[19,20]. However, how this happens is unclear. Here, we describe a mechanism by which reductions in SIRT1 expression in breast cancer cells alter lysosomal activity, resulting in increased numbers of exosomes shed from the cells and significant changes in the composition of their cargo. Specifically, we show that SIRT1-knockdown or pharmacological inhibition of this enzyme destabilizes the mRNA encoding the A subunit of the lysosomal vacuolar-type H+ ATPase (V-ATPase) proton pump (ATP6V1A), causing a reduction in its expression. This decrease in ATP6V1A levels impairs lysosomal degradative activity and causes the enlargement of MVBs, which then fuse with the plasma membrane and release exosomes that contain distinct cargo and strongly promote cell survival and migration. We further demonstrate that upon reduction of SIRT1 expression, there is a marked increase in the secretion of soluble lysosomal luminal proteins, i.e., cathepsins, which degrade the extracellular matrix, allowing tumor cells to invade surrounding tissues[21,22]. Taken together, these findings show how SIRT1 plays an important role in a fundamental aspect of cell biology by ensuring proper lysosomal function and, in doing so, influences the secretome of cells. Moreover, they provide an explanation for how reducing SIRT1 expression contributes to the aggressiveness of breast cancer cells.

Results

Decreasing SIRT1 Expression Levels Promotes Exosome Release

SIRT1 has been suggested to be a tumor suppressor in breast cancer, as its expression is downregulated in aggressive forms of the disease[7,8,23]. When we used Cancer RNA-Nexus[24] (GSE58135) to examine triple-negative breast cancers (TNBCs), compared to normal tissues found adjacent to the TNBC tumors (NTNBCs), more than 80% (34/42) of the tumor samples showed a marked reduction in SIRT1 transcript levels (**Figure 2.1A**). The protein expression levels of SIRT1 also tended to be lower in TNBC cell lines than in non-TNBC cell types (**Figure 2.1B**). Similar reductions in the transcript levels of the highly related SIRT6 and SIRT7 proteins were not observed (**Figures 2.1C and 2.1D**).

We obtained a clue regarding how reduced SIRT1 expression affects the behavior of breast cancer cells, when examining the intra-cellular features of SIRT1-knockdown MDA-MB-231 cells, versus control MDA-MB-231 cells (**Figure 2.1E**). Specifically, we found differences in the MVBs between the two cell types when immunofluorescence microscopy was performed using an antibody against the MVB marker protein CD63. While a comparable number of MVBs were detected in each sample, many MVBs in cells with reduced SIRT1 expression were noticeably larger (**Figures 2.1F and 2.1G**).

We further showed that short hairpin RNA (shRNA)-mediated knockdown of SIRT1 in normal human astrocytes and primary human dermal fibroblasts (**Figure 2.1H**) caused similar increases in MVB size (**Figures 2.1I and 2.1J**). We also deleted SIRT1 from MDA-MB-231 cells using CRISPR-Cas9. Clones that lost a single copy ($SIRT1^{+/-}$) or both copies ($SIRT1^{-/-}$) of the SIRT1 gene were shown to have enlarged MVBs, compared to wild-type ($SIRT1^{+/+}$) cells (**Figures 2.1K-2.1M**).

Figure 2.1 Downregulation of SIRT1 in triple-negative breast cancer results in enlarged MVBs. (A) SIRT1 transcript levels were determined in triple-negative breast cancer (TNBC) tumors and normal tissues adjacent to the TNBC tumors (NTNBC) using RNA sequencing (RNA-seq) Nexus (GEO accession: GSE58135). (B) Western blot analysis of SIRT1 and lactate dehydrogenase A (LDHA) levels in Triple-Negative Breast Cancer (TNBC) and non-TNBC cell lines. Lactate dehydrogenase A (LDHA) was used as the loading control. The line in the blots represents a small section of the blots that was deleted. The transcript levels of (C) SIRT6 and (D) SIRT7 were determined in TNBC tumors, and normal tissues adjacent to the TNBC tumors (NTNBC) using RNA-Seq Nexus (GEO accession: GSE58135). (E) Western blot analysis of SIRT1 and β-actin levels in whole-cell lysates (WCL) of sham-shRNA-expressing control (CTRL) and SIRT1-knockdown (KD) MDA-MB-231 cells. (F) Fluorescence microscopy images of the cells in (E) immunostained for CD63 (green) and stained with DAPI (blue). The periphery of each cell is outlined (dashed lines), and insets are higher magnifications of boxed areas. Scale bar, 4 μm. (G) Quantification of MVB diameter for each condition in (E). (H) Western blot analysis of SIRT1 levels in sham shRNA expressing control (CTRL), and SIRT1 knock down (KD), normal human astrocytes (top) and human dermal fibroblasts (bottom). (I) Fluorescence microscopy images of the cells in (H) immunostained for CD63 (green), and stained with DAPI (blue). Insets are higher magnifications of boxed areas. Scale bar, 6.25 μm. (J) Quantification of MVB diameter for each condition in (I). (K) Western blot analysis of SIRT1 expression levels in wildtype MDA-MB-231 cells (SIRT1 +/+), cells lacking one copy of the gene encoding SIRT1 (SIRT1 +/-), or in cells lacking both copies of the gene encoding SIRT1 (SIRT1 -/-). (L) Fluorescence microscopy images of the cells in (K), immunostained for CD63 (green), and stained with DAPI (blue). Insets are higher magnifications of boxed areas. Scale bar, 4 μm. (M) Quantification of MVB diameter for each condition in (L).

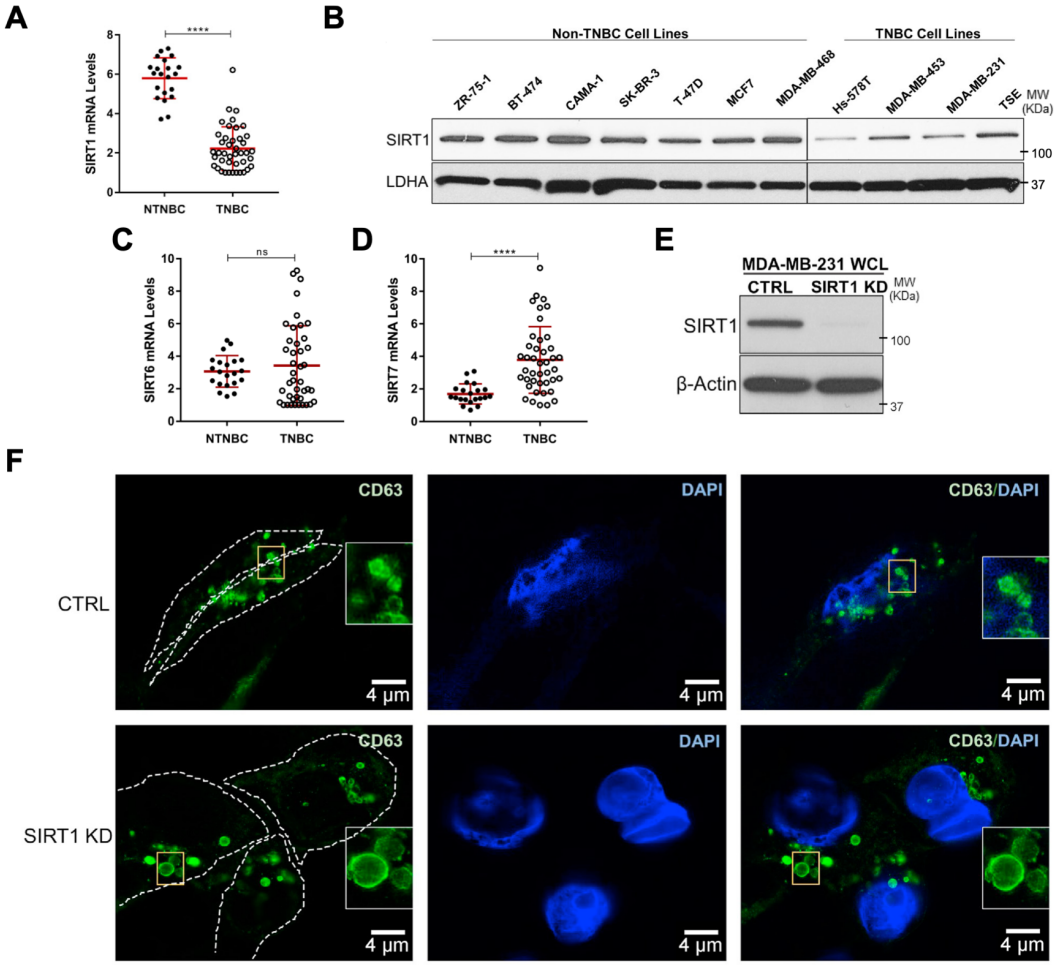
A
SIRT1 mRNA Levels
****
NTNBC
TNBC
B
Non-TNBC Cell Lines
TNBC Cell Lines
ZR-75-1
BT-474
CAMA-1
SK-BR-3
T-47D
MCF7
MDA-MB-468
Hs-578T
MDA-MB-453
MDA-MB-231
TSE
MW (KDa)
SIRT1
LDHA
100
37
C
SIRT6 mRNA Levels
ns
NTNBC
TNBC
D
SIRT7 mRNA Levels
****
NTNBC
TNBC
E
MDA-MB-231 WCL
CTRL
SIRT1 KD
MW (KDa)
SIRT1
β-Actin
100
37
F
CTRL
SIRT1 KD
CD63
DAPI
CD63/DAPI
4 μm

Figure 2.1 (Continued)

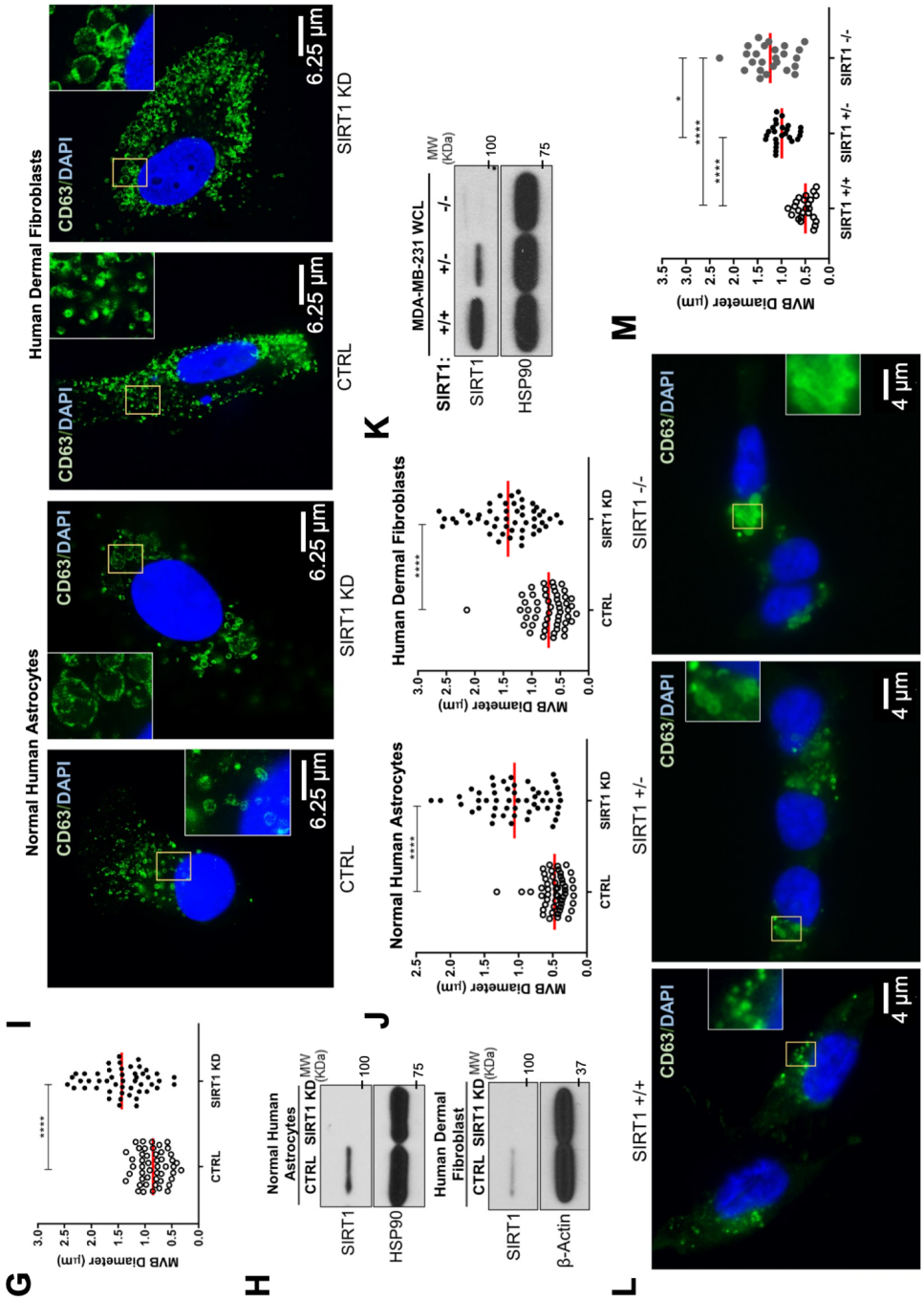

These observations raised the question of whether the changes in MVB size observed in SIRT1-knockdown cells reflected differences in their ability to generate exosomes. Therefore, we examined whether SIRT1, as well as the related SIRT6 or SIRT7 proteins, could impact exosome formation in MDA-MB-231 cells. shRNAs that specifically target each of these enzymes, or a control sham shRNA, were introduced into MDA-MB-231 cells, which are capable of generating EVs[11–13]. The expression levels of SIRT1, SIRT6, and SIRT7 were each knocked down by at least 85%, compared to control cells (**Figure 2.2A**). The amount of EVs in the conditioned media from an equivalent number of control cells, or cells depleted of SIRT1, SIRT6, or SIRT7, was determined using nanoparticle tracking analysis (NTA). Knocking down SIRT6 and SIRT7 caused only modest changes in the amount of EVs produced by the cells, whereas knockdown of SIRT1 resulted in a significant increase in EVs, with a greater than 3-fold increase in the number of exosome-sized vesicles (i.e., 40–150 nm vesicles) (**Figures 2.2B and 2.2C**). Depleting SIRT1 in U87 glioma cells and human kidney (HK)-2 cells led to similar increases in exosome production (**Figures 2.2D and 2.2E**).

The exosomes and MVs released into the media by control or SIRT1-knockdown MDA-MB-231 cells were then isolated using a combination of filtration and ultracentrifugation steps (**Figure 2.2F**). The isolation of each type of EV, as well as the media depleted of EVs (i.e., the vesicle-free medium; VFM), was verified by immunoblotting for specific EV cargo and selected soluble proteins (**Figure 2.2G**). HSP90, which is expressed in both classes of EVs, was detected in each fraction (bottom panel)[25] while the exosome marker CD63 was found only in the exosome fractions (middle panel). IKBα was detected only in the cell lysates (top panel), demonstrating that the EV and media fractions do not contain cytosolic contaminants. Electron microscopy carried out on the exosomes isolated from control and SIRT1-

Figure 2.2 Downregulation of SIRT1 in triple-negative breast cancer results in increased exosome secretion. (A) Western blot analysis of nuclear sirtuins and heat shock protein 90 (HSP90) levels in WCLs of sham-shRNA-expressing CTRL, SIRT1-KD, SIRT6-KD, and SIRT7-KD MDA-MB-231 cells. The expression level of each sirtuin was quantified relative to HSP90 and included in the blot. (B) Nanoparticle tracking analysis (NTA) was performed on the conditioned media collected from an equivalent number of serum-starved sham-shRNA-expressing CTRL, SIRT1-KD, SIRT6-KD, and SIRT7-KD cells. (C) Quantification of exosomes generated for each of the conditions in (B). (D) Western blot analysis of SIRT1 levels in sham shRNA expressing control (CTRL), and SIRT1 KD, HK-2 (left) and U87 (right) cells. (E) Quantification of exosomes generated for each condition in (D). (F) Approach used to prepare microvesicles, exosomes, and vesicle free medium (VFM) from conditioned media. (G) Western blot analysis of IκBα, CD63, and HSP90 levels in WCLs, microvesicles (MVs), exosomes (EXOs), and vesicle-free medium (VFM) prepared from sham-shRNA-expressing CTRL, and SIRT1 KD, MDA-MB-231 cells. (H) Electron microscopy images of exosomes derived from control (EXO-CTRL), and SIRT1 KD (EXO-SIRT1 KD), cells. Scale bar, 100 nm.

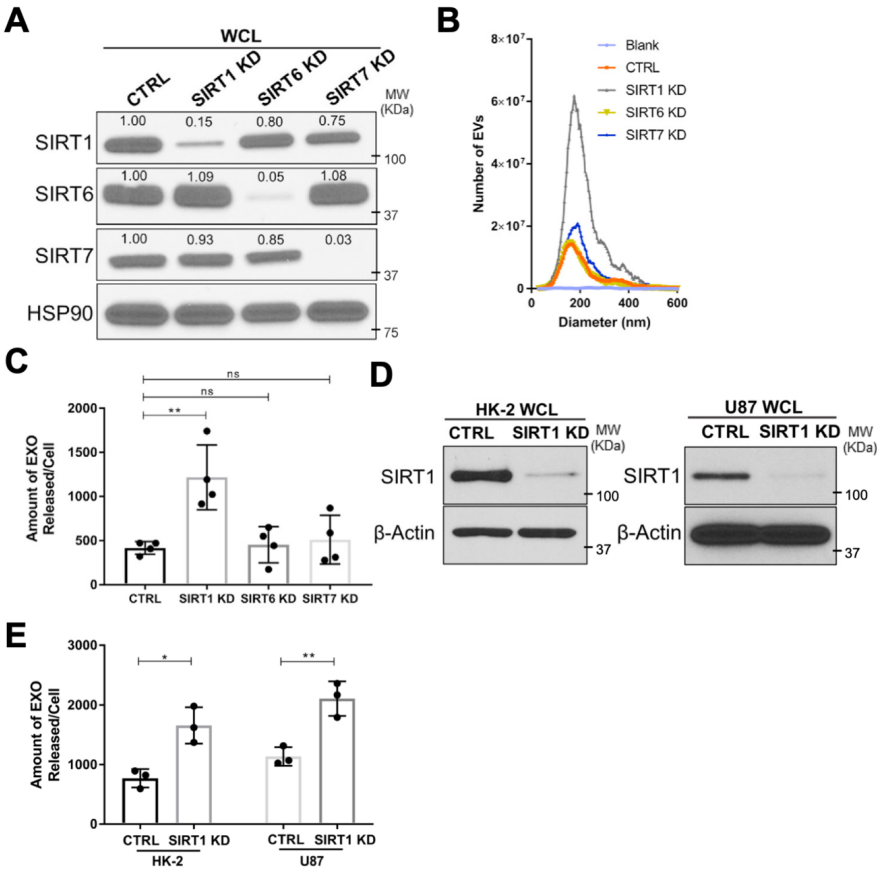
A
WCL
CTRL
SIRT1 KD
SIRT6 KD
SIRT7 KD
MW (KDa)
SIRT1
1.00 0.15 0.80 0.75
100
SIRT6
1.00 1.09 0.05 1.08
37
SIRT7
1.00 0.93 0.85 0.03
37
HSP90
75
B
Blank
CTRL
SIRT1 KD
SIRT6 KD
SIRT7 KD
Number of EVs
Diameter (nm)
C
Amount of EXO Released/Cell
ns
ns
**
CTRL
SIRT1 KD
SIRT6 KD
SIRT7 KD
D
HK-2 WCL
CTRL SIRT1 KD MW (KDa)
SIRT1
β-Actin
100
37
U87 WCL
CTRL SIRT1 KD MW (KDa)
SIRT1
β-Actin
100
37
E
Amount of EXO Released/Cell
*
**
CTRL SIRT1 KD
HK-2
CTRL SIRT1 KD
U87

Figure 2.2 (Continued)

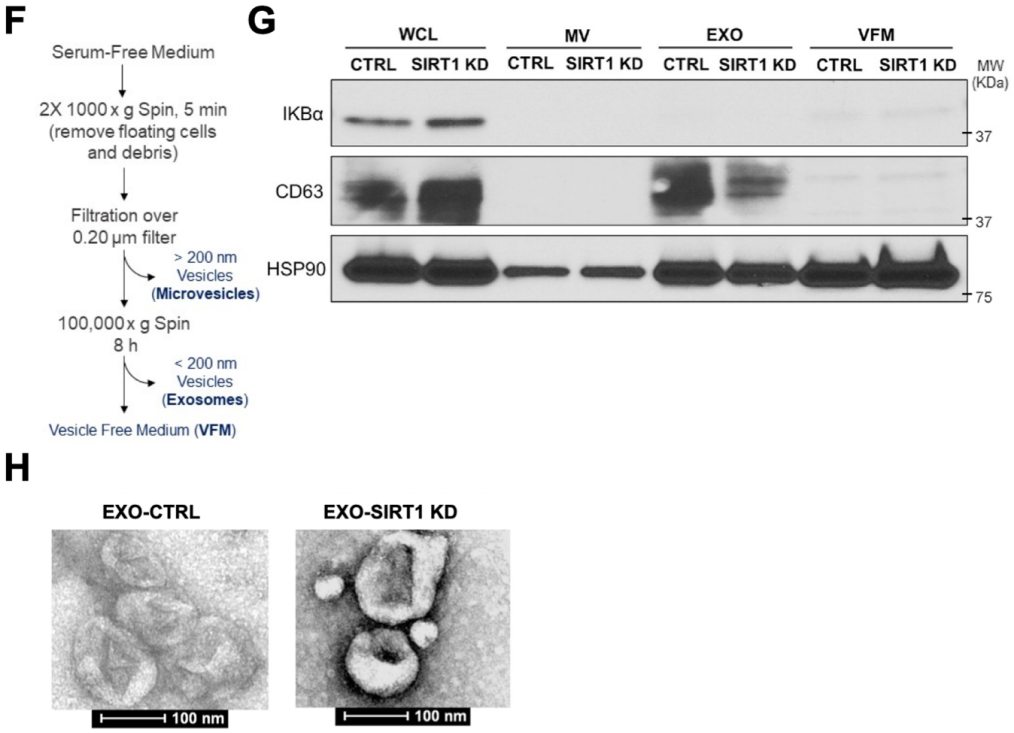

depleted MDA-MB-231 cells (**Figure 2.2H**) showed that these vesicles were similar in size and morphology.

Exosomes from SIRT1-Knockdown Cells Contain Distinct Protein Cargo

Exosomes generated by cells depleted of SIRT1 contain a protein composition distinct from exosomes produced by control cells, as evident when performing SDS-PAGE and Coomassie blue staining of their protein cargo. Whereas the whole-cell lysates (WCLs) showed no obvious differences in protein expression between control MDA-MB-231 cells and cells lacking SIRT1 (**Figure 2.3A**, lanes labeled WCL), the amounts of some proteins were noticeably reduced (blue arrows), while others were significantly increased (red arrow), in exosomes derived from SIRT1-knockdown cells. This was further indicated when stable isotope labeling with amino acids in cell culture (SILAC) was performed on exosomes from control and SIRT1-knockdown MDA-MB-231 cells (**Figure 2.3B**). **Figure 2.3C** lists proteins whose levels were either the most enriched (left table) or reduced (right table) in exosomes derived from SIRT1-knockdown cells, compared to exosomes from control cells. Immunoblotting experiments confirmed the SILAC results; two examples are presented in **Figure 2.3D**, where the increased levels of 14-3-3 zeta/delta and the decreased levels of CD81, as indicated by SILAC (**Figure 2.3C**, proteins in red), were also observed in immunoblots. DAVID gene ontology (GO) analysis performed on the proteins enriched in exosomes from SIRT1-depleted cells showed they are involved in diverse cellular processes and come from different cellular localizations (**Figure 2.3E**).

MVBs and their contents either are directed to the lysosome and degraded or reach the cell surface where they fuse with the plasma membrane. A critical step in MVB formation, where protein sorting occurs, involves the maturation of intraluminal vesicles[26]. Endosomal sorting complexes required for transport (ESCRTs) are

Figure 2.3 Exosomes from SIRT1-KD Cells Contain Distinct Protein Cargo
(A) Coomassie Blue-stained SDS-PAGE gel of whole cell lysates (WCL) and exosomes (EXO) from sham shRNA expressing control (CTRL), and SIRT1 knock down (KD), cells. The blue arrows indicate proteins that are enriched in exosomes from control cells, while the red arrow indicates a protein that is enriched in exosomes from SIRT1 KD cells. (B) The approach used to quantify protein levels in exosomes from sham shRNA expressing control (CTRL), and SIRT1 KD, cells. (C) Tables listing some of the most enriched (left), or depleted (right), proteins in exosomes from SIRT1 KD cells (relative to exosomes from control cells). (D) Western blot analysis of two differentially expressed proteins identified in exosomes (EXO) from SIRT1 KD cells (highlighted in red in Figure 3C). HSP90 was used as the loading controls. (E) DAVID GO-Cellular Component analysis of proteins that are enriched in exosomes derived from SIRT1 KD cells, compared to control cells. (F) Western blot analysis of ubiquitinated protein and β-actin levels in WCL of sham-shRNA-expressing CTRL (CTRL) and SIRT1-KD cells. The amount of ubiquitinated proteins detected in each lysate was quantified relative to β-actin and included in the blot. (G) Western blot analysis of ubiquitinated protein and HSP90 levels in EXOs from sham-shRNA-expressing CTRL, SIRT1-KD, SIRT6-KD, and SIRT7-KD cells. The amount of ubiquitinated proteins detected in each lysate was quantified relative to HSP90 and included in the blot. (H) Quantification of ubiquitinated protein levels for each condition in (G). (I) Western blot analysis of ubiquitinated protein levels in EXOs from cells treated with DMSO or EX-527 (50 μM) for 16 h. (J) Western blot analysis of ubiquitinated protein and Flotillin-2 levels in EXOs from wild-type MDA-MB-231 cells (SIRT1+/+) or cells in which both copies of the SIRT1 gene were genetically deleted (SIRT1−/−). The amount of ubiquitinated protein detected in each lysate was quantified relative to Flotiliin-2 and included in the blot. (K) Western blot analysis of ubiquitinated Histone 2A (UB-H2A), ubiquitinated histone H2B (UB-H2B), and Survivin levels in EXOs from sham-shRNA-expressing CTRL and SIRT1-KD cells. (L) Left Panel: Western blot analysis of SIRT1 levels in WCL of MDA-MB-453 cells ectopically expressing either the vector alone (Vector) or SIRT1 (SIRT1 overexpression; OE). Right Panel: Western blot analysis of ubiquitinated protein levels in exosomes isolated from these cells (MDA-MB-453 EXO).

A

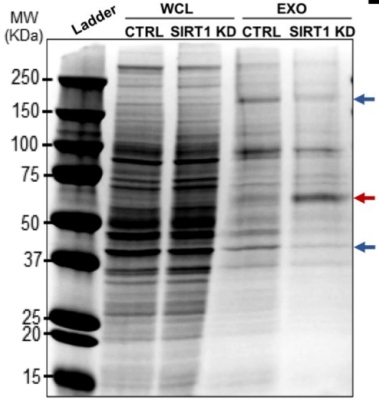

B

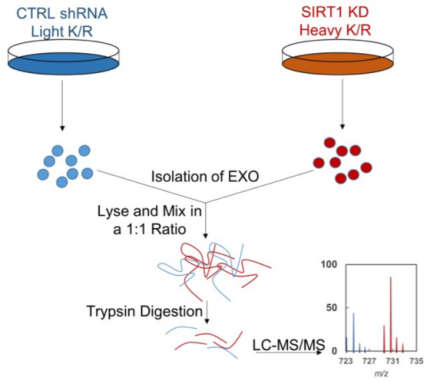

C

Proteins Enriched in EXO from SIRT1 KD Cells

Protein Name	H/L Ratio
14-3-3 protein zeta/delta	**184.797**
highly similar to Homo sapiens thyroid autoantigen 70kDa	24.558
SFPQ protein (Fragment)	16.114
highly similar to Homo sapiens EIF2S3	10.811
Annexin	9.645
Elongation factor 1-delta (Fragment)	9.292
highly similar to 14-3-3 protein gamma	8.755
Perilipin-3 (Fragment)	8.505
Galectin-1	8.485
Ribonuclease/angiogenin inhibitor 1, isoform CRA_a	8.448
Histone H2B	2.001
Histone H2A type 1-H	1.936

Proteins Depleted in EXO from SIRT1 KD Cells

Protein Name	H/L Ratio
Fibronectin 1, isoform CRA	0.038
Plectin	0.020
highly similar to ADP-ribosylation factor 1	0.020
Desmoglein-1	0.020
GEMIN5 protein	0.019
DNA helicase (Fragment)	0.019
GYG1 protein (Fragment)	0.018
Heparan sulfate proteoglycan 2 (Perlecan)	0.018
RNA-binding protein 14	0.018
Eukaryotic translation initiation factor 3 subunit B	0.017
Tetraspanin, CD81	**0.275**

D

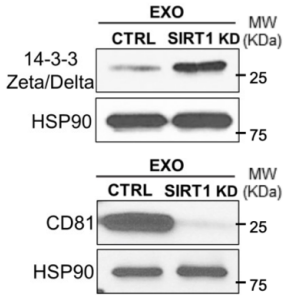

E

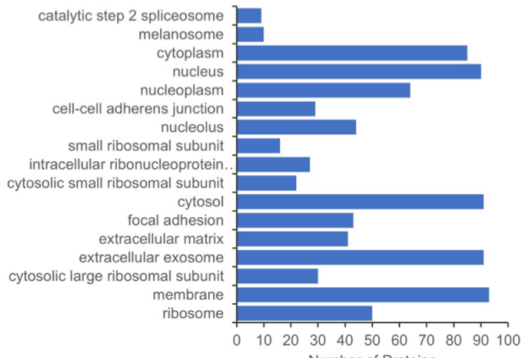

Figure 2.3 (Continued)

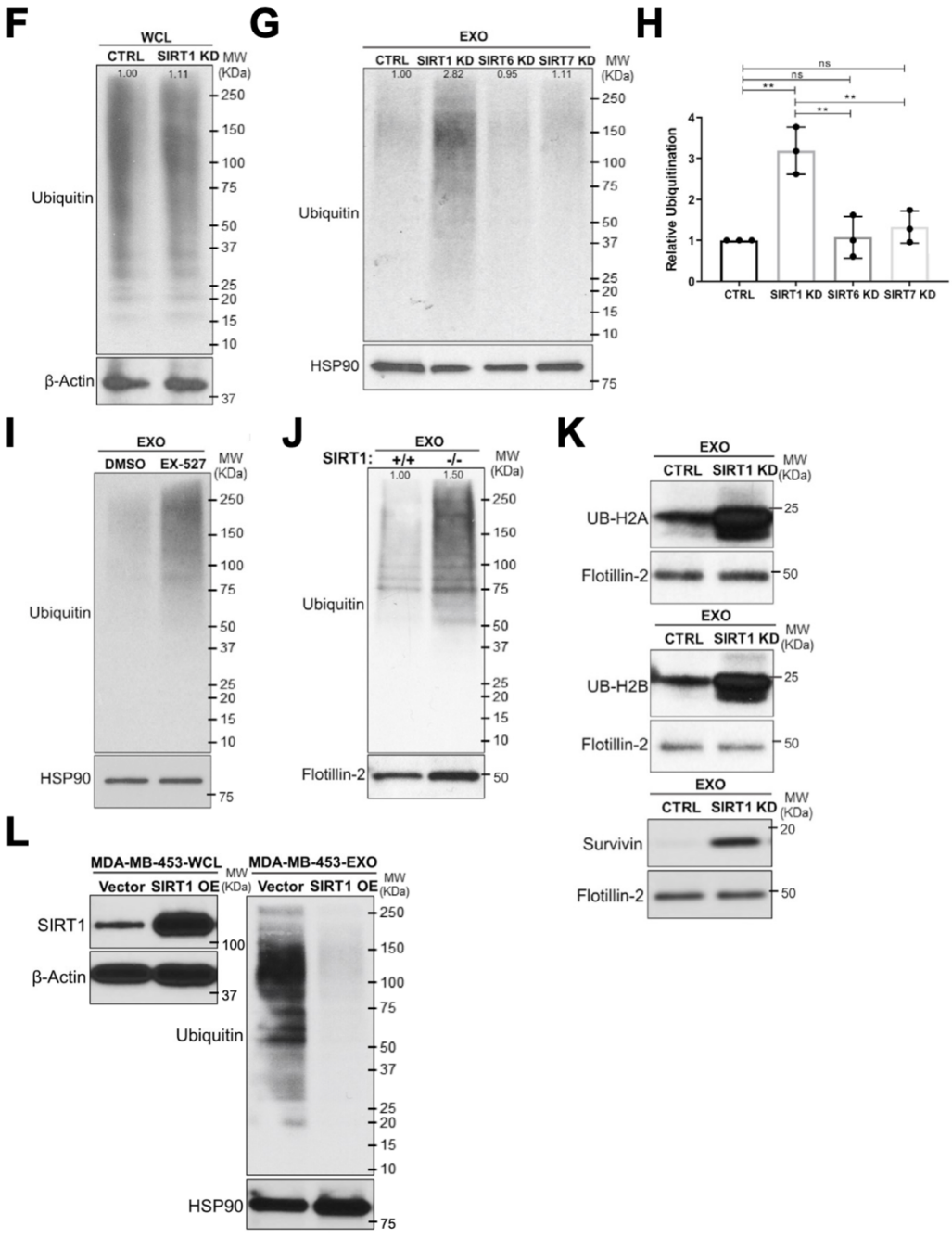

responsible for recognizing and importing ubiquitinated proteins into a subset of intraluminal vesicles that are eventually degraded when MVBs fuse with lysosomes. Thus, we examined whether knocking down SIRT1 in MDA-MB-231 cells altered the amount of ubiquitinated cargo in their exosomes. While no significant differences in the levels of ubiquitinated proteins were detected in WCLs upon knockdown of SIRT1 (**Figure 2.3F**), there was a clear increase in the amounts of ubiquitinated cargo in exosomes isolated from cells depleted of SIRT1 (**Figures 2.3G** and **2.3H**). Treatment of MDA-MB-231 cells with the SIRT1 inhibitor, EX-527, or deleting SIRT1 from cells by CRISPR-Cas9 also resulted in the generation of exosomes enriched with ubiquitinated proteins (**Figures 2.3I** and **2.3J**), while knocking down SIRT6 or SIRT7 expression did not have the same effect (**Figures 2.3G** and **2.3H**). Histone 2A (H2A) and 2B (H2B), which are known to be ubiquitinated, were identified by SILAC to be enriched in exosomes derived from MDA-MB-231 cells depleted of SIRT1 (**Figure 2.3C**) and shown to exit the cells as ubiquitinated species in these vesicles (**Figure 2.3K**, top and middle panels). Exosomes isolated from SIRT1-knockdown cells were also highly enriched in Survivin (**Figure 2.3K**, bottom panel), which is specifically expressed in aggressive cancer cells and degraded in a ubiquitin-dependent manner[27].

Since reducing SIRT1 levels in cells increases the amount of ubiquitinated cargo present in their exosomes, we next examined whether the ectopic expression of SIRT1 in cells could reverse this effect. The triple-negative MDA-MB-453 breast cancer cell line was used for this experiment because it expresses low levels of SIRT1 and generates exosomes containing considerable amounts of ubiquitinated cargo (**Figure 2.3L**). When SIRT1 was ectopically expressed in MDA-MB-453 cells, the levels of ubiquitinated proteins present in exosomes isolated from these cells were reduced (**Figure 2.3L**).

To further examine how decreased SIRT1 levels result in more MVB content (i.e., exosomes) being released into the extracellular environment, we used an approach that isolates intact lysosomes and MVBs from cells[28]. The endolysosomal fractions immunoprecipitated using a FLAG antibody from control and SIRT1-knockdown MDA-MB-231 cells expressing a FLAG-tagged form of the MVB-lysosomal resident protein TMEM192 (FLAG-TMEM192), were subjected to western blot analysis using antibodies against RAB27A and the MVB marker mannose-6-phosphate receptor (M6PR). Under conditions where equivalent amounts of M6PR-positive vesicles were immunoprecipitated (**Figure 2.4A**, bottom panel), a greater amount of RAB27A associated with MVBs immunoprecipitated from SIRT1-depleted cells (**Figure 2.4A**, top panel). Consistent with the role of RAB27A in promoting late endosomal trafficking to the plasma membrane[29], knocking down RAB27A in cells lacking SIRT1 led to the accumulation of large MVBs (**Figure 2.4B-4D**). These findings support the idea that RAB27A is recruited to MVBs in cells depleted of SIRT1 to help mediate their transport and fusion with the plasma membrane.

Next, we considered the possibility that reduced SIRT1 levels could interfere with the ability of MVBs to be degraded in lysosomes. If so, knocking down Rab7 (**Figure 2.4E**), which mediates MVB-lysosome fusion[30] and causes a significant enlargement in the size of MVBs (**Figures 2.4F** and **2.4G**), should have a similar effect on exosome production. Immunoblotting the exosomes generated by cells depleted of Rab7 showed that they were highly enriched in ubiquitinated cargo and Survivin (**Figure 2.4H**, left and right panels), similar to the SIRT1-expression knockdown. These findings suggest that reduced SIRT1 levels cause MVBs that normally would be degraded in lysosomes to instead become enlarged and fuse with the cell surface to release their contents.

Figure 2.4 SIRT1 KD Impacts Endolysosomal Trafficking
(A) Western blot analysis of RAB27A levels in endolysosomal fractions immunoprecipitated from sham-shRNA-expressing CTRL and SIRT1-KD cells ectopically expressing FLAG-tagged TMEM192. (B) Western blot analysis of RAB27A, SIRT1, and β-Actin levels in WCL from sham shRNA expressing control (CTRL), RAB27 KD, SIRT1 KD, and SIRT1/RAB27 KD MDA-MB-231 cells. (C) Fluorescence microscopy images of the cells in (B) immunostained for CD63 (green), and stained with DAPI (blue). Insets are higher magnifications of boxed areas. Scale bar, 4 μm. (D) Quantification of MVB diameter for each condition in (C). (E) Western blot analysis of RAB7, SIRT1, and β-actin levels in the WCL of sham-shRNA-expressing CTRL and RAB7-KD MDA-MB-231 cells. (F) Fluorescence microscopy images of the cells in (E), immunostained for CD63 (green) and stained with DAPI (blue). Insets are higher magnifications of boxed areas. Scale bar, 4 μm. (G) Quantification of MVB diameter for each condition in (F). (H) Western blot analysis of ubiquitinated protein (left) and Survivin (right) levels in EXO from CTRL and RAB7-KD cells. (I) Coomassie Blue-stained SDS-PAGE gel of vesicle free medium (VFM) proteins collected from sham shRNA expressing control (CTRL), and SIRT1 KD, cells. The red arrows indicate proteins that are enriched in the VFM from SIRT1 KD cells, while the blue arrow indicates a protein enriched in the VFM from control cells. (J) DAVID-GO-cellular-component analysis of proteins enriched in VFM collected from SIRT1-KD cells compared to control cells. (K) Western blot analysis of cathepsin B and HSP90 levels in MVs, EXOs, and VFM fractions from sham-shRNA-expressing CTRL and SIRT1-KD cells. The unprocessed and processed forms of cathepsin B are indicated. (L) Western blot analysis of Cathepsin B levels in vesicle free media (VFM) isolated from cells treated with DMSO, or EX-527 (50 μM), for 16 hours. The unprocessed and processed forms of Cathepsin B are indicated. (M) Levels of cathepsin B activity in the conditioned medium (CM) from CTRL and SIRT1-KD MDA-MB-231 cells treated without or with CA-074 (10 μM) for 30 min. (N) Western blot analysis of Cathepsin B levels in vesicle free media (VFM) isolated from sham shRNA expressing control (CTRL), SIRT1 KD, SIRT6 KD, and SIRT7 KD cells. The unprocessed and processed forms of Cathepsin B are indicated. (O) Western blot analysis of MMP7 and MMP9 levels in the WCL prepared from sham shRNA expressing control (CTRL), and SIRT1 KD, cells, as well as in the vesicle free media (VFM) collected from these cells.

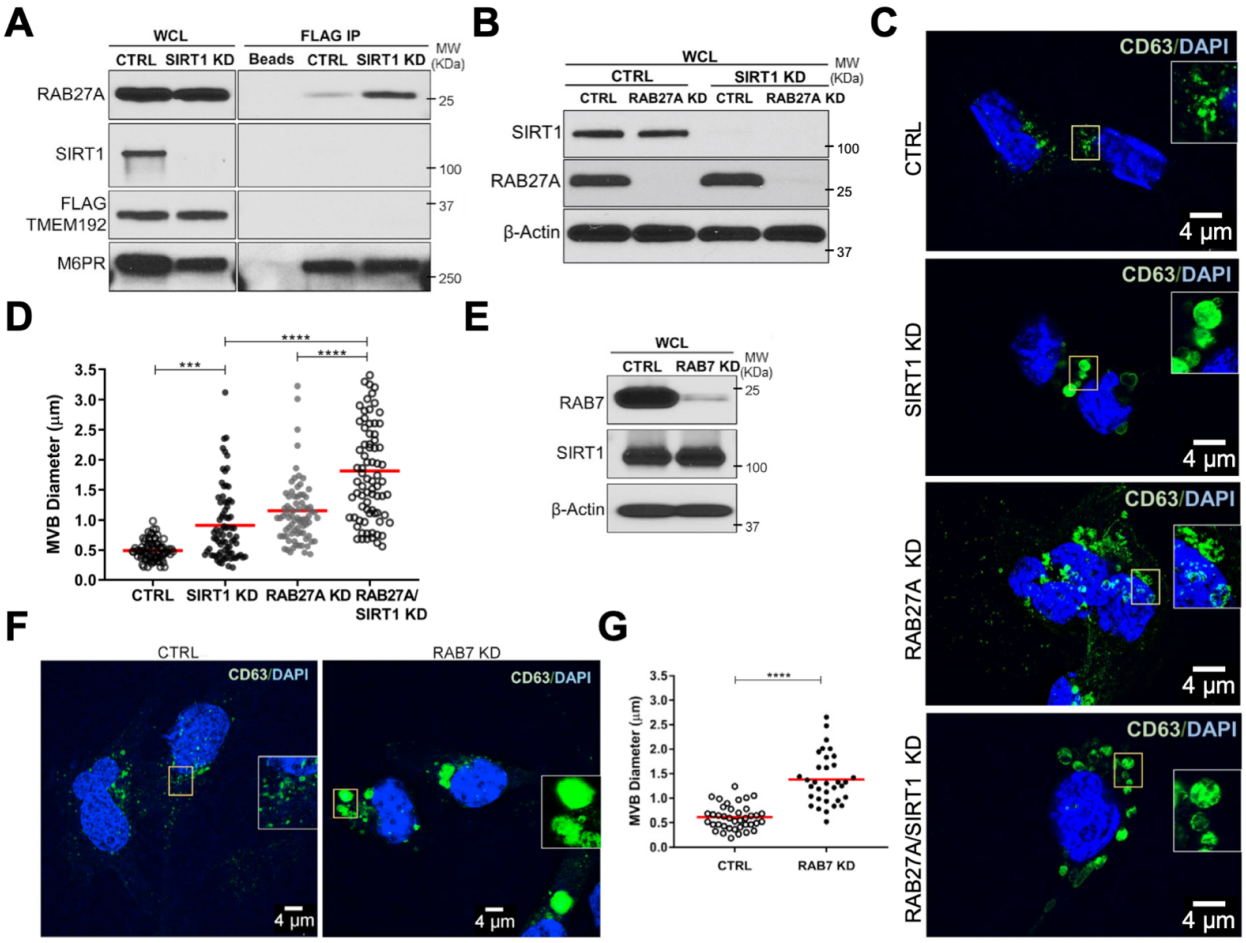
A
WCL
FLAG IP
CTRL SIRT1 KD
Beads CTRL SIRT1 KD
MW (KDa)
RAB27A
SIRT1
FLAG TMEM192
M6PR
25
100
37
250
B
WCL
CTRL
SIRT1 KD
CTRL RAB27A KD CTRL RAB27A KD
SIRT1
RAB27A
β-Actin
100
25
37
C
CD63/DAPI
CTRL
SIRT1 KD
RAB27A KD
RAB27A/SIRT1 KD
4 μm
D
MVB Diameter (μm)
***
****
****
CTRL SIRT1 KD RAB27A KD RAB27A/ SIRT1 KD
E
WCL
CTRL RAB7 KD
RAB7
SIRT1
β-Actin
F
CTRL
RAB7 KD
CD63/DAPI
4 μm
G
MVB Diameter (μm)
****
CTRL
RAB7 KD

Figure 2.4 (Continued)

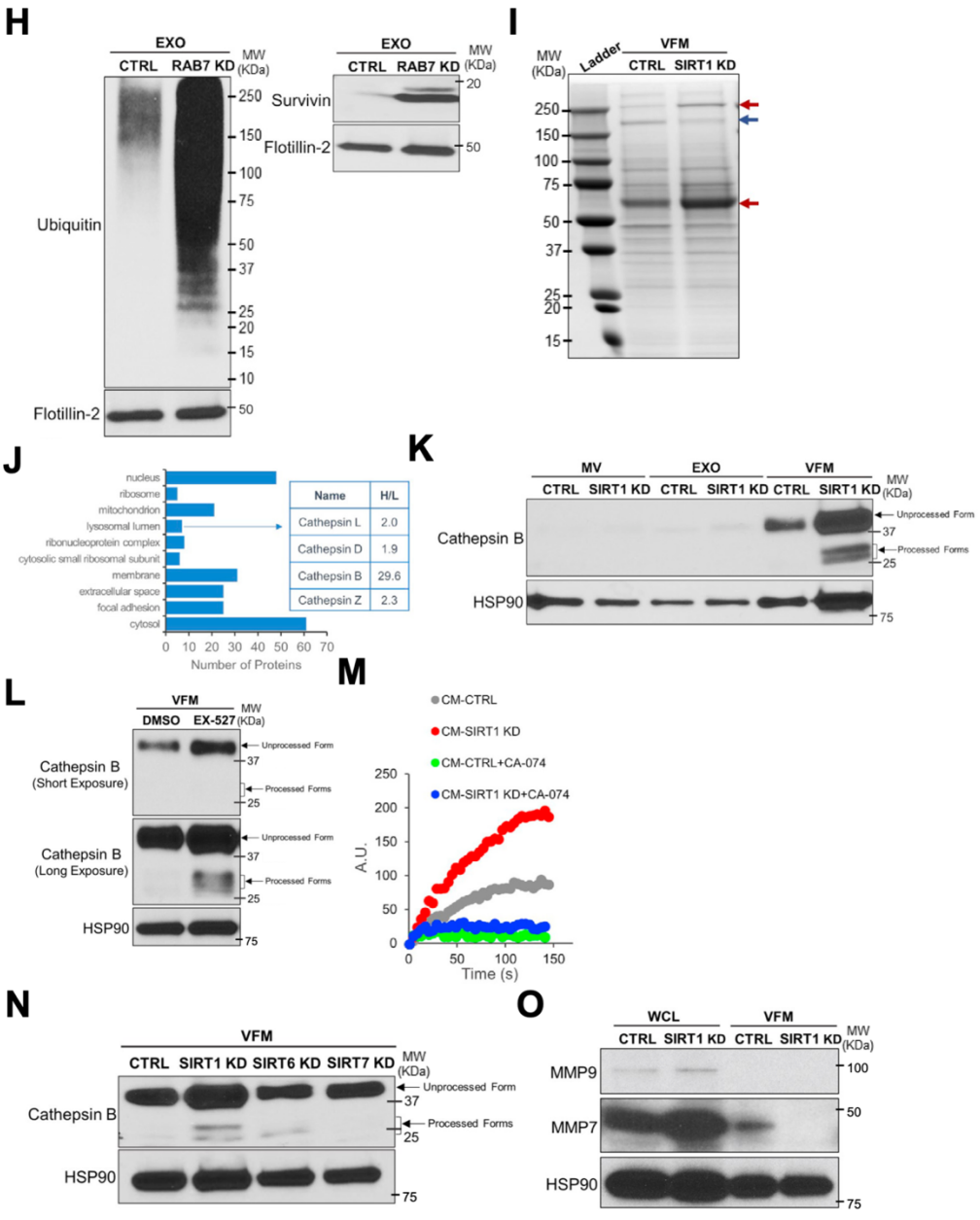

We then examined whether SIRT1-knockdown cells also secrete soluble proteins that reside in MVBs. The conditioned media depleted of exosomes and MVs (i.e., VFM) from control and SIRT1-knockdown MDA-MB-231 cells were resolved by SDS-PAGE and stained with Coomassie blue. The resulting gel (**Figure 2.4I**) showed that the VFM collected from SIRT1-depleted cells contained both increased (red arrows) and decreased (blue arrow) amounts of various proteins. SILAC analysis performed on these same preparations identified several lysosomal luminal proteins, namely members of the cathepsin hydrolase family, that were enriched in the VFM collected from cells depleted of SIRT1 (**Figure 2.4J**), with cathepsin B showing the greatest increase (heavy-light ratio (H-L~30)). This result was confirmed by immunoblotting, which showed that smaller processed (i.e., active), as well as larger unprocessed (i.e., less active), forms of this enzyme were detectable in the VFM isolated from SIRT1-knockdown cells (**Figure 2.4K**, lanes labeled VFM). A smaller amount of unprocessed cathepsin B was found in the VFM from control cells, while it was absent in MVs or exosomes isolated from either control or SIRT1-knockdown cells (**Figure 2.4K**). Increases in cathepsin B levels were also detected in the VFM collected from cells treated with the SIRT1 inhibitor EX-527 (**Figure 2.4L**), and conditioned media from SIRT1-depleted cells exhibited significantly higher cathepsin B activity, compared to conditioned media from control cells (**Figure 2.4M**). This increase in activity was completely blocked upon treatment of the medium derived from SIRT1-knockdown cells with CA-074, a cathepsin-B-specific inhibitor.

Experiments examining whether cathepsin B secretion was increased to the same extent in cells depleted of SIRT6 and SIRT7 showed that this was not the case

Figure 2.5 SIRT1 Depletion Resembles Lysosomal Impairment.
(A) Fluorescence microscopy images of sham-shRNA-expressing CTRL and SIRT1-KD cells immunostained for LAMP1 (red) and stained with DAPI (blue). Insets are higher magnifications of boxed areas. Scale bar, 4 μm. (B) Quantification of lysosome diameter for each condition in (A). (C) Fluorescence microscopy images of DMSO-, Chloroquine (50 μM)-, or Bafilomycin-A (200 nM)-treated cells (for 16 hours) immunostained for LAMP1 (red), and stained with DAPI (blue). Insets are higher magnifications of boxed areas. Scale bar, 4 μm. (D) Quantification of lysosome diameter for each condition in (C). (E) Fluorescence microscopy images of DMSO-, Chloroquine (50 μm)-, or Bafilomycin-A (200 nm)-treated cells (for 16 hours) immunostained for CD63 (green), and stained with DAPI (blue). Insets are higher magnifications of boxed areas. Scale bar, 4 μm. (F) Quantification of lysosome diameter for each condition in (E).

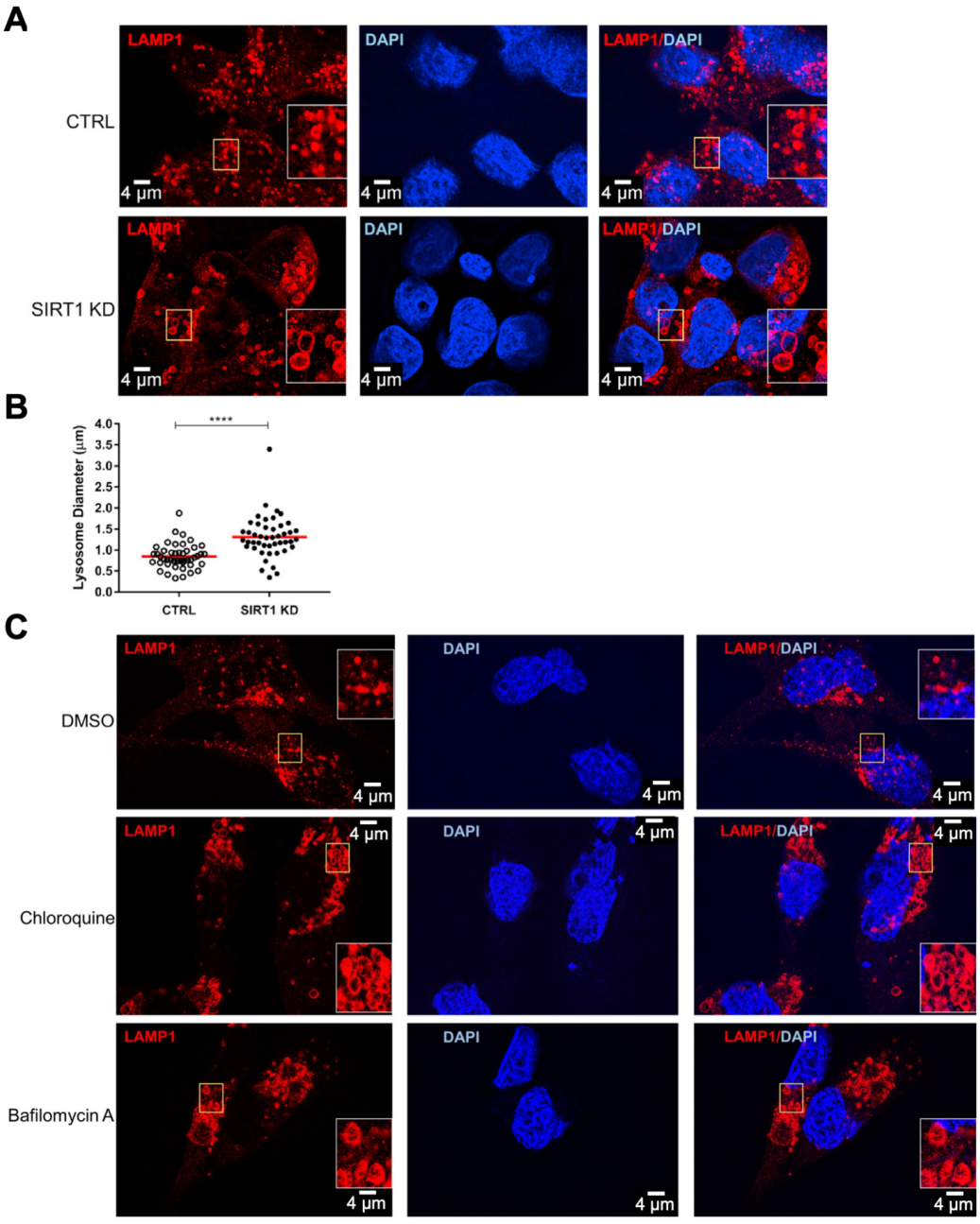
A
CTRL
SIRT1 KD
LAMP1
DAPI
LAMP1/DAPI
4 µm
B
Lysosome Diameter (µm)
4.0
3.5
3.0
2.5
2.0
1.5
1.0
0.5
0.0
****
CTRL
SIRT1 KD
C
DMSO
Chloroquine
Bafilomycin A
LAMP1
DAPI
LAMP1/DAPI
4 µm

Figure 2.5 (Continued)

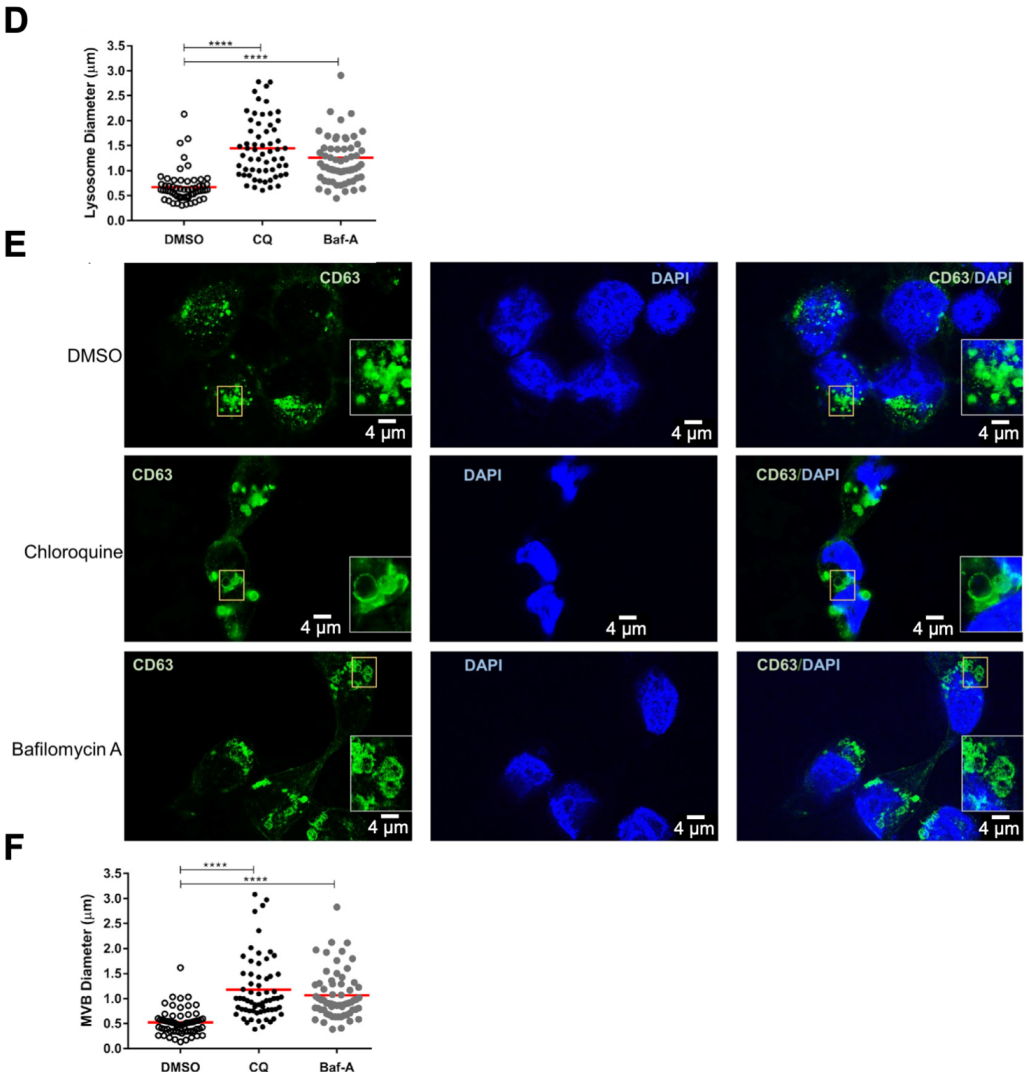

(**Figure 2.4N**). Similarly, non-lysosomal metalloproteases MMP7 and MMP9 were not enriched in the VFM collected from SIRT1-depleted cells (**Figure 2.4O**).

SIRT1 Depletion Causes Lysosomal Impairment

Given the effects of reduced SIRT1 expression levels on MVB maturation and the contents of the secretome, we then examined whether SIRT1 influences lysosomal function. Immunofluorescent microscopy performed on control MDA-MB-231 cells showed LAMP1-positive lysosomes located near the nucleus of each cell (**Figure 2.5A,** top panel). However, lysosomes in SIRT1-knockdown cells contained significantly larger LAMP1-positive structures (**Figure 2.5A**, bottom panel, and **Figure 2.5B**), suggesting lysosomal impairment[31,32]. Treatment of cells with either chloroquine or bafilomycin-A to inhibit lysosomal activity yielded similar effects (**Figures 2.5C** and **2.5D**). Treating MDA-MB-231 cells with either of these inhibitors also resulted in cells with enlarged CD63-positive MVBs (**Figures 2.5E** and **2.5F**) and gave rise to exosomes with increased amounts of ubiquitinated proteins (**Figure 2.6A**) and Survivin (**Figure 2.6B**). Moreover, treatment of MDA-MB-231 cells with bafilomycin-A led to not only an increased exosome release (**Figure 2.6C**) but also an increase in the levels of cathepsin B in the medium (i.e., the VFM) (**Figure 2.6D**). Additional evidence that lysosomes in cells with limiting amounts of SIRT1 are not functioning properly came from an experiment where cathepsin B maturation was examined. Cathepsins undergo a maturation process, along the endocytic pathway, that involves multiple glycosylation and cleavage events[33]. Thus, we immunoblotted WCLs from control MDA-MB-231 cells and MDA-MB-231 cells depleted of SIRT1 for cathepsin B. While cathepsin B was detected primarily as a mature, fully processed enzyme, in control cells, their SIRT1-knockdown counterparts had little detectable fully processed enzyme (**Figure 2.6E**). Instead, they predominantly expressed a

Figure 2.6 SIRT1 Depletion Resembles Lysosomal Impairment.
(A) Western blot analysis of ubiquitinated protein and Flotillin-2 levels in EXOs from cells treated with DMSO, Baf-A (200 nM), or CQ (50 μM), for 16 h. The amount of ubiquitinated protein detected in each lysate was quantified relative to Flotillin-2 and included in the blot. (B) Western blot analysis of Survivin levels in the exosomes (EXO) isolated from cells in each condition in (A). (C) Quantification of exosomes generated by cells treated with DMSO or Baf-A (200 nM) for 16 h. (D) Western blot analysis of Cathepsin B levels in vesicle free media (VFM) isolated from cells in each condition in (A). (E) Western blot analysis of Cathepsin B levels in sham shRNA expressing control (CTRL), and SIRT1 KD, cells. (F) Western blot analysis of Cathepsin B levels from cellular extracts of each condition in (A). (G) Fluorescence microscopy images of sham-shRNA-expressing CTRL and SIRT1-KD cells immunostained for cathepsin B (red) and LAMP1 (green). The cells were also stained with DAPI (blue). Scale bar, 8 μm. The images of the SIRT1-KD cells are a composite of two separate pictures. Insets are higher magnifications of boxed areas. (H) Fluorescence microscopy images of sham shRNA expressing control (CTRL), and SIRT1 KD, cells immunostained for Cathepsin B (red) and CD63 (green). The cells were also stained with DAPI (blue) to label nuclei. The insets are higher magnifications of boxed areas. Scale bar, 3.4 μm.

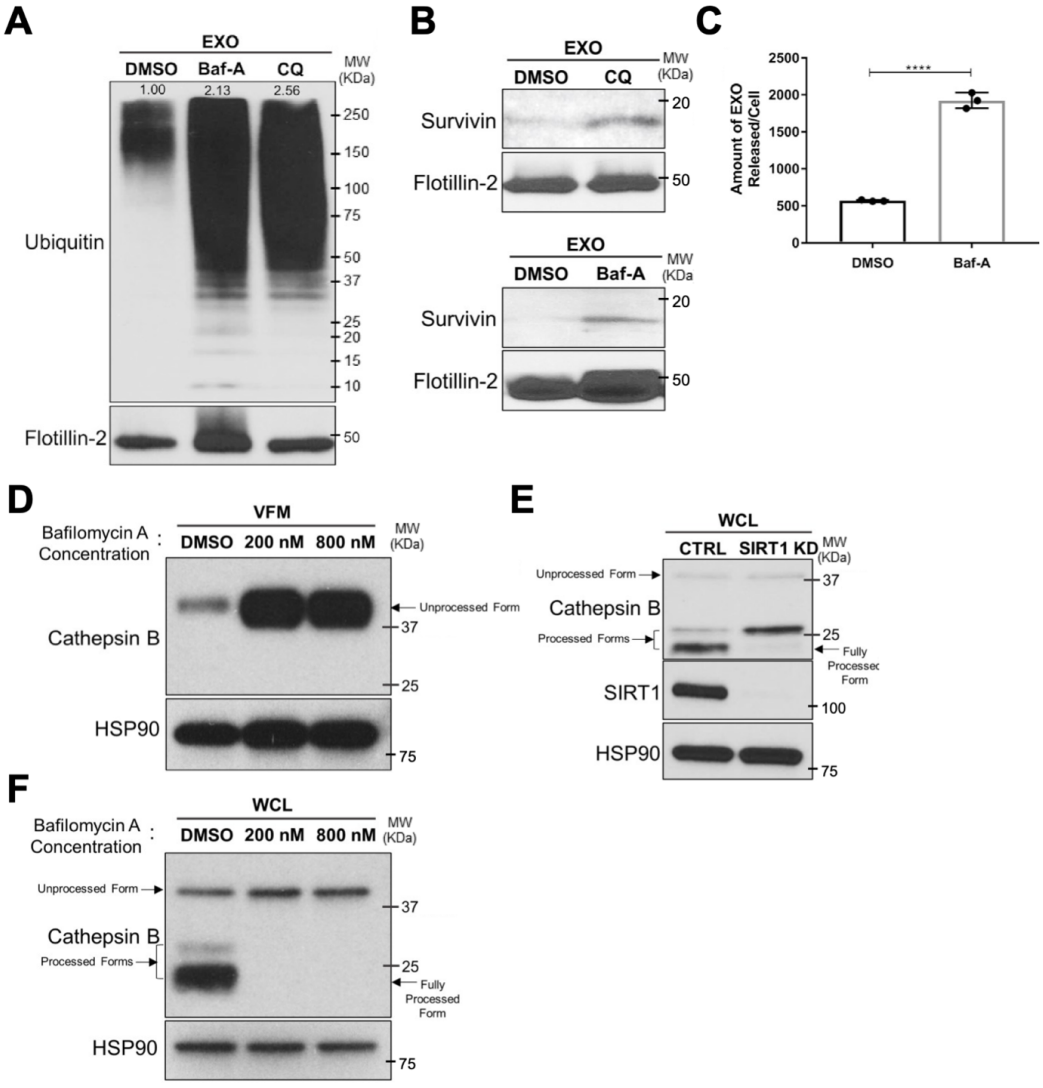
A
EXO
DMSO
Baf-A
CQ
1.00
2.13
2.56
MW (KDa)
250
150
100
75
50
37
25
20
15
10
Ubiquitin
Flotillin-2
50
B
EXO
DMSO
CQ
MW (KDa)
Survivin
20
Flotillin-2
50
EXO
DMSO
Baf-A
MW (KDa
Survivin
20
Flotillin-2
50
C
Amount of EXO Released/Cell
2500
2000
1500
1000
500
0
****
DMSO
Baf-A
D
VFM
Bafilomycin A Concentration :
DMSO
200 nM
800 nM
MW (KDa)
Unprocessed Form
Cathepsin B
37
25
HSP90
75
E
WCL
CTRL
SIRT1 KD
MW (KDa)
Unprocessed Form
37
Cathepsin B
Processed Forms
25
Fully Processed Form
SIRT1
100
HSP90
75
F
WCL
Bafilomycin A Concentration :
DMSO
200 nM
800 nM
MW (KDa)
Unprocessed Form
37
Cathepsin B
Processed Forms
25
Fully Processed Form
HSP90
75

Figure 2.6 (Continued)

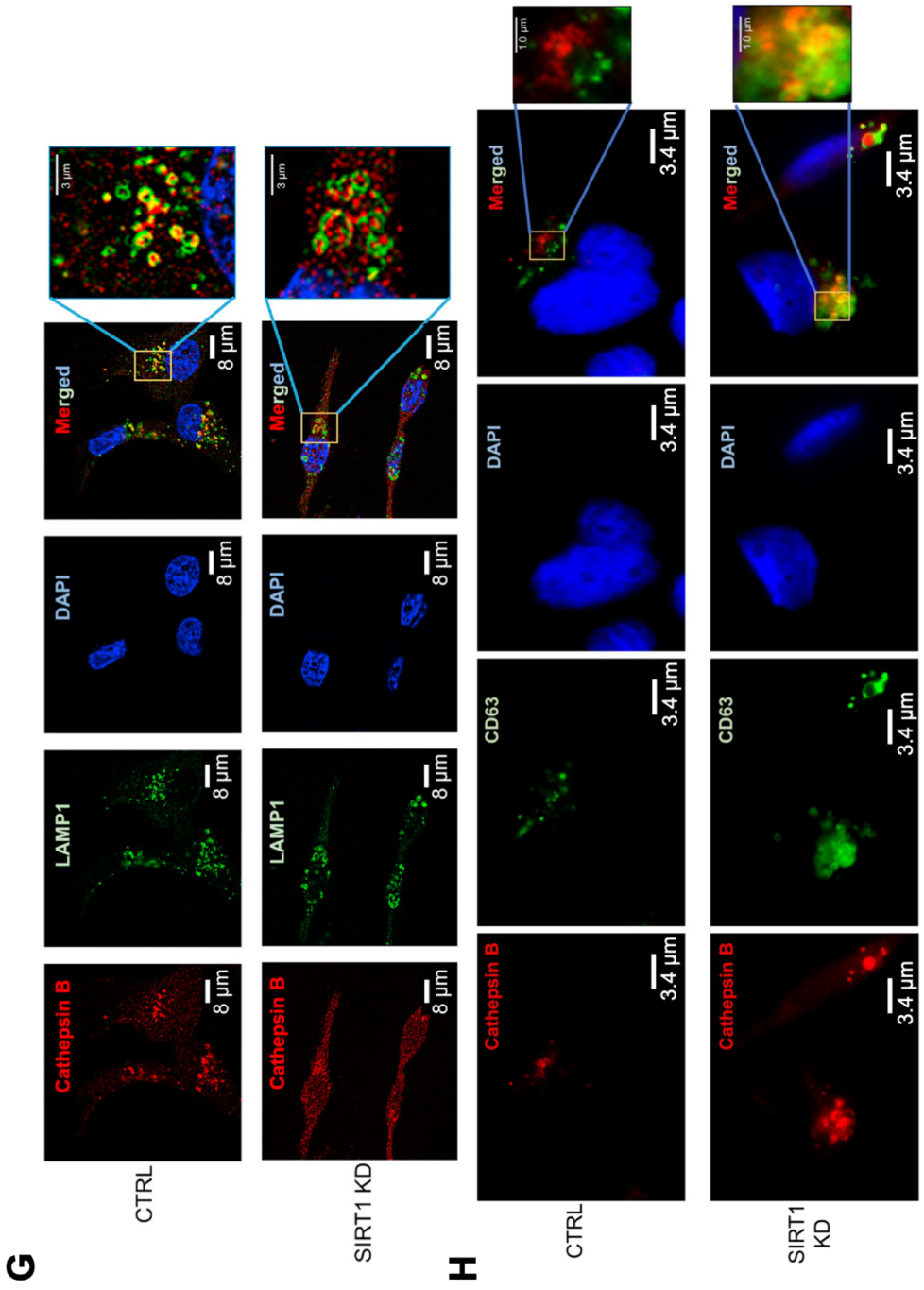

partially processed form of cathepsin B, while parental MDA-MB-231 cells treated with increasing amounts of bafilomycin-A showed a complete loss of the processed forms of cathepsin B (**Figure 2.6F**). Immunofluorescence microscopy carried out on SIRT1-knockdown cells using a cathepsin B antibody showed a marked difference in the localization of this hydrolase. Specifically, cathepsin B predominantly localized with LAMP1-positive lysosomes in control cells (**Figure 2.6G**, top panel), as expected. However, in cells depleted of SIRT1, there was less localization of cathepsin B with LAMP1-positive lysosomes (**Figure 2.6G**, bottom panel); instead, it predominantly localized with CD63-positive MVBs (**Figure 2.6H**). Such changes were previously shown to be associated with its secretion from cancer cells, where its hydrolase activity played an important role in degrading the extracellular matrix and promoting tumor invasiveness[21,22,33].

SIRT1 Loss Inhibits Lysosomal Acidification

We next determined whether SIRT1 directly impacted lysosomal function by assaying the pH of lysosomes in control and SIRT1-knockdown MDA-MB-231 cells using LysoSensor yellow-blue dextran ratiometric dye. Based on the calibration curve shown in **Figure 2.7A**, we found that the pH of lysosomes in control cells was 4.7 (**Figure 2.7B**), matching the reported pH of properly functioning lysosomes[34], while the pH of lysosomes in cells depleted of SIRT1 was slightly above 5.6 (**Figure 2.7B**).

We then examined whether the increase in lysosomal pH associated with SIRT1-knockdown cells is due to a defective proton pump. Lysosomal re-acidification assays were performed (**Figure 2.7C**, diagram), where the pH of lysosomes in control and SIRT1-knockdown cells was first increased by bafilomycin-A treatment, followed by the addition of LysoTracker to determine how quickly the pH of the lysosomes recovered. The pH of lysosomes in control cells fully recovered within 60 min (**Figure**

Figure 2.7 SIRT1 Loss Disrupts Lysosomal Acidification
(A) Calibration curve used to determine lysosomal pH in control of MDA-MB-231 cells using LysoSensor Dextran®. (B) Lysosomal pH measurements were determined for sham-shRNA-expressing CTRL and SIRT1 KD MDA-MB-231 cells based calibration curve in (A). (C) Scheme of the lysosome re-acidification assay (top) and the percent of lysosomal re-acidification determined using LysoTracker Green DND-26 in sham-shRNA-expressing CTRL and SIRT1-KD cells. (D) SILAC results showing the ratio of ATP6V1A protein levels in SIRT1-KD cells compared to control cells (top). Western blot analysis of ATP6V1A, ATP6V0D1, SIRT1, and HDAC6 protein levels in CTRL and SIRT1-KD cells (bottom). The expression levels of ATP6V1A in each lysate was quantified relative to HDAC6 and included in the blot. (E) Western blot analysis of ATP6V1A, SIRT1, and β-Actin protein levels in sham shRNA expressing control (CTRL), and SIRT1 KD, MDA-MB-453 and Hs-578T cells. The expression levels of ATP6V1A were quantified relative to β-Actin and included in the blot. (F) Western blot analysis of ATP6V1A, SIRT1, and HSP90 levels in CTRL and ATP6V1A-KD cells. The expression levels of ATP6V1A was quantified relative to HSP90 and included in the blot. (G) NTA was performed on the conditioned media from an equal number of serum-starved sham-shRNA-expressing CTRL and ATP6V1A-KD cells. (H) Quantification of exosomes generated for each condition in (G). (I) Western blot analysis of ubiquitinated protein, Survivin, and Flotillin-2 levels in EXOs generated by the cells in (F). The amount of ubiquitinated proteins detected in each lysate was quantified relative to Flotillin-2 and included in the blot. (J) Western blot analysis of SIRT1, ATP6V1A, and β-actin levels in sham-shRNA-expressing CTRL and SIRT1-KD cells ectopically expressing either the vector alone (Vector) or overexpressing ATP6V1A (ATP6V1A OE). (K) Quantification of exosomes generated for each condition in (J). (L) Western blot analysis of ubiquitinated protein, cathepsin B, and HSP90 levels in EXOs (left panel) and VFM (right panel) collected from these cells. The amounts of ubiquitinated protein and cathepsin B detected in each lysate were quantified relative to HSP90 and included in the blots. The unprocessed and processed forms of cathepsin B are also indicated.

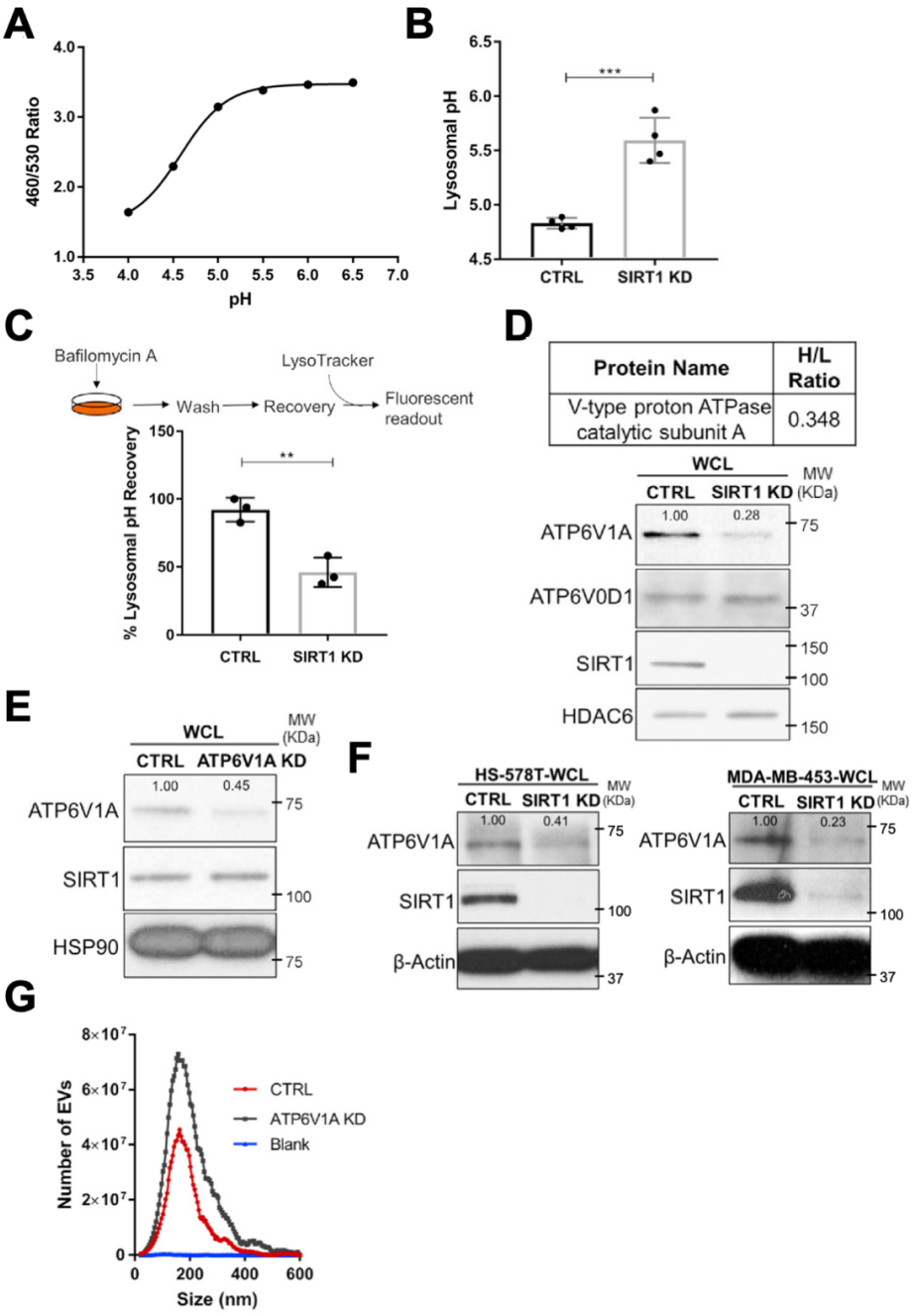
A
460/530 Ratio
pH
B
Lysosomal pH
***
CTRL
SIRT1 KD
C
Bafilomycin A
Wash
Recovery
LysoTracker
Fluorescent readout
% Lysosomal pH Recovery
**
CTRL
SIRT1 KD
D
Protein Name
H/L Ratio
V-type proton ATPase catalytic subunit A
0.348
WCL
CTRL
SIRT1 KD
MW (KDa)
ATP6V1A
ATP6V0D1
SIRT1
HDAC6
1.00
0.28
E
WCL
CTRL
ATP6V1A KD
MW (KDa)
ATP6V1A
SIRT1
HSP90
1.00
0.45
F
HS-578T-WCL
MDA-MB-453-WCL
CTRL
SIRT1 KD
MW (KDa)
ATP6V1A
SIRT1
β-Actin
1.00
0.41
1.00
0.23
G
Number of EVs
Size (nm)
CTRL
ATP6V1A KD
Blank

Figure 2.7 (Continued)

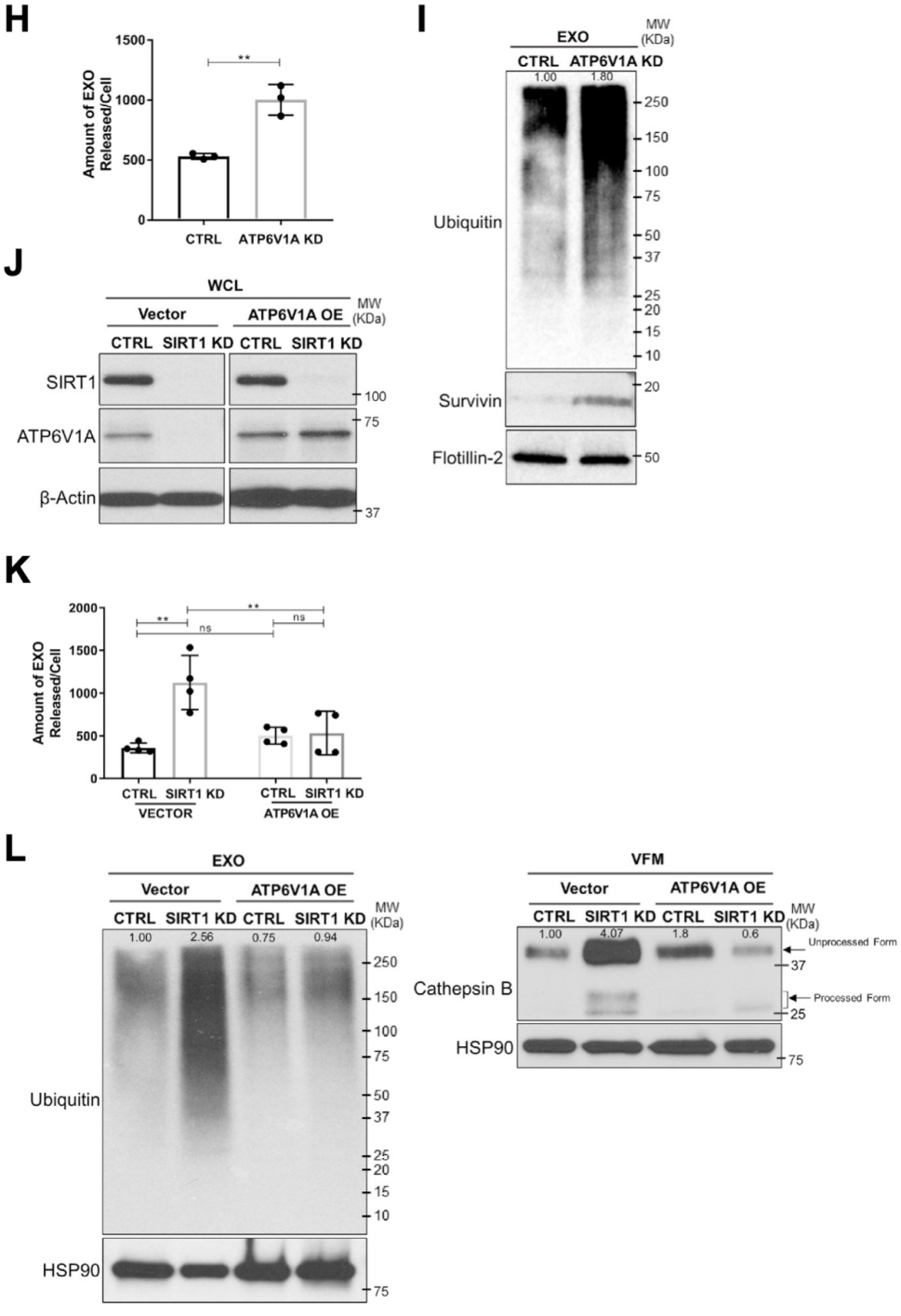

2.7C, graph). In contrast, the pH recovery of lysosomes in cells lacking SIRT1 was significantly slower.

Based on these findings, we turned our attention to the proton pump. V-ATPases are multi-subunit enzymes that are responsible for the acidification of late endosomes and lysosomes[35], and alterations in the expression of any component of this pump can disrupt the ability of lysosomes to maintain proper pH[36,37]. Analysis of our SILAC results performed on SIRT1-knockdown cells revealed that the expression of subunit A of V1 (ATP6V1A) is downregulated by 65%, compared to control cells. This was confirmed by western blot analysis (**Figure 2.7D**), whereas the expression of the ATP6V0D1 subunit was unchanged by SIRT1 knockdown (**Figure 2.7D**). Knocking down SIRT1 in two other breast cancer cell lines, i.e., Hs-578T and MDA-MB-453 cells, similarly affected ATP6V1A protein levels (**Figure 2.7E**), while knocking down the expression of ATP6V1A in MDA-MB-231 cells (**Figure 2.7F**), mirrored the effects of knocking down SIRT1 and increased the release of exosomes, with these vesicles being enriched in Survivin and ubiquitinated proteins (**Figures 2.7G-2.7I**). However, the ectopic expression of ATP6V1A in cells depleted of SIRT1 (**Figure 2.7J**) rescued the effects of knocking down SIRT1, thereby reducing exosome numbers (**Figure 2.7K**) and the amount of ubiquitinated proteins detected in their exosomes as well as the level of cathepsin B in the VFM (**Figure 2.7L**).

SIRT1 Regulates ATP6V1A mRNA Stability

The reduction in ATP6V1A protein levels observed in cells lacking SIRT1 was accompanied by a corresponding decrease in its mRNA levels, as determined by performing RT-qPCR using two independent primer sets that target the ATP6V1A mRNA (**Figure 2.8A**). The expression levels of a number of lysosomal genes are known to be regulated by the transcription factor EB (TFEB), which binds to

Figure 2.8 SIRT1 Regulates ATP6V1A mRNA Stability
(A) RT-qPCR was performed using two primer sets to determine ATP6V1A transcript levels (relative to actin) in sham-shRNA-expressing CTRL and SIRT1-KD cells. The transcript levels of SIRT1 were also determined as a control. (B) Dual-reporter luciferase assays were performed on the promoter region of the ATP6V1A gene. Top: a schematic of the luciferase reporter used. Bottom: the ratio of luciferase luminescence to Renilla luminescence in sham-shRNA-expressing CTRL and SIRT1-KD MDA-MB-231 cells expressing the reporter construct. (C) RT-qPCR analysis was performed to determine the transcript levels of several TFEB target genes (relative to actin) in sham shRNA expressing control (CTRL), and SIRT1 KD, cells. (D) Western blot analysis of ubiquitinated protein and Flotillin-2 levels in exosomes (EXO) derived from control (CTRL), and SIRT1 KD, cells that were treated with DMSO, Rapamycin (RAP; 1 μM), or Torin 1 (250 nM), for 16 hours. The amount of ubiquitinated protein detected in each lysate was quantified relative to Flotillin-2 and included in the blots. (E) RT-qPCR was performed to determine ATP6V1A transcript levels (relative to actin) in control (CTRL), and SIRT1 KD, cells that were treated with DMSO, Rapamycin (RAP; 1 μM), or Torin 1 (250 nM) for 12 hours. The transcript levels of CLCN7 in the cells were also determined as a positive control. (F) RT-qPCR was performed to determine ATP6V1A transcript levels (relative to actin) in control (CTRL), and SIRT1 KD, cells treated with DMSO, or JQ1 (400 nM), for 9 hours. The transcript levels of SQSTM1 and CLCN7 in the cells were also determined as positive and negative controls, respectively. (G) Number of the various types of AREs and U-stretches identified in the 3′UTRs of transcripts encoding the indicated lysosomal proteins. (H) ATP6V1A mRNA stability assays were performed on actinomycin-A-treated MDA-MB-231 cells treated with DMSO or EX-527 (20 μM) or ectopically expressing SIRT1 (SIRT1 OE) for the indicated times. (I) ATP6V1A mRNA stability assays were performed on cells ectopically expressing ATP6V1A mRNA containing (UTR) or lacking (CDS) its 3′ UTR sequence and treated with either DMSO or EX-527 (20 μM) for the indicated times. (J) ATP6V1A transcript levels were determined in TNBC tumors and NTNBC using RNA-seq Nexus (GEO accession: GSE58135). (K) Correlation of ATP6V1A and SIRT1 mRNA levels in the tumor samples in (J), as well as in (L) the GDC TCGA Breast Cancer dataset.

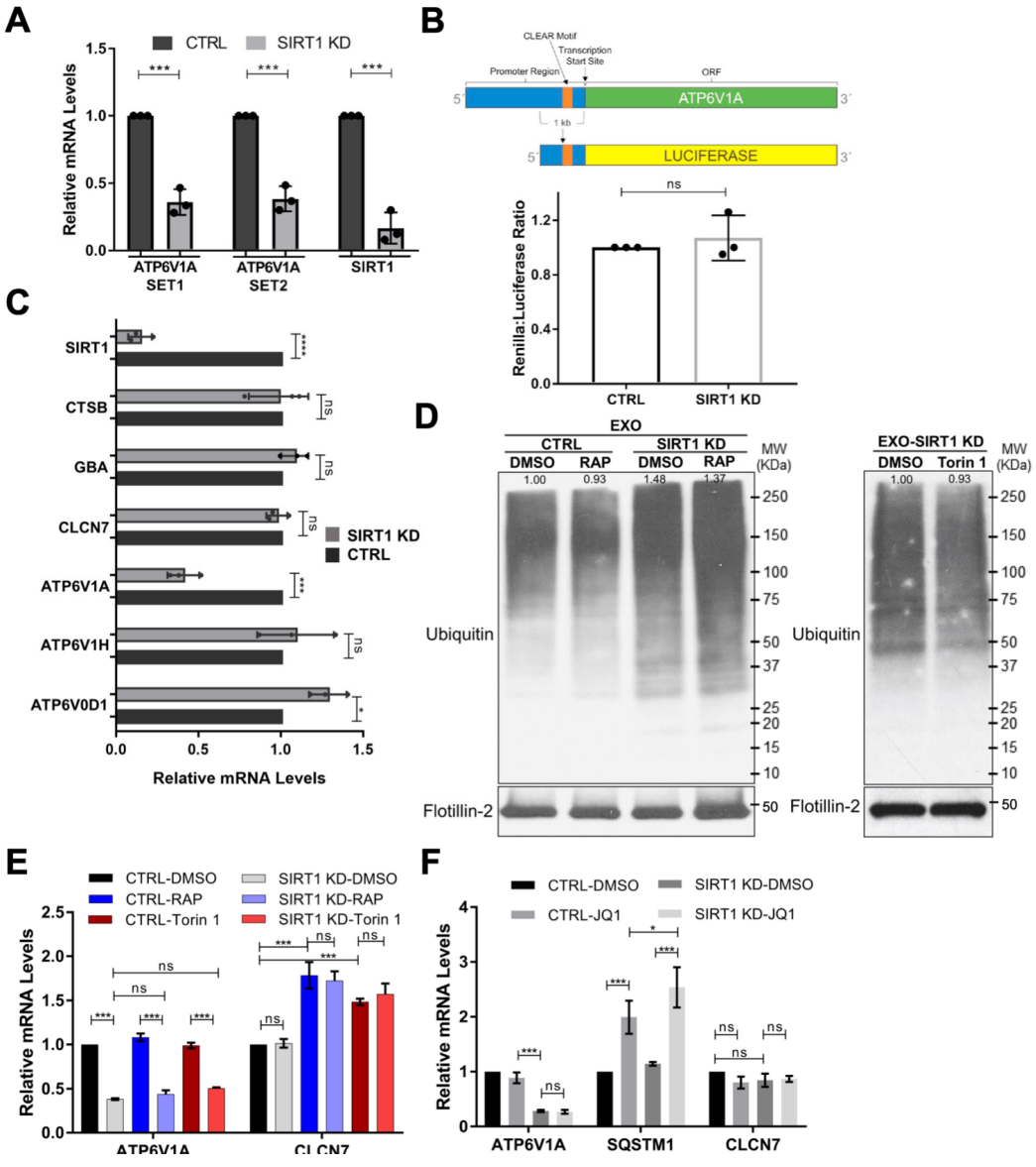
A
CTRL
SIRT1 KD
Relative mRNA Levels
ATP6V1A SET1
ATP6V1A SET2
SIRT1
B
CLEAR Motif
Transcription Start Site
Promoter Region
ORF
ATP6V1A
LUCIFERASE
1 kb
Renilla:Luciferase Ratio
ns
CTRL
SIRT1 KD
C
SIRT1
CTSB
GBA
CLCN7
ATP6V1A
ATP6V1H
ATP6V0D1
SIRT1 KD
CTRL
Relative mRNA Levels
D
EXO
CTRL
SIRT1 KD
DMSO
RAP
MW (KDa)
1.00
0.93
1.48
1.37
Ubiquitin
Flotillin-2
EXO-SIRT1 KD
DMSO
Torin 1
E
CTRL-DMSO
CTRL-RAP
CTRL-Torin 1
SIRT1 KD-DMSO
SIRT1 KD-RAP
SIRT1 KD-Torin 1
Relative mRNA Levels
F
CTRL-DMSO
CTRL-JQ1
SIRT1 KD-DMSO
SIRT1 KD-JQ1
Relative mRNA Levels
ATP6V1A
SQSTM1
CLCN7

Figure 2.8 (Continued)

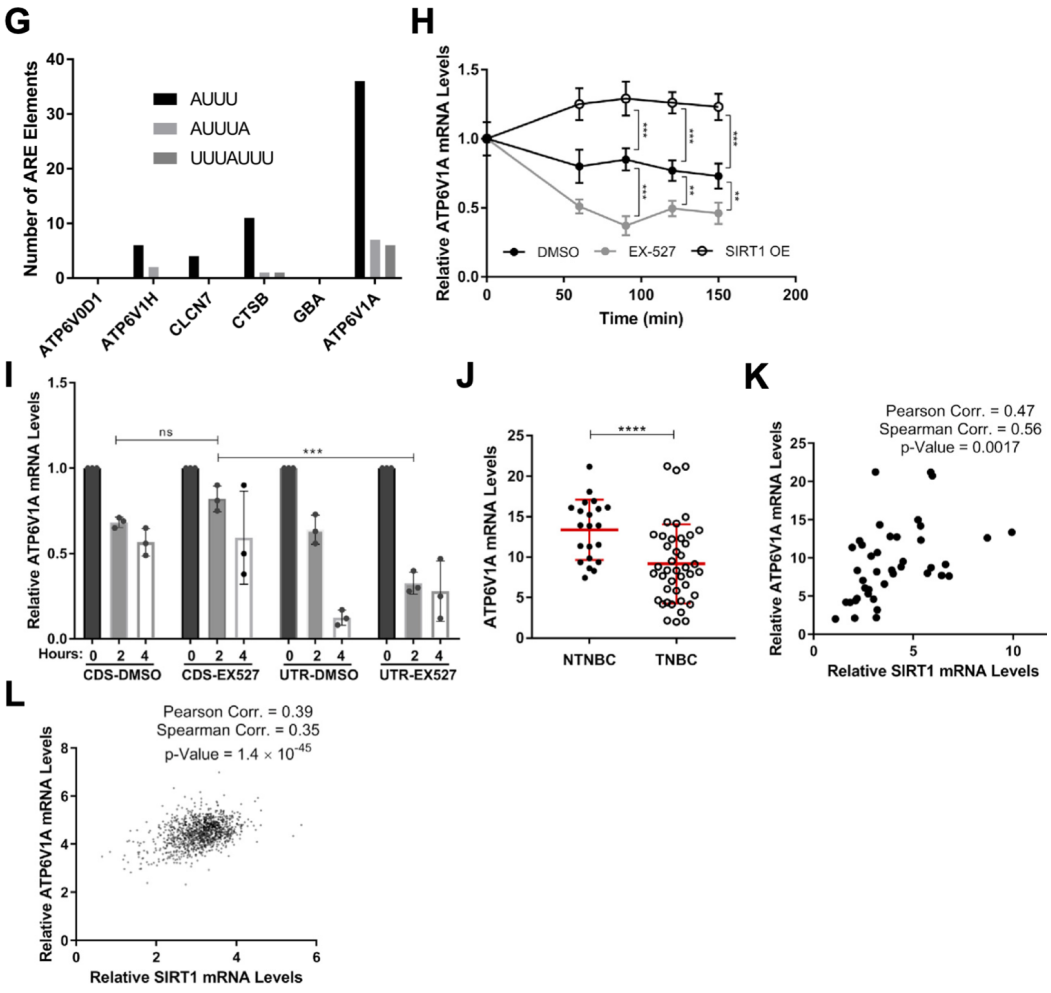

coordinated lysosomal expression and regulation (CLEAR) elements in the promoter regions of these genes and promotes their transcription[38]. Because there is a putative CLEAR motif upstream of the ATP6V1A transcriptional start site (**Figure 2.8B**, diagram) and given a recent study identifying SIRT1 as a positive regulator of the transcriptional activity of TFEB[39], we examined whether knocking down SIRT1 inhibited TFEB transcriptional activity and reduced ATP6V1A mRNA levels. However, using a dual-luciferase reporter whose expression was under the control of the ATP6V1A promoter (**Figure 2.8B**, diagram), no differences in luciferase luminescence between control and SIRT1-knockdown cells were detected (**Figure 2.8B**, graph). Moreover, the mRNA levels of several known TFEB targets were not affected to the same extent as ATP6V1A levels under conditions where SIRT1 expression was inhibited using shRNAs (**Figure 2.8C**).

Mechanistic target of rapamycin complex 1 (mTORC1) is another known regulator of lysosomal function, based on its ability to inhibit TFEB activity and reduce the levels of several components of the proton pump[40]. However, treatment of SIRT1-knockdown cells with rapamycin or Torin 1, two inhibitors of mTORC1, had no effect on the enrichment of ubiquitinated cargo in exosomes or ATP6V1A mRNA levels (**Figures 2.8D and 2.8E**).

While this manuscript was in preparation, another study was published showing that SIRT1 was capable of promoting the transcription of genes involved in autophagy and lysosomal biogenesis by inhibiting a negative regulator of transcription, bromodomain-containing protein 4 (BRD4). To investigate whether BRD4 binding might be responsible for the reduced ATP6V1A mRNA levels in SIRT1-knockdown cells, we used a specific inhibitor of BRD4, (i.e., JQ1). While JQ1 treatment of SIRT1-knockdown cells increased the mRNA levels of SQSTM1 mRNA,

as previously reported[41], the inhibitor had no effect on ATP6V1A or CLCN7 mRNA levels in control or SIRT1-depleted cells (**Figure 2.8F**).

We then examined whether SIRT1 influences the turnover of the ATP6V1A RNA transcript. A key factor that affects the stability of RNA transcripts is the presence of A-U rich elements (AREs) and U-stretches in their 3′ untranslated regions (3′ UTRs). Certain RNA-binding proteins bind AREs and U-stretches in mRNA transcripts and alter their half-lives[42]. Analysis of the 3′ UTR of the ATP6V1A mRNA revealed an unusually large number of AREs and U-stretches, compared to other lysosomal genes (**Figure 2.8G**). This led us to determine whether ATP6V1A mRNA stability was affected by SIRT1. MDA-MB-231 cells transcriptionally inhibited by actinomycin-D treatment were further treated with either DMSO or the SIRT1 inhibitor EX-527 for increasing lengths of time. The RNA was then isolated from these cells and analyzed for ATP6V1A transcript levels. The results showed that the ATP6V1A mRNA in cells treated with EX-527 had a much shorter half-life, compared to cells treated with DMSO (**Figure 2.8H**). Ectopic expression of SIRT1 in the same cells resulted in the further stabilization of the ATP6V1A transcript. Moreover, EX-527 treatment did not have detrimental effects on the stability of an ectopically expressed ATP6V1A construct that lacked its 3′ UTR. In contrast, the inclusion of the 3′ UTR in this construct resulted in a significant reduction in the stability of the ectopically expressed ATP6V1A transcript upon treatment of the cells with EX-527 (**Figure 2.8I**).

Because SIRT1 is frequently downregulated in TNBC (**Figure 2.1A**), we examined whether there was a corresponding decrease in ATP6V1A mRNA levels in these tumor samples. Indeed, ATP6V1A transcript levels were significantly lower in TNBC tissues, compared to the normal adjacent tissues (**Figure 2.8J**). Moreover, there was a positive correlation between SIRT1 and ATP6V1A mRNA levels within

the same tumors in this dataset (**Figure 2.8K**), as well as when analyzing a larger dataset of breast tumors using The Cancer Genome Atlas (TCGA) database (Genomic Data Commons (GDC) TCGA Breast Cancer, **Figure 2.8L**).

The Secretome of SIRT1-Depleted Breast Cancer Cells Promotes Cell Survival and Invasive Activity

To determine the biological effects of exosomes derived from SIRT1-knockdown cells, we first wanted to demonstrate the transfer of cargo in exosomes to recipient cells. A yellow fluorescent protein (YFP)-tagged form of Survivin (YFP-SURV), when ectopically expressed in MDA-MB-231 cells, could be detected in their exosomes (**Figure 2.9A**). When treating the non-invasive MCF10AT1 breast cancer cell line with these exosomes, YFP-tagged Survivin was detected within the cells, as indicated by western blot analysis (**Figure 2.9B**) and immunofluorescent microscopy (**Figure 2.9C**). We then investigated whether the exosomes and cathepsins present in the secretome of cancer cells with reduced expression of SIRT1 work together to promote a cancer cell phenotype. To examine this possibility, spheres of non-invasive MCF10AT1 cells were generated and embedded in a collagen matrix (**Figure 2.9D**). The cells were cultured in the absence (untreated control) or presence of equivalent amounts of exosomes and/or VFM isolated from control, and SIRT1-depleted MDA-MB-231 cells. The addition of exosomes or VFM from either of these two cell types had only minimal effects on MCF10AT1 sprouting (invasion) (**Figures 2.9E and 2.9F**). However, the combination of exosomes and VFM derived from the SIRT1-knockdown MDA-MB-231 cells strongly promoted this invasive phenotype (i.e., day 4 in **Figure 2.9G**).

We also ectopically expressed a green fluorescent protein (GFP) construct in the cells to visualize them embedded in the collagen matrix by fluorescent microscopy. Again, the addition of exosomes and VFM from SIRT1-depleted MDA-

Figure 2.9 The Secretome of SIRT1-Depleted Breast Cancer Cells Promote Invasion

(A) Western blot analysis of YFP-Survivin levels in WCL (left) and exosomes (right) collected from MDA-MB-231 cells ectopically expressing either the vector alone (Vector), or YFP-tagged Survivin (YFP-SURV). (B) Western blot analysis of YFP-tagged Survivin levels in MCF10AT1 cells that were left untreated, or treated with exosomes from MDA-MB-231 cells ectopically expressing YFP-tagged Survivin, for 4 hours. (C) Fluorescence microscopy images of MCF10AT1 cells left untreated, or treated with exosomes from MDA-MB-231 cells ectopically expressing YFP-tagged Survivin, for 4 hours. The cells were immunostained with a GFP antibody (yellow). The cells were also stained with rhodamine-conjugated Phalloidin (purple) to label F-actin, and DAPI (blue) to label nuclei. Scale bar, 5 μm. (D) Diagram of the invasion assay. Spheroids of MCF10AT1cells were prepared, embedded in a collagen matrix, and cultured under different conditions, and the extent to which they migrated was determined. (E–G) Images of invasion assays performed on MCF10AT1 cells treated with equivalent amounts of (E) EXOs, (F) VFM, or (G) EXOs and VFM from either sham-shRNA-expressing CTRL or SIRT1-KD MDA-MB-231 cells. Images show the extent of cell outgrowths on days 0, 2, and 4 of the experiment. Arrows highlight areas of invasion, and the insets are higher magnifications of boxed areas. Scale bar, 0.3 mm. (H) Fluorescent microscopy and second-harmonic generation (SHG) images of invasion assays performed on GFP-expressing MCF10AT1 cells treated with an equivalent amount of EXOs and VFM collected from sham-shRNA-expressing CTRL and SIRT1 KD MDA-MB-231 cells or from SIRT1-KD MDA-MB-231 cells ectopically expressing ATP6V1A (SIRT1 KD/V1A OE). Some of the cells were also treated with CA-074 (10 μM). Arrowheads indicate areas where cells have invaded into the collagen. Scale bar, 100 μm. (I) Quantification of invasion area for each condition in (H). (J) Fluorescent microscopy and second-harmonic generation (SHG) images of GFP-expressing MCF10AT1 cells embedded in a collagen matrix and treated with an equivalent amount of exosomes and vesicle free media (VFM) from MDA-MB-231 cells treated with DMSO, or Bafilomycin-A, (200 nM), for 16 hours. Arrow heads indicated some of the areas where cells have invaded into the collagen the most. Scale bar, 100 μm. (K) Quantification of invasion area for each condition in (J).

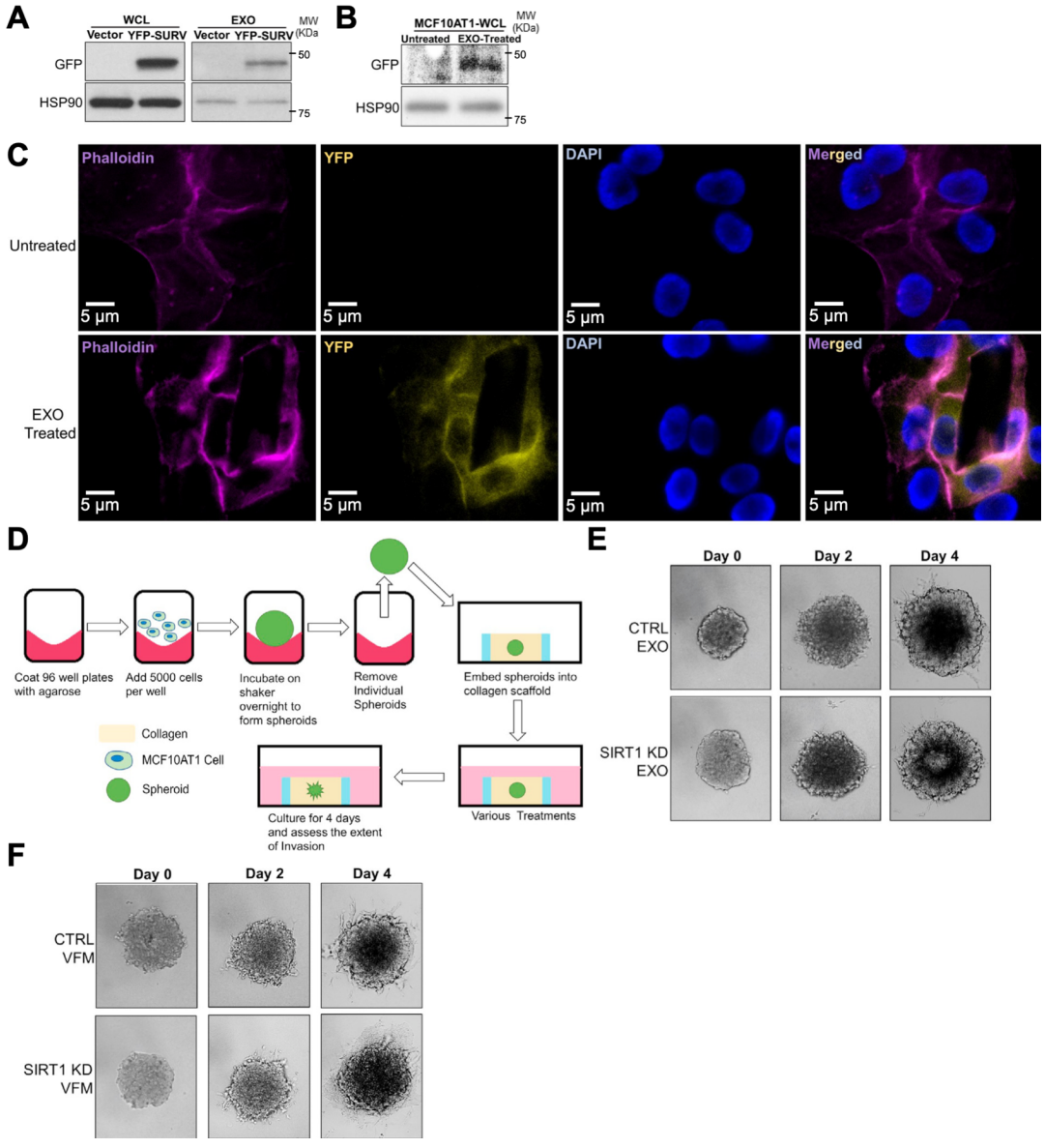
A
WCL
Vector YFP-SURV
EXO
Vector YFP-SURV
MW (KDa)
GFP
HSP90
50
75
B
MCF10AT1-WCL
Untreated EXO-Treated
MW (KDa)
GFP
HSP90
50
75
C
Phalloidin
YFP
DAPI
Merged
Untreated
EXO Treated
5 µm
D
Coat 96 well plates with agarose
Add 5000 cells per well
Incubate on shaker overnight to form spheroids
Remove Individual Spheroids
Embed spheroids into collagen scaffold
Collagen
MCF10AT1 Cell
Spheroid
Culture for 4 days and assess the extent of Invasion
Various Treatments
E
Day 0
Day 2
Day 4
CTRL EXO
SIRT1 KD EXO
F
Day 0
Day 2
Day 4
CTRL VFM
SIRT1 KD VFM

Figure 2.9 (Continued)

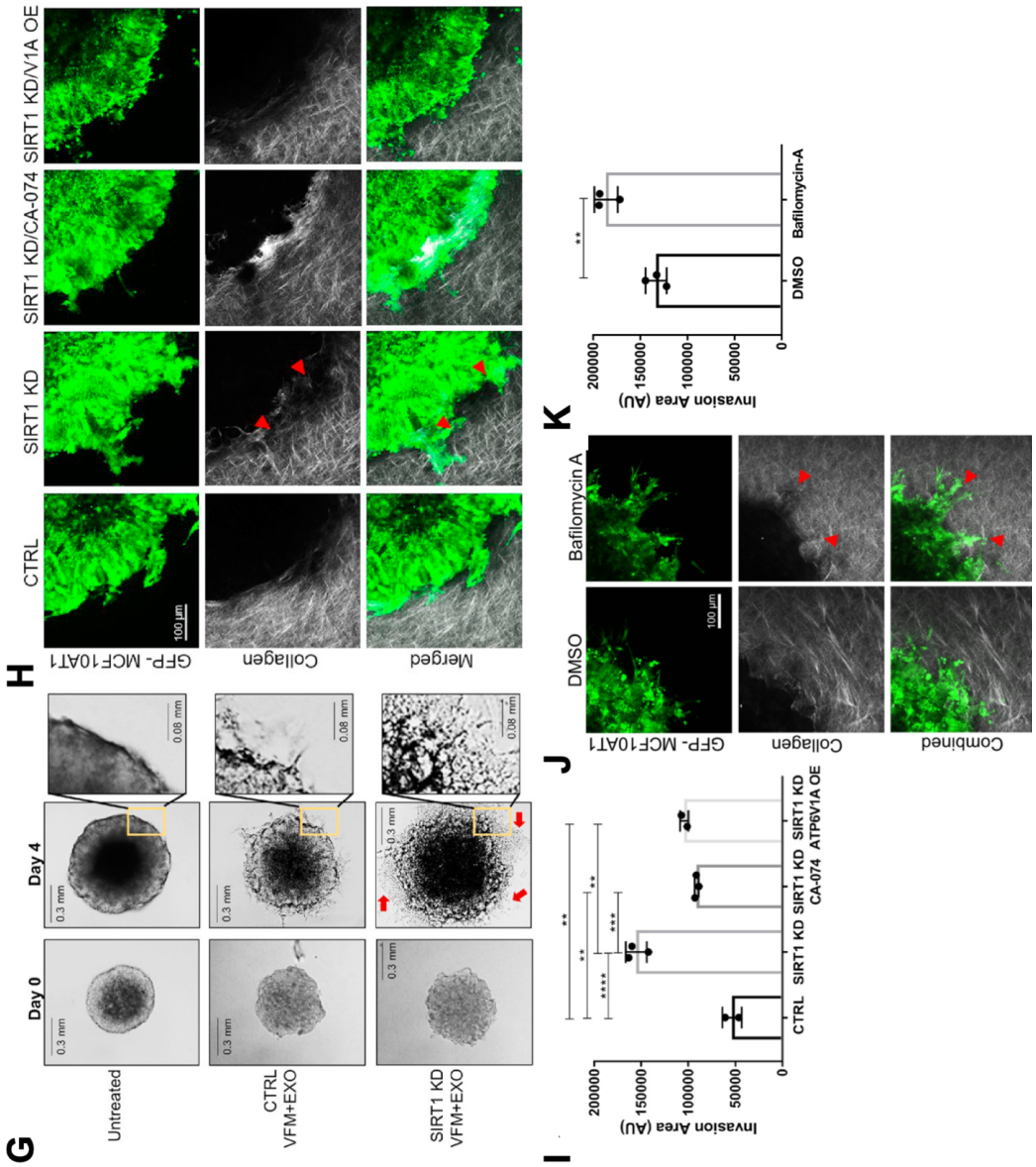

MB-231 cells increased the invasion of GFP-expressing MCF10AT1 cells compared to cells treated with exosomes and VFM from control MDA-MB-231 cells (**Figure 2.9H**, top panels, and **Figure 2.6I**). This approach also allowed for the visualization of areas where collagen was invaded by the cells (**Figure 2.9H**, see arrows in the middle and bottom panels). The increase in cell invasion caused by exosomes and VFM from SIRT1-knockdown cells was significantly reduced when MCF10AT1 cells were treated with the cathepsin B inhibitor CA-074 or when ATP6V1A was ectopically expressed in the SIRT1-knockdown MDA-MB-231 cells prior to collecting their exosomes (**Figures 2.9H and 2.9I**). Consistent with our findings that SIRT1 inhibits lysosomal function to generate a unique secretome, an increase in the invasiveness of GFP-expressing MCF10AT1 cells was promoted by exosomes and VFM derived from MDA-MB-231 cells treated with bafilomycin-A (**Figures 2.9J and 2.9K**).

Survival and wound-healing (scratch) assays were also performed. Exosomes isolated from MDA-MB-231 cells depleted of SIRT1 were more effective at promoting the survival of serum-deprived MCF10AT1 cells, compared to an equivalent amount of exosomes from control cells (**Figure 2.10A**), and they strongly stimulated MCF10AT1 cell migration, as determined in wound-closure assays (**Figures 2.10B and 2.10C**). Because exosomes derived from SIRT1-knockdown cells are enriched with Survivin, a protein known to promote cell survival and migration[43,44], we determined whether it was important for mediating these effects. Control and SIRT1-knockdown MDA-MB-231 cells were treated with phosphate-buffered saline (PBS) as a control or with YM155, a small molecule that inhibits Survivin expression (**Figure 2.10D**) such that it is absent from exosomes generated by SIRT1-knockdown cells (**Figure 2.10E**). Exosomes from control cells treated without (PBS treated) or with YM155 caused only a modest enhancement in the survival and migration of MCF10AT1 cells (**Figures 2.10F-2.10H**). However, exosomes from SIRT1-

Figure 2.10 The Secretome of SIRT1-Depleted Breast Cancer Cells Promote Migration and Survival

(A) Cell death assays were performed on MCF10AT1 cells that were left untreated (serum starved) or were treated with EXOs isolated from either sham-shRNA-expressing control (EXO-CTRL) or SIRT1-KD cells (EXO-SIRT1 KD). As a control, cells were cultured with media containing 2% fetal bovine serum (FBS). (B) Wound healing assays performed on MCF10AT1 cells cultured for 8 h in serum free media (8-hr-No treatment), or serum free medium supplemented with an equivalent amount of exosomes derived from either control (8 hr-EXO-CTRL), or SIRT1 KD (8 hr - EXO-SIRT1KD), MDA-MB-231 cells. (C) Images of the wound healing assay performed in (B). The initial width of the wounds struck are shown (0 hr) and highlighted using dashed lines. (D) Western blot analysis of Survivin levels in WCL of SIRT1 KD cells treated with phosphate buffer saline (PBS), or YM155 (30 nM), for 48 hours. (E) Western blot analysis of Survivin levels in the exosomes generated by the cells in (D). (F) Serum starvation-induced cell death assays were performed on MCF10AT1 cells that were left untreated (No Serum), or were treated with exosomes isolated from control (EXO-CTRL), or SIRT1 KD, cells (EXO-SIRT1 KD) that had been treated with either PBS, or YM155 (30 nM), for 48 hours. (G) Wound healing assays performed on MCF10AT1 cells cultured for 8 h in serum free medium supplemented with an equivalent amount of exosomes derived from control (8 hr-EXO-CTRL), or SIRT1 KD, MDA-MB-231 cells (8 hr - EXO-SIRT1KD) that had been treated with either PBS, or YM155 (30 nM), for 48 hours. (H) Images of the wound healing assay performed in (I). The initial width of the wounds struck are shown (0 hr) and highlighted using dashed lines.

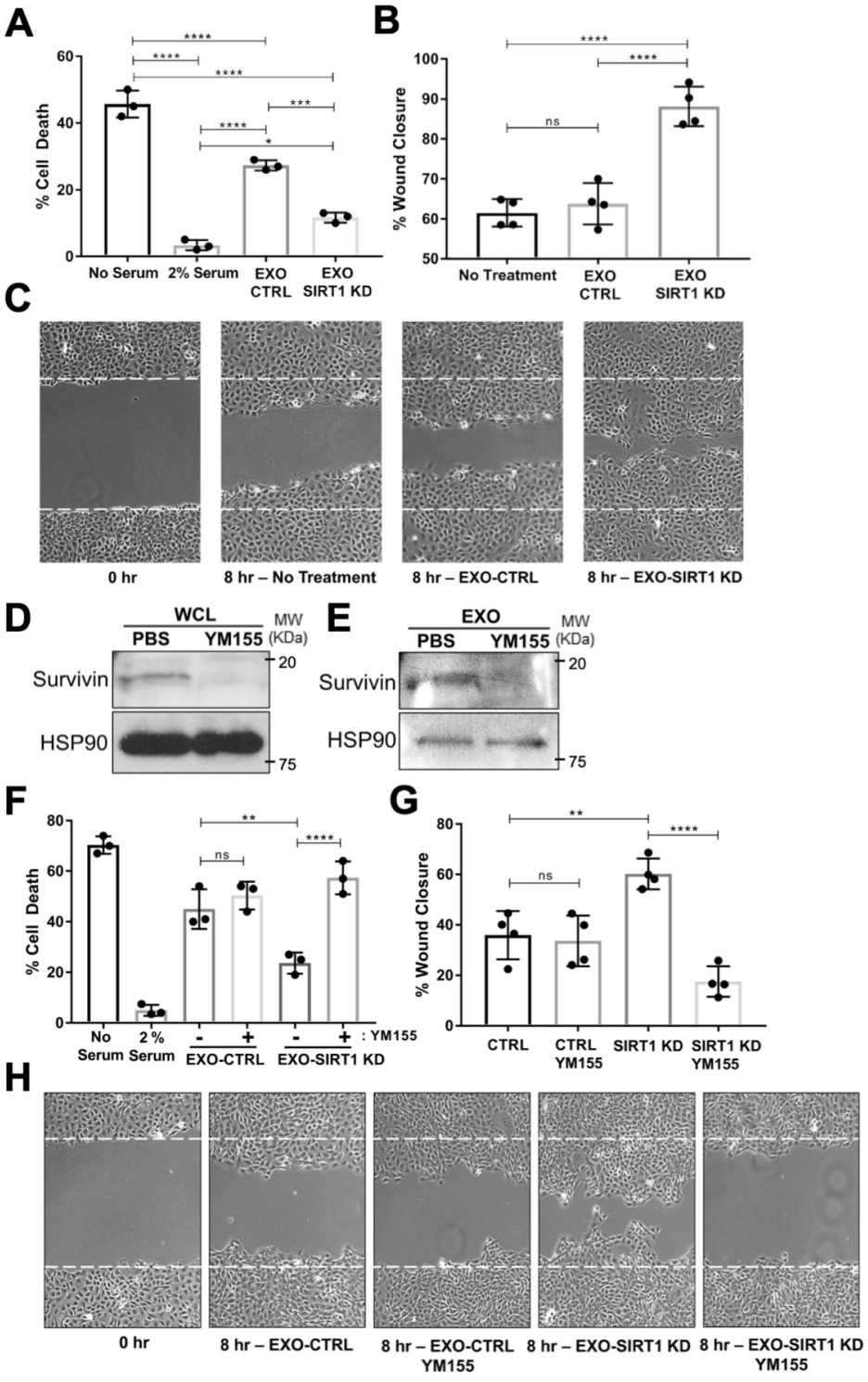
A
% Cell Death
No Serum
2% Serum
EXO CTRL
EXO SIRT1 KD
B
% Wound Closure
No Treatment
EXO CTRL
EXO SIRT1 KD
ns
C
0 hr
8 hr – No Treatment
8 hr – EXO-CTRL
8 hr – EXO-SIRT1 KD
D
WCL
PBS
YM155
MW (KDa)
Survivin
HSP90
E
EXO
F
No Serum
2% Serum
EXO-CTRL
EXO-SIRT1 KD
: YM155
G
CTRL
CTRL YM155
SIRT1 KD
SIRT1 KD YM155
H
0 hr
8 hr – EXO-CTRL
8 hr – EXO-CTRL YM155
8 hr – EXO-SIRT1 KD
8 hr – EXO-SIRT1 KD YM155

knockdown cells treated with YM155 no longer promoted cell survival and migration as effectively as exosomes from SIRT1-knockdown cells treated with only PBS (**Figures 2.10F-2.10H**).

Discussion

Lysosomes help maintain cellular homeostasis by degrading unwanted proteins, RNA, and DNA. This occurs as MVBs containing intraluminal vesicles and soluble proteins are trafficked to, and fused with, lysosomes, exposing their contents to the acidic and hydrolase-rich environment of the lysosomal lumen[45]. However, some MVBs are directed to the cell surface, where they give rise to a class of EVs referred to as exosomes. Research involving EVs has been attracting increasing attention from diverse fields of biology and the pharmaceutical industry, primarily because it is now recognized that virtually all cells form and shed distinct classes of EVs that contain cargo reflecting their cellular origin. EVs can be transferred to other cells, resulting in phenotypic changes that have an impact on several biological processes and diseases and have been extensively studied in the context of cancer[10]. Exosomes derived from highly aggressive cancer cells have been shown to promote cell growth and survival as well as invasive and metastatic activities[18,46,47]. Still, there remain large gaps in our understanding of EVs, especially regarding the mechanisms that regulate exosome biogenesis.

Our findings, summarized in **Figure 2.11**, identify a connection between SIRT1, lysosomal activity, and the formation of a secretome with unique characteristics. Specifically, we discovered that knocking down SIRT1 in breast cancer cells decreases the protein levels of the ATP6V1A subunit of the V-ATPase proton pump located on lysosomal membranes. This results in a poorly functioning pump and the inability of lysosomes to maintain the low pH needed for degradative

Figure 2.11 SIRT1 Downregulation Alters the Secretome of Breast Cancer Cells by Impairing Lysosomal Function
Model describing the role of SIRT1 in regulating exosome biogenesis and hydrolase secretion. Decreasing SIRT1 levels in breast cancer cells reduces the stability of the ATP6V1A transcript and causes a corresponding loss in the expression of the ATP6V1A protein. This impairs lysosomal function and results in MVBs that would normally be degraded in the lysosomes to instead fuse with plasma membrane and release their content, i.e., exosomes and hydrolases.

SIRT1 KD
MDA-MB-231 Cell
Early Endosomes
MVB
RAB27
Lysosome
Loss of SIRT1
ATP6V1A mRNA
Degradation
V-ATPase Proton
Pump Poorly
Functioning
Control
MDA-MB-231 Cell
Early Endosomes
MVB
SIRT1
ATP6V1A mRNA
Stabilization
ATP6V1A
Protein
Lysosome
V-ATPase
Proton Pump
Functioning
ATP6V1A mRNA
ATP6V1A Gene
Nucleus
V-ATPase Proton Pump
Intra-Luminal Vesicles/Exosomes
Unprocessed Cathepsin B
Processed Cathepsin B
RNA Degradation Machinery
Plasma Membrane

activity. Thus, in cells lacking sufficient amounts of SIRT1 expression or activity to sustain proper lysosomal function, MVBs that would typically be degraded in lysosomes, instead fuse with the plasma membrane and release their contents (i.e., exosomes with unique cargo and hydrolases that normally reside in the lysosomes to degrade proteins) into the extracellular environment.

A possible explanation for the increased release of exosomes in SIRT1-depleted cells involves the V-ATPase machinery directly impacting exocytosis. The V0 and V1 domains of the V-ATPase assemble together on late MVBs and lysosomes to acidify the lumens of these structures. However, it has been recently shown that the V0 domain can dissociate from the V1 domain to promote exocytosis[48,49]. Since knocking down SIRT1 decreases the expression of ATP6V1A, a subunit of the V1 domain, it was plausible that this could be sufficient to cause the dissociation of the V0 domain and increase exosome release. Although we cannot completely rule out this possibility, inhibiting lysosomal function using chloroquine or bafilomycin-A or interfering with the ability of MVBs to fuse with lysosomes (by knocking down RAB7) showed the same effects as reducing SIRT1 levels. It is also worth noting that treating cells with chloroquine has been shown to enhance the assembly of the V1-V0 subunits[50], further suggesting that inhibiting the acidification of lysosomes is sufficient to produce a unique secretome.

Using 3D cultures of non-invasive MCF10AT1 breast cancer cells, we showed that distinct components within the secretome of SIRT1-deficient breast cancer cells act synergistically to promote cell survival and invasive activity. Specifically, the increased amounts of lysosomal hydrolases secreted by SIRT1-knockdown breast cancer cells, particularly cathepsin B, degrade extracellular matrix components, while exosomes enriched in Survivin derived from these cells strongly promote cell survival and migration. The release of exosomes and soluble factors by highly aggressive

cancer cells may be important for cancer progression, as tumors are composed of a heterogeneous collection of cells. Thus, more aggressive cells may produce a secretome that alters the behavior of less aggressive cells within the tumor, making them more invasive and drug resistant.

While it is well accepted that the multi-subunit V-ATPase proton pump is essential for maintaining the acidification and function of lysosomes[51], how the components of this pump are regulated, as well as the consequences of deregulating lysosomal activity in cancer[52], is poorly understood. Thus, the regulation of lysosomal function by SIRT1 offers new insights into these questions. The expression of the ATP6V1A subunit of the V-ATPase proton pump was reduced by ~65% in SIRT1-knockdown MDA-MB-231 cells, compared to control cells, because of decreased ATP6V1A transcript levels. Based on previous findings[2,53], we initially suspected that knocking down SIRT1 would inhibit the transcription of the ATP6V1A gene. However, the transcription of this gene was similar in both control and SIRT1-knockdown cells. Instead, we found that depleting cells of SIRT1 decreased the half-life of the ATP6V1A transcript. One likely possibility for this effect is that depleting cells of SIRT1 leads to the acetylation and inactivation of a protein that binds to and stabilizes the ATP6V1A transcript, and we are currently attempting to identify such a SIRT1 substrate.

SIRT1 is best known for its role in extending lifespan[4,54]. More recently, there have been suggestions that it also can function as a tumor suppressor[1], as reducing SIRT1 expression levels frequently occurs in TNBCs. However, how SIRT1 might act to inhibit cancer progression has been an open question. Our findings showing that knocking down SIRT1 expression in cancer cells impairs lysosomal activity and results in the generation of a secretome capable of strongly promoting cell survival and invasive activity now offer a plausible explanation. This previously unappreciated

connection between SIRT1 and lysosomal function may also help to shed light on how reducing SIRT1 levels can negatively impact aging and certain neurodegenerative disorders that are characterized by the loss of SIRT1 expression[55,56].

Materials and Methods

Reagent and Resources

The reagent and resources used for the experiments described in this study are listed in Table 1:

Table 1. List of reagents and resources used in this study

REAGENT or RESOURCE	SOURCE	IDENTIFIER
Antibodies		
Anti-SIRT1 antibody	Cell Signaling Technology	2493S; RRID: AB_2188359
Anti-SIRT6 antibody	Cell Signaling Technology	12486S; RRID: AB_2636969
Anti-SIRT7 antibody	Cell Signaling Technology	5360S; RRID: AB_2716764
Anti-RAB27A antibody	Cell Signaling Technology	95394S
Anti-RAB7A antibody	Cell Signaling Technology	9367S; RRID: AB_1904103
Anti-IkBα antibody	Cell Signaling Technology	4812S; RRID: AB_10694416
Anti-β-Actin antibody	Cell Signaling Technology	3700S; RRID: AB_2242334
Anti-Survivin antibody	Novus Biologicals	NB500-201; RRID: AB_10001517

Anti-GFP antibody	Cell Signaling Technology	2956S; RRID: AB_1196615
Anti-HDAC6 antibody	Cell Signaling Technology	7558S; RRID: AB_10891804
Anti-Flotillin-2 antibody	Cell Signaling Technology	3436S; RRID: AB_2106572
Anti-Flag antibody	Cell Signaling Technology	8146S; RRID: AB_10950495
Anti-HSP90 antibody	Cell Signaling Technology	4877S; RRID: AB_2233307
Anti-LAMP1 antibody	Cell Signaling Technology	9091S; RRID: AB_2687579
Anti-LDHA	Cell Signaling Technology	3582S; RRID: AB_2066887
Anti-CD63 antibody	Abcam	ab59479; RRID: AB_940915
Anti-M6PR Antibody	Cell Signaling Technology	14364S
Anti-CD81 antibody	Millipore	MABF2061
Anti-ATP6V1A antibody	Abcam	ab137574; RRID: AB_2722516
Anti-ATP6V0D1 antibody	Abcam	ab56441; RRID: AB_940402
Anti-MMP7 antibody	Cell Signaling Technology	71031S
Anti-MMP9 antibody	Cell Signaling Technology	13667S
Anti-Cathepsin B antibody	Cell Signaling Technology	31718S; RRID: AB_2687580
Anti-Ubiquitin antibody	Santa Cruz Biotechnology	sc-8017; RRID: AB_628423

Anti-UB H2A antibody	Cell Signaling Technology	8240S; RRID: AB_10891618
Anti-UB H2B antibody	Cell Signaling Technology	5546S; RRID: AB_10693452
Anti-14-3-3 Zeta/Delta antibody	Cell Signaling Technology	7413S; RRID: AB_10950820
Anti-Rabbit IgG-HRP Conjugate antibody	Cell Signaling Technology	7074S; RRID: AB_2099233
Anti-Mouse IgG-HRP Conjugate antibody	Cell Signaling Technology	7076S; RRID: AB_330924
Anti-Mouse IgG-Alexa 488 Conjugate antibody	Thermo Fisher	A-11029; RRID: AB_2534088
Anti-Rabbit IgG-Alexa 568 Conjugate antibody	Thermo Fisher	A-11036; RRID: AB_10563566
Bacterial and Virus Strains		
E.coli: Stellar Competent Cells	Clonetech	636763
E.coli: One Shot Stbl3 Chemically competent cells	Thermo Fisher	C737303
Chemicals, Peptides, and Recombinant Proteins		
Leupeptin	Sigma	L9783
Aprotinin	Sigma	10236624001
Dithiothreitol (DTT)	Sigma	10197777001
Dimethylsulfoxide (DMSO)	Sigma	D8418
Chloroquine	Cayman Chemicals	14194

Bafilomycin-A	Cayman Chemicals	11038
LysoTracker™ Green DND-26	Thermo Fisher	L7526
LysoSensor™ Yellow/Blue dextran, 10,000 MW	Thermo Fisher	L22460
EX-527	Cayman Chemicals	10009798
Rapamycin	Cayman Chemicals	13346
Torin 1	Cayman Chemicals	10997
YM155	Tocris	6491
Nigercin	Sigma	N7143
Monesin	Sigma	M5273
Actinomycin D	Cayman Chemicals	11421
Puromycin	Sigma	P9620
Alexa Fluor™ 594 Phalloidin	Thermo Fisher	A12381
Keratinocyte Serum Free Medium (K-SFM)	Thermo Fisher	17005042
Bovine Pituitary Extract (BPE)	Thermo Fisher	13028014
Gibco™ Amphotericin B	Thermo Fisher	15290026
DAPI	Sigma	D9542
CA-074	Tocris	4863
EGF	Millipore	01-107
DMEM	Gibco	11965-092
RPMI	Gibco	11875-093
DMEM/F12	Gibco	12634-010
SILAC RPMI	Thermo Fisher	89984
Fetal Bovine Serum	Gibco	10437028

Calf Serum	Gibco	16010159
Horse Serum	Gibco	16050-122
Pen-Strep	Gibco	15140122
Dialyzed FBS	HyClone	SH30079.02HI
[$^{13}C_6$,$^{15}N_2$]-L-lysine	Sigma	608041
[$^{13}C_6$,$^{15}N_4$]-L-arginine	Sigma	608033
Insulin	Sigma	I2643-50MG
Hydrocortisone	Sigma	H4001-1G
Choleratoxin	Sigma	C8052-1MG

Critical Commercial Assays		
RNA Isolation Kit	Invitrogen	12183018A
Dual-Reporter Luciferase Assay	Promega	E1910
InFusion Cloning Kit	Clonetech	638909
Superscript III Reverse Transcriptase	Invitrogen	18080044
Cathepsin B activity assay kit	Immunochem Technologies	937

Experimental Models: Cell Lines		
Human: HEK-293T	ATCC	N/A
Human: MDA-MB-231	ATCC	N/A
Human: MDA-MB-453	ATCC	N/A
Human: Hs-578T	ATCC	N/A
Human: ZR-75-1	ATCC	N/A
Human: BT-474	ATCC	N/A

Human: CAMA-1	ATCC	N/A
Human: SK-BR-3	ATCC	N/A
Human: T-47D	ATCC	N/A
Human: MCF7	ATCC	N/A
Human: MDA-MB-468	ATCC	N/A
Human: TSE	ATCC	N/A
Human: Human Dermal Fibroblasts	Zenbio	DF-F
Human: Normal Human Astrocytes	Provided by Ichiro Nakano, University of Alabama	N/A
Human: U87	ATCC	HTB-14
Human: HK-2	ATCC	CRL2190
Human: MCF10AT1	Provided by Claudia Fischbach, Cornell Univeristy	N/A
Human: GFP-MCF10AT1	This Paper	N/A
Human: ATP6V1A-CDS MDA-MB-231	This Paper	N/A
Human: ATP6V1A-UTR MDA-MB-231	This Paper	N/A

Oligonucleotides		
Control shRNA Sequence: CCGGCAACAAGATGAAG AGCACCAACTCGAGTTG GTGCTCTTCATCTTGTTG TTTTT	Sigma Mission ShRNA	SHC002

shRNA Targeting Sequence: SIRT1 : GTACCGGCATGAAGTGC CTCAGATATTACTCG AGTAATATCTGAGGCACT TCATGTTTTTTG	Sigma Mission ShRNA	TRCN0000218734
shRNA Targeting Sequence: SIRT6 : CCGGGAAGAATGTGCCA AGTGTAAGCTCGAG CTTACACTTGGCACATTC TTCTTTTTG	Sigma Mission ShRNA	TRCN0000232528
shRNA Targeting Sequence: SIRT7 : CCGGGTCCAGCCTGAAG GTTCTAAACTCGAG TTTAGAACCTTCAGGCTG GACTTTTTG	Sigma Mission ShRNA	TRCN0000359663
shRNA Targeting Sequence: RAB27A : GTACCGGGATCTTCTCTA TGATTGATACCTCG AGGTATCAATCATAGAGA AGATCTTTTTTG	Sigma Mission ShRNA	TRCN0000380306

shRNA Targeting Sequence: RAB7A : GTACCGGGGTTATCATCC TGGGAGATTCCTCG AGGAATCTCCCAGGATG ATAACCTTTTTTG	Sigma Mission ShRNA	TRCN0000380577
shRNA Targeting Sequence: ATP6V1A : CCGGGCTGTCCAACATG ATTGCATTCTCGAGA ATGCAATCATGTTGGACA GCTTTTT	Sigma Mission ShRNA	TRCN0000029539
sgRNA-1 targeting SIRT1: CACCGGCTCCCCGGCGG GGGACGACG	This Paper	N/A
sgRNA-2 targeting SIRT1: CACCGTCGTACAAGTTGT CGGCCAG	This Paper	N/A
Recombinant DNA		
pLJM1-LAMP1-mRFP-FLAG	Zoncu et al[57], 2011	Addgene Plasmid #34611
pGL3 Luciferase Reporter Vector - Basic	Promega	E1751

pRL Renilla Luciferase Control Reporter Vector	Promega	E2231
pMD2.G-VSV-G-expressing envelope plasmid	From Didier Trono	Addgene Plasmid #12259
pCMV delta R8.2-Lentiviral Packaging plasmid	From Didier Trono	Addgene Plasmid #12263
pUMVC-Retroviral Packaging plasmid	Stewart et al[58], 2003	Addgene Plasmid #8449
pYESir2-puro plasmid	Vaziri et al[59], 2001	Addgene Plasmid # 1769
LentiCRISPRv2-Blast	From Mohan Babu	Addgene Plasmid # 83480
LentiCRISPRv2GFP	Walter et al[60], 2017	Addgene Plasmid # 82416
pLJC5-Tmem192-2xFlag	Abu-Remaileh et al[28], 2017	Addgene Plasmid # 102929
pLJM1-ATP6V1A-CDS plasmid		This Paper
pLJM1-ATP6V1A-CDS+UTR plasmid		This Paper

Software and Algorithms		
Snapgene Viewer	GSL Biotech	snapgene.com
ImageJ	NIH	https://imagej.nih.gov/ij/
Fiji open source image analysis software	Fiji	https://fiji.sc/

DAVID Bioinformatics Resource	Huang et al.[61,62], 2008, 2009	https://david.ncifcrf.gov/
Prism	Graphpad	https://www.graphpad.com
Xcalibur 2.2	Thermo Fisher	

Other		
SYBR Green Supermix	Bio-Rad	1725121
Fugene 6 Transfection Reagent	Promega	E2692
Trypsin – Lys-C Mix	Promega	V5073
Sep-Pak C18 Columns	Waters	186000308
0.22 µm Steriflip Filter	Millipore	SEM1M179M6
Amicon Ultra-15 Centrifugal Filter Units – 10 KDa	Millipore	UFC901024
NheI	New England Biolab	R3131S
EcoRI	New England Biolab	R3101S

Experimental Model and Subject Details

Cell Lines. Human embryonic kidney (HEK)-293T, MDA-MB-231, MDA-MB-453, and Hs-578T breast cancer cells, U87 glial cells, and Human Kidney-2 (HK-2) cells were obtained from the ATCC (https://www.atcc.org/), while the primary Human Dermal Fibroblast were purchased from Zenbio. The MCF10AT1 cells were provided by Claudia Fischbach, Cornell University, and the Normal Human Astrocytes were from Ichiro Nakano, University of Alabama. HEK-293T cells were cultured in Dulbecco's Modified Eagle Medium (DMEM) supplemented with 10% calf serum (CS). MDA-MB-231, MDA-MB-453, Hs-578T, ZR-75-1, BT-474, CAMA-1, SK-BR-3, T-47D, MCF7,

MDA-MB-468, TSE, and U87 cells were cultured in Roswell Park Memorial Institute 1640 (RPMI-1640) medium supplemented with 10% fetal bovine serum (FBS). MCF10AT1 were cultured in DMEM/F12 medium supplemented with 5% horse serum, 10 μg/mL insulin, 0.5 μg/mL hydrocortisone, 100 ng/mL cholera toxin, 20 ng/mL EGF, 100 I.U./mL penicillin, and 100 μg/mL streptomycin. Primary Human Dermal Fibroblast were cultured in DMEM supplemented with 10% FBS, 100 I.U./mL penicillin, 100 μg/mL streptomycin, and 0.25 μg/mL Amphotericin B. Normal Human Astrocytes were cultured in DMEM/F-12 supplemented with 10% FBS. HK-2 cells were cultured in Keratinocyte Serum Free Medium (K-SFM) supplemented with 0.05 mg/ml bovine pituitary extract (BPE), and 5 ng/mL EGF. All cell lines were maintained at 37°C with 5% CO2.

Cells stably expressing constructs of interest were selected for, and maintained by, supplementing the growth medium with 2 μg/mL puromycin.

Method details

Plasmid Generation, Virus Production, and Cell Infection. The pLJM1-LAMP1-mRFP-FLAG (#34611) construct was purchased from Addgene, and the ATP6V1A transcript, lacking or containing its 3′UTR, were cloned into the pLJM1 plasmid using the following primers:

ATP6V1A-CDS-Forward:

CGTCAGATCCGCTAGCATGGATTTTTCCAAGCTACCC,

ATP6V1A-CDS-Reverse:

TCGAGGTCGAGAATTCCTAATCTTCAAGGCTACGGAATGC,

ATP6V1A-UTR-Forward:

CGTCAGATCCGCTAGCATGGATTTTTCCAAGCTACC,

ATP6V1A-UTR-Reverse:

TCGAGGTCGAGAATTCTGTTAATTTAAATCCACTTTTTATT.

For the luciferase reporter assay, the 500 bp region immediately upstream of the ATP6V1A transcription start site was cloned into the pGL3-Luciferase reporter vector (E1751), and for transfection efficiency normalization the pRL-Renilla reporter (E2231) was purchased from Promega. All shRNA constructs were from Sigma.

Lentiviruses were generated by transfecting HEK-293T cells with the shRNA plasmids (Sigma) and the packaging plasmids (#12259 and #12263, Addgene) using Fugene 6 (Promega). The viruses shed into the medium by the cells were harvested 24 and 48 h after transfection. The viruses were then used to infect the target cells using Polybrene (8 μg/mL).

To generate SIRT1 knockout MDA-MB-231 cells, CRISPR/Cas9 was used. Two sgRNAs were used to induce double-strand DNA breaks and clones that lost one copy of SIRT1 gene, or both copies of this gene, were derived by selection with 5 μg/mL blasticidin. The results were confirmed with PCR.

RNA Isolation and Quantitative (q) RT-PCR Analysis. Total RNA was isolated from cells using the PureLink RNA Mini Kit (Invitrogen), and the mRNA transcripts were converted to cDNA using Superscript III Reverse Transcriptase (Invitrogen) and oligo dT_{20}. The cDNA was then used to determine the expression levels of the indicated transcripts using SYBR Green Supermix (Bio-Rad) and the Applied Biosystems® 7500 Real-Time PCR System with the T method (ABI). The following primers were used for the RT-qPCR analyses are shown in **Table 2.2**.

Table 2.2. List of primers used in this study

PRIMER	SEQUENCE
SIRT1-FW	AAGTTGACTGTGAAGCTGTACG
SIRT1-RW	TGCTACTGGTCTTACTTTGAGGG

ATP6V1A-S1-FW	ACATCCCCAGAGGAGTAAACG
ATP6V1A-S1-RW	ACTACCAACCCGTAGGTTTTTG
ATP6V1A-S2-FW	GAGATCCTGTACTTCGCACTGG
ATP6V1A-S2-RW	GGGGATGTAGATGCTTTGGGT
ATP6V1A-CDS and UTR-FW	CAAAGACGATGACGACAAGa
ATP6V1A-CDS and UTR-RW	CCCACTCTCACCAGCTCATA
GBA-FW	ATGGAGCGGTGAATGGGAAG
GBA-RW	GTGCTCAGCATAGGCATCCAG
CTSB-FW	ACAACGTGGACATGAGCTACT
CTSB-RW	TCGGTAAACATAACTCTCTGGGG
CLCN7-FW	CCCACACAACGAGAAGCTCC
CLCN7-RW	ACTTGTCGATATTGCCCTTGATG
ATP6V1H-FW	CAGAAGTTCGTGCAAACAAAGTC
ATP6V1H-RW	TCAGGGCTTCGTTTCATTTCAA
ATP6V0D1-FW	GCATCACCTCTGACGGTGTC
ATP6V0D1-RW	CTCCTTAATGTCACGCACGAT
ACTB-FW	CATGTACGTTGCTATCCAGGC
ACTB-RW	CTCCTTAATGTCACGCACGAT
SQSTM1-FW	GACTACGACTTGTGTAGCGTC
SQSTM1-RW	AGTGTCCGTGTTTCACCTTCC

RNA Stability Assay. To determine the stability of the endogenously or exogenously expressed ATP6V1A transcripts in control or SIRT1 KD MDA-MB-231 cells, the RNA from these cells was collected at different times (up to 3 h) following their treatment

with Actinomycin D (Cayman Chemicals, 4 μg/mL). The levels of each transcript were then determined by RT-qPCR using the primer sets listed in the RNA Isolation and Quantitative (q) RT-PCR Analysis section.

Dual Reporter Luciferase Assay. The pGL3-Luciferase reporter construct containing the ATP6V1A promoter (5 μg) and the pRL-Renilla reporter construct (0.5 μg) were transfected into control and SIRT1 KD MDA-MB-231 cells using Fugene 6. After 16 h, the luciferase and the renilla bioluminescence was measured using a BioTek Synergy 2 plate reader according to the manufacturer's instructions.

EV and Vesicle Free Medium Preparation. The conditioned medium collected from 2.0 × 106 serum starved cells was subjected to two consecutive centrifugations at 700 × g to clarify the medium of cells and cell debris. The partially clarified medium was filtered using a 0.22 μm pore size Steriflip PVDF filter (Millipore). The filter was rinsed two times with 5 mL of Phosphate buffered saline (PBS) to remove any remaining exosome sized EVs (less than 0.22 μm) from the filter. The EVs larger than 0.22 μm retained by the filter were lysed using 250 μL of lysis buffer (25 mM Tris, 100 mM NaCl, 1% Triton X-100, 1 mM EDTA, 1 mM DTT, 1 mM NaVO4, 1 mM β-glycerol phosphate, and 1 μg/ml each aprotinin and leupeptin). This was considered the microvesicle (MV) lysate. The filtrate was then subjected to ultracentrifugation at 100,000 × g for 8 h. The pelleted exosomes were either lysed using 250 μL of lysis buffer, or resuspended in 500 μL of serum free medium for cell-based assays. The supernatant depleted of MVs and exosomes was concentrated using 10 KDa centricons (Amicon). This was considered the vesicle-free medium (VFM). Whole cell lysates (WCL) were prepared by rinsing dishes of cells with PBS, adding 800 μL of lysis buffer, and scraping the cells off the plate. The resulting MV, exosome, and cell

lysates were centrifuged at 16,000 x g for 10 min, and then the supernatants were subjected to Western blot analysis.

SILAC and Mass Spectrometry. Quantitative proteomics using SILAC was performed on samples as described in Zhang et al.[63], 2016. Briefly, MDA-MB-231 cells were cultured in SILAC RPMI-1640 media supplemented with Dialyzed FBS (HyClone) and either [13C6,15N2]-L-lysine (Sigma) and [13C6,15N4]-L-arginine (Sigma) or L-lysine (Sigma) and L-arginine (Sigma) for five generations. The MDA-MB-231 cell line that was grown with heavy L-lysine and L-arginine was then treated with lentivirus containing shRNA targeting SIRT1, whereas the MDA-MB-231 cell line grown in normal L-lysine and L-arginine was treated with control lentivirus shRNA. After 48 h, the cells, and the exosomes released by these cells, were lysed in lysis buffer, while the vesicle free media (VFM) samples were prepared as described above. The protein concentrations of the samples were determined by Bradford assay, and an equivalent amount of each sample (30 µg) was processed as outlined in Zhang et al.[64], 2017. The resulting lyophilized peptides were then analyzed using nano LC-MS/MS (Cornell University, Proteomics Facility). All data was acquired using Xcalibur 2.2 operation software.

Endolysosomal Immunoprecipitation. Endolysosomal immunoprecipitations were performed as described in Abu-Remaileh et al.[28], 2017. Briefly, 30 million cells stably expressing FLAG-tagged TMEM192 were infected with control shRNA, or SIRT1 targeting shRNA. After 48 hours, the cells were washed twice with PBS before being removed from the dish using a cell scraper and resuspended in 1.0 mL KPBS (136 mM KCl, 10 mM KH2PO4, pH 7.25). The cells were centrifuged at 1000 x g for 2 min at 4°C, and the cell pellets were resuspended in 950 µL of KPBS, 25 µL of which was

used as a loading control. After homogenization of the remaining cells using a dounce homogenizer, the samples were centrifuged at 1000 x g for 2 min at 4°C. The resulting supernatant was then incubated with 100 µL of magnetic anti-FLAG beads for 15 minutes. The beads were captured using a magnet and washed three times with KPBS before being lysed with 100 uL of lysis buffer. The loading controls, as well as the various immunoprecipitates, were analyzed using Western blot analysis

Lysosomal pH Measurement. Lysosomal pH was determined as described previously (Zoncu et al.[57], 2011) with slight modifications. 1.0 x 106 sham shRNA expressing control, or SIRT1 knock down, MDA-MB-231 cells were treated with 50 µg/mL of Lysosensor yellow-blue Dextran® for 12 hours, before being amino acid starved for an additional 2 hours. The cells were then rinsed twice with PBS, and resuspended in physiological buffer (136mM NaCl, 2.5mM KCl, 2mM CaCl2, 1.3mM MgCl2, 5mM Glucose, 10mM HEPES pH 7.4), and transferred to individual wells of a black 96-well plate. Lysosensor fluorescence emission was recorded at 460 nm and 540 nm upon excitation at 360 nm using a BioTek Synergy 2 Plate Reader. To measure the lysosomal pH, the 460/540 fluorescence emission ratios were interpolated to a calibration curve that was established by resuspending the cells containing lysosensor in 200 µL aliquots of pH calibration buffers (145 mM KCl, 10 mM glucose, 1 mM MgCl2, and 20 mM of either HEPES, MES, or acetate supplemented with 10 µg/ml nigericin), buffered to pH ranging from 3.5 to 8.0.

Lysosomal pH Recovery Assay. Lysosomal pH was determined as described previously (Chen et al.[65], 2017) with slight modifications. Sham shRNA expressing control, and SIRT1 KD, MDA-MB-231 cells (5 × 103) plated in 24 well plates were treated with either DMSO, or 100 nM Bafilomycin-A, for 1 h, at which point the cells

were rinsed extensively with media and allowed to recover for 1 h. The cells were then treated with LysoTracker® Green DND 26 (Thermo Fisher) for 1 h, washed twice with PBS, and were lysed in 200 µL of RIPA buffer (10 mM Tris, 140 mM NaCl, 1% Triton X-100, 1 mM EDTA, 0.1% SDS, 0.1% sodium deoxycholate and 1 µg/ml each aprotinin and leupeptin). The fluorescence of each sample was measured in a 96-well plate using a BioTek Synergy 2 Plate Reader; EX: 485 nm and EM: 520 nm. The percent recovery was calculated as follows:

100% : DMSO for the whole duration of the assay

0%: Baf-A for the whole duration of the assay

$$\% \text{ recovery} = (AR - A0)/(A100 - A0)$$

Western Blot Analysis. The protein concentrations of cell, microvesicle, and exosome lysates, as well as of vesicle free media samples, were determined using the Bradford protein assay. The lysates were normalized by protein concentration, resolved by SDS-PAGE, and the proteins were transferred to PVDF membranes. Membranes were blocked with 5% bovine serum albumin (Sigma) in TBST (19 mM Tris Base, 2.7 mM KCl, 137 mM NaCl, and 0.5 % Tween-20) for 1 h and the membranes were incubated with the indicated primary antibodies overnight, followed by detection with HRP-conjugated secondary antibodies (Cell Signaling Technology) and exposure to ECL reagent (Pierce).

Immunofluorescence Microscopy. Cells grown on glass coverslips were treated as indicated, fixed and permeabilized with methanol. The slides were then blocked with 10% bovine serum albumin diluted in PBS. For each antibody used, the cells were incubated for 90 min using the following dilutions: CD63 (1:200, Abcam), LAMP1

(1:100, Cell Signaling Technologies), Cathepsin B (1:800, Cell Signaling Technologies), GFP (1:100, Cell Signaling Technologies). Anti-Mouse IgG-Alexa 488 Conjugate antibody (1:400, Thermo Fisher) and anti-Rabbit IgG-Alexa 568 Conjugate antibody (1:400, Thermo Fisher). DAPI (Sigma) was used to label nuclei, and conjugated Phalloidin (1:2000) was used to label actin. The cells were visualized with Super Resolution Structured Illumination Microscopy using a Zeiss Elyra Super Resolution Microscope with a 63x oil objective lens (Cornell University, Biotechnology Resource Center). Image processing and quantification was performed with ImageJ software.

Nanoparticle Tracking Analysis. The sizes and concentrations of EVs in a given sample were determined using a NanoSight NS300 (Malvern, Cornell NanoScale Science and Technology Facility) as described in Kreger et al.[47], 2016. Briefly, the samples were diluted in serum free RPMI-1640 and injected into the beam path to capture movies of EVs as points of diffracted light moving rapidly under Brownian motion. Five 45-s digital videos of each sample were taken and analyzed to determine the concentration and size of the individual EVs based on their movement, and then results were averaged together.

Electron Microscopy. Transmission Electron Microscopy (TEM) on exosomes was performed as described in Desrochers et al.[66], 2016. Briefly, 5 µL of an exosome preparation derived from either control or SIRT1 KD MDA-MB-231 cells were diluted in PBS, added to a carbon-coated 300-mesh copper grid, and then stained with 1.75% uranyl acetate. Once dry, the samples were imaged using the FEI T12 Spirit 120 kV Field Emission Transmission Electron Microscope at Cornell's Center for Materials Research (CCMR), supported by NSF MRSEC award number: NSF DMR-1120296.

Cathepsin B Activity Assay. The Magic Red substrate for the Cathepsin B Activity Assay Kit (Immunochem Technologies) was diluted in PBS to a 20X concentration. Then, 95 µL of concentrated conditioned media (prepared using 10 KDa centricons (Amicon)) collected from an equivalent number of either sham shRNA expressing control, or SIRT1 KD, MDA-MB 231 cells were added to each well of a 96-well plate containing 5 µL of 20X Magic Red. In some cases, 10 µM of CA-074 was added to the samples for 30 minutes. The resulting fluorescence that occurred over time was readout using a Cary Eclipse Fluorescence Spectrophotometer; EM: 530 nm and EX: 595 nm.

Cell Death Assays. MCF10AT1 cells grown in 6-well dishes were placed in serum-free medium supplemented with nothing (serum starved) or an equivalent amount (5.0 x 107 exosomes/mL) exosomes from sham shRNA expressing control, or SIRT1 KD, MDA-MB-231 cells. Approximately 40 h later, the cells were stained with DAPI to label nuclei. The cells were visualized by fluorescent microscopy and nuclear condensation and/or blebbing was used to identify dead or dying cells.

Wound Healing Assay. Confluent cultures of MCF10AT1 cells were placed in serum free medium supplemented with nothing, or equivalent amounts of exosomes (5.0 x 107 exosomes/mL) from control or SIRT1 KD MDA-MB-231 cells that had been left untreated, or were treated with either PBS or YM155, for 12 h. Wounds were then struck through the cells using a pipette tip and the medium on the cells was replaced. Approximately 8 h later, the cells were fixed with 4% paraformaldehyde and then imaged using phase contrast microscopy. The extend of wound closure for each condition was determined using ImageJ software.

Invasion Assay. Poly(dimethylsiloxane) (PDMS, Dow Corning) was cast onto a petri dish (150 mm) to form a 1.0 mm thick layer. Biopsy punches of 6 and 8 mm were generated in the PDMS to create a ring pattern. The PDMS rings were treated with plasma cleaner and covalently bond to a glass coverslip followed by treatment with 1% [v/v] polyethyleneimine (Sigma) and 0.1% [v/v] glutaraldehyde (Fisher). To generate spheroids of MCF10AT1 cells, the wells of a 96-well plate were coated with 50 μL of 1.5% agarose diluted in PBS to form a non-adhesive layer. 5 × 103 MCF10AT1, or GFP expressing MCF10AT1, cells were added to each well, and the plates were placed in a shaking incubator at 37°C overnight. The resulting spheroids that formed were individually selected using a glass pasteur pipette, mixed with collagen (Corning), and cast into the center of each PDMS ring. The samples were then subjected to consecutive temperature changes from ice cold, to room temperature, to 37°C at 15 min intervals. After the collagen solidified, each well was treated with various combinations of exosomes (5.0 x 107 exosomes/mL), VFM (400 μg/mL), and inhibitors, as indicated for 4 days and fixed with paraformaldehyde. Bright field images of the cells were taken every day and their media was changed every other day. The GFP expressing MCF10AT1 cells, and the collagen matrix adjacent to the cells, were subjected to fluorescent and second-harmonic generation (SHG) imaging microscopy, respectively. The extent of invasion was calculated as the area of sprouting and outgrowth for each spheroid.

Quantification and Statistical Analysis. Quantitative data are presented as means ± SD. All experiments were independently performed at least three times. Statistical significance was calculated by ANOVA (Tukey's test) for experiments involving comparing more than two conditions, and student's t test for experiments involving

comparing two conditions. Error bars represents the mean ± SD. ∗p ≤ 0.05, ∗∗p ≤ 0.01, ∗∗∗p<0.001, ∗∗∗∗p<0.0001, n.s. = non-significant.

Research Contributions

The author would like to acknowledge the following researchers at Cornell University for their help with this study: Lu Ling, for 3D invasion assays; Amrit Hingorani and Amdiel Clement, for their help in development of plasmids used in this study, Eric Johansen, for help with the endolysosomal IP assays; Xiaoyu Zhang, for SILAC experiments; and John Hartman, for electron microscopy images.

REFERENCES

1. Chalkiadaki A, Guarente L. The multifaceted functions of sirtuins in cancer. *Nat Rev Cancer*. 2015;**15**:608-624

2. Jing H, Lin H. Sirtuins in epigenetic regulation. *Chem Rev*. 2015;**115**:2350-2375.

3. Cohen HY, Miller C, Bitterman KJ, et al. Calorie restriction promotes mammalian cell survival by inducing the SIRT1 Deacetylase. *Science*. 2004;**305**:390-392

4. Lin SJ, Defossez PA, Guarente L. Requirement of NAD and SIR2 for life-span extension by calorie restriction in Saccharomyces cerevisiae. *Science*. 2000;**289**:2126-2128

5. Chung YR, Kim H, Park SY, et al. Distinctive role of SIRT1 expression on tumor invasion and metastasis in breast cancer by molecular subtype. *Hum Pathol*. 2015;**46**:1027-1035

6. Wu M, Wei W, Xiao X, et al. Expression of SIRT1 is associated with lymph node metastasis and poor prognosis in both operable triple-negative and non-triple-negative breast cancer. *Med Oncol*. 2012;**29**:3240-3249

7. Simic P, Williams E, Bell E, Gong J, Bonkowski M, Guarente L. SIRT1 suppresses the epithelial-to-mesenchymal transition in cancer metastasis and organ fibrosis. *Cell Rep*. 2013;**3**:1175-1186

8. Wang RH, Zheng Y, Kim HS, et al. Interplay among BRCA1, SIRT1, and Survivin during BRCA1-associated tumorigenesis. *Mol Cell*. 2008;**32**:11-20

9. Wang RH, Sengupta K, Li C, et al. Impaired DNA damage response, genome instability, and tumorigenesis in SIRT1 mutant mice. *Cancer Cell*. 2008;**14**:312-323

10. Desrochers LM, Antonyak MA, Cerione RA. Extracellular vesicles: satellites of information transfer in cancer and stem cell biology. *Dev Cell*. 2016;**37**:301-309

11. Antonyak MA, Li B, Boroughs LK, et al. Cancer cell-derived microvesicles induce transformation by transferring tissue transglutaminase and fibronectin to recipient cells. *Proc Natl Acad Sci*. 2011;**108**:4852-4857

12. Li B, Antonyak MA, Zhang J, Cerione RA. RhoA triggers a specific signaling pathway that generates transforming microvesicles in cancer cells. *Oncogene*. 2012;**31**:4740-4749

13. Kreger BT, Dougherty AL, Greene KS, Cerione RA, Antonyak MA.

Microvesicle cargo and function changes upon induction of cellular transformation. *J Biol Chem*. 2016;**291**:19774-19785.

14. Qu L, Ding J, Chen C, et al. Exosome-Transmitted lncARSR Promotes sunitinib resistance in renal cancer by acting as a competing endogenous RNA. *Cancer Cell*. 2016;**29**:653-668

15. Feng Q, Zhang C, Lum D, et al. A class of extracellular vesicles from breast cancer cells activates VEGF receptors and tumour angiogenesis. *Nat Commun*. 2017;**8**:14450

16. Zhao H, Yang L, Baddour J, et al. Tumor microenvironment derived exosomes pleiotropically modulate cancer cell metabolism. *Elife*. 2016;**5**:e10250

17. Costa-Silva B, Aiello NM, Ocean AJ, et al. Pancreatic cancer exosomes initiate pre-metastatic niche formation in the liver. *Nat Cell Biol*. 2015;**17**:1-7

18. Hoshino A, Costa-Silva B, Shen T-L, et al. Tumour exosome integrins determine organotropic metastasis. *Nature*. 2015;**527**:329-335

19. Miao Y, Li G, Zhang X, Xu H, Abraham SN. A TRP channel senses lysosome neutralization by pathogens to trigger their expulsion. *Cell*. 2015;**161**:1306-1319

20. Alvarez-Erviti L, Seow Y, Schapira AH, et al. Lysosomal dysfunction increases exosome-mediated alpha-synuclein release and transmission. *Neurobiol Dis*. 2011;**42**:360-367

21. Gocheva V, Joyce JA. Cysteine cathepsins and the cutting edge of cancer invasion. *Cell Cycle*. 2007;**6**:60-64

22. Mitrović A, Pečar Fonović U, Kos J. Cysteine cathepsins B and X promote epithelial-mesenchymal transition of tumor cells. *Eur J Cell Biol*. 2017;**96**:622-631

23. Shi L, Tang X, Qian M, et al. A SIRT1-centered circuitry regulates breast cancer stemness and metastasis. *Oncogene*. 2018;**37**:6299-6315

24. Varley KE, Gertz J, Roberts BS, et al. Recurrent read-through fusion transcripts in breast cancer. *Breast Cancer Res Treat*. 2014;**146**:287-297

25. Li W, Sahu D, Tsen F. Secreted heat shock protein-90 (Hsp90) in wound healing and cancer. *Biochim Biophys Acta - Mol Cell Res*. 2012;**1823**:730-741

26. Villarroya-Beltri C, Baixauli F, Gutiérrez-Vázquez C, Sánchez-Madrid F, Mittelbrunn M. Sorting it out: Regulation of exosome loading. *Semin Cancer Biol*. 2014;**28**:3-13

27. Li Z, Pei X-H, Yan J, et al. CUL9 Mediates the Functions of the 3M complex

and ubiquitylates Survivin to maintain genome integrity. *Mol Cell*. 2014;**54**:805-819

28. Abu-Remaileh M, Wyant GA, Kim C, et al. Lysosomal metabolomics reveals V-ATPase and mTOR-dependent regulation of amino acid efflux from lysosomes. *Science.* 2017;**358**:807-813.

29. Ostrowski M, Carmo NB, Krumeich S, et al. Rab27a and Rab27b control different steps of the exosome secretion pathway. *Nat Cell Biol*. 2010;**12**:19-30

30. Vanlandingham PA, Ceresa BP. Rab7 regulates late endocytic trafficking downstream of multivesicular body biogenesis and cargo sequestration. *J Biol Chem*. 2009;**284**:12110-12124

31. Bret Evers AM, Rodriguez-Navas C, Tesla RJ, Yu G, White III CL. Lipidomic and transcriptomic basis of lysosomal dysfunction in progranulin deficiency. *Cell Reports*. 2017;**20**:2565-2574

32. Kilpatrick BS, Eden ER, Hockey LN, Futter CE, Patel S. Methods for monitoring lysosomal morphology. *Methods Cell Biol*. 2015;**126**:1-19

33. Olson OC, Joyce JA. Cysteine cathepsin proteases: regulators of cancer progression and therapeutic response. *Nat Rev Cancer*. 2015;**15**:712-729.

34. Diwu Z, Chen CS, Zhang C, Klaubert DH, Haugland RP. A novel acidotropic pH indicator and its potential application in labeling acidic organelles of live cells. *Chem Biol*. 1999;**6**:411-418

35. Settembre C, Fraldi A, Medina DL, Ballabio A. Signals from the lysosome: a control centre for cellular clearance and energy metabolism. *Nat Rev Mol Cell Biol*. 2013;**14**:283-296

36. Lee JH, Yu WH, Kumar A, et al. Lysosomal proteolysis and autophagy require presenilin 1 and are disrupted by Alzheimer-related PS1 mutations. *Cell*. 2010;**141**:1146-1158

37. Meo-Evoli N, Almacellas E, Massucci FA, et al. V-ATPase: a master effector of E2F1-mediated lysosomal trafficking, mTORC1 activation and autophagy. *Oncotarget*. 2015;**6**:28057-28070

38. Sardiello M. Transcription factor EB: from master coordinator of lysosomal pathways to candidate therapeutic target in degenerative storage diseases. *Ann N Y Acad Sci*. 2016;**1371**:3-14

39. Bao J, Zheng L, Zhang Q, et al. Deacetylation of TFEB promotes fibrillar Aβ degradation by upregulating lysosomal biogenesis in microglia. *Protein Cell*. 2016;**7**:417-433

40. Peña-Llopis S, Vega-Rubin-de-Celis S, Schwartz JC, et al. Regulation of TFEB and v-ATPases by mTORC1. *EMBO J*. 2011;**30**:3242-3258

41. Sakamaki J, Wilkinson S, Hahn M, et al. Bromodomain protein BRD4 is a transcriptional repressor of autophagy and lysosomal function. *Mol Cell*. 2017;**66**:517-532

42. Schoenberg DR, Maquat LE. Regulation of cytoplasmic mRNA decay. *Nat Rev Genet*. 2012;**13**:246-259

43. Li Y, Zhou Y, Zheng J, et al. Downregulation of survivin inhibits proliferation and migration of human gastric carcinoma cells. *Int J Clin Exp Pathol*. 2015;**8**:1731-1736

44. Mckenzie JA, Liu T, Goodson AG, Grossman D. Survivin enhances motility of melanoma Cells by supporting Akt activation and α5 integrin upregulation. *Cancer Res.* 2010;**20**:7927-7937

45. Davidson SM, Vander Heiden MG. Critical functions of the lysosome in cancer biology. *Annu Rev Pharmacol Toxicol*. 2017;**57**:481-507

46. Costa-Silva B, Aiello NM, Ocean AJ, et al. Pancreatic cancer exosomes initiate pre-metastatic niche formation in the liver. *Nat Cell Biol*. 2015;**17**:816-826

47. Kreger B, Johansen E, Cerione R, Antonyak M. The enrichment of Survivin in exosomes from breast cancer cells treated with paclitaxel promotes cell survival and chemoresistance. *Cancers (Basel)*. 2016;**8**:111

48. Liégeois S, Benedetto A, Garnier J-M, Schwab Y, Labouesse M. The V0-ATPase mediates apical secretion of exosomes containing Hedgehog-related proteins in Caenorhabditis elegans. *J Cell Biol*. 2006;**173**:949-961

49. Poëa-Guyon S, Ammar MR, Erard M, et al. The V-ATPase membrane domain is a sensor of granular pH that controls the exocytotic machinery. *J Cell Biol*. 2013;**203**:283-298

50. Stransky LA, Forgac M. Amino Acid Availability Modulates Vacuolar H+-ATPase Assembly. *J Biol Chem*. 2015;**290**:27360-27369

51. Cotter K, Stransky L, McGuire C, Forgac M. Recent insights into the structure, regulation, and function of the V-ATPases. *Trends Biochem Sci*. 2015;**40**:611-622

52. Kallunki T, Olsen OD, Jäättelä M. Cancer-associated lysosomal changes: friends or foes? *Oncogene*. 2013;**32**:1995-2004

53. Shan P, Fan G, Sun L, et al. SIRT1 Functions as a negative regulator of eukaryotic poly(A)RNA transport. *Curr Biol*. 2017;**27**:2271-2284

54. Cohen HY. Calorie restriction promotes mammalian cell survival by inducing the SIRT1 deacetylase. *Science*. 2004;**305**:390-392

55. Kim D, Nguyen MD, Dobbin MM, et al. SIRT1 deacetylase protects against

neurodegeneration in models for Alzheimer's disease and amyotrophic lateral sclerosis. *EMBO J*. 2007;**26**:3169-3179

56. Min SW, Cho SH, Zhou Y, et al. Acetylation of tau inhibits its degradation and contributes to tauopathy. *Neuron*. 2010;**67**:953-966

57. Zoncu R, Bar-Peled L, Efeyan A, Wang S, Sancak Y, Sabatini DM. mTORC1 senses lysosomal amino acids through an inside-out mechanism that requires the vacuolar H^+-ATPase. *Science*. 2011;**334**:678-683

58. Stewart SA, Dykxhoorn DM, Palliser D, et al. Lentivirus-delivered stable gene silencing by RNAi in primary cells. *Rna*. 2003;**9**:493-501

59. Vaziri H, Dessain SK, Eaton EN, et al. hSIR2SIRT1 functions as an NAD-dependent p53 deacetylase. *Cell*. 2001;**107**:149-159

60. Walter DM, Venancio OS, Buza EL, et al. Systematic in vivo inactivation of chromatin- regulating enzymes identifies Setd2 as a potent tumor suppressor in lung adenocarcinoma. *Cancer Res*. 2017;**77**:1719-1729

61. Huang DW, Sherman BT, Lempicki RA. Systematic and integrative analysis of large gene lists using DAVID bioinformatics resources. *Nat Protoc*. 2008;**4**:44-57

62. Huang DW, Sherman BT, Lempicki RA. Bioinformatics enrichment tools: Paths toward the comprehensive functional analysis of large gene lists. *Nucleic Acids Res*. 2009;**37**:1-13

63. Zhang X, Khan S, Jiang H, et al. Identifying the functional contribution of the defatty-acylase activity of SIRT6. *Nat Chem Biol*. 2016;**12**:614-620

64. Zhang X, Spiegelman NA, Nelson OD, Jing H, Lin H. SIRT6 regulates Ras-related protein R-Ras2 by lysine defatty-acylation. *Elife*. 2017;**6**:e25158

65. Chen Y-C, Backus KM, Merkulova M, et al. Covalent modulators of the vacuolar ATPase. *J Am Chem Soc*. 2017;**139**:639-642

66. Desrochers LM, Bordeleau F, Reinhart-King CA, Cerione RA, Antonyak MA. Microvesicles provide a mechanism for intercellular communication by embryonic stem cells during embryo implantation. *Nat Commun*. 2016;**7**:11958

CHAPTER 3

SIRT1 Regulates V-ATPase Expression and Lysosomal Function Through the RNA Binding Protein IGF2BP2

The downregulation of the NAD^+-dependent deacetylase SIRT1 that occurs in aggressive breast cancer cells leads to their increased secretion of exosomes and cathepsins, resulting in enhanced invasive activity and metastatic spread. These effects are due to a decreased half-life for the RNA transcript encoding the ATP6V1A subunit of the v-ATPase, thus impairing lysosomal function. Here we show that SIRT1 stabilizes ATP6V1A transcript levels by catalyzing the deacetylation of insulin-like growth factor 2 mRNA binding protein 2 (IGF2BP2). This prevents IGF2BP2 from recruiting the nuclease XRN2 that degrades the RNA transcript encoding ATP6V1A. These findings identify a previously unrecognized role for SIRT1 in maintaining RNA stability and lysosomal function by ensuring the proper expression of a major subunit of the v-ATPase.

Introduction

Lysosomes are the main degradative organelle in mammalian cells, and their impaired function gives rise to several different physiological processes and pathological disorders, including aging[1], neurodegeneration[2,3], and cancer[4–6]. However, the mechanisms that regulate lysosomal activity in these different contexts are still unclear. We recently showed that downregulation of SIRT1 expression in breast cancer cells results in the production of a secretome that strongly promotes cell survival, as well as cell migration and invasion[5]. We further determined that these effects were caused by reducing the stability of the transcript encoding ATP6V1A, the catalytic component of the v-ATPase that is essential for maintaining the highly acidic environment of lysosomes. Thus, when SIRT1 expression is downregulated in aggressive breast cancer cells, bio-active materials that would normally be targeted to lysosomes are instead released from the cells as exosomes and soluble proteins that collectively promote aggressive phenotypes. However, the mechanism by which SIRT1 regulates ATP6V1A mRNA levels is still unknown. Here, we show that SIRT1 is modulating the RNA stability of the ATP6V1A transcript through deacetylating IGF2BP2, an RNA binding protein that binds to the 3'-untranslated region (UTR) of this transcript. Mechanistically, acetylation of IGF2BP2, under conditions where SIRT1 is downregulated, results in recruitment of the exonuclease XRN2, which promotes the degradation of the ATP6V1A mRNA.

Results

SIRT1 downregulation promotes tumor progression *in vivo*

To further demonstrate the consequences of reduced SIRT1 function in breast cancer progression, we used the PyMT mouse model of breast cancer. PyMT-positive mice rapidly develop mammary tumors, and they frequently metastasize to the lung[7] (**Figure 3.1A**). Primary mammary tumors were collected from these mice at various

time-points after they were detected by palpation (from 8-14 weeks). The tumor samples were lysed and Western blotted for SIRT1. **Figure 3.1B** shows SIRT1 expression decreased during tumor progression (top panel). Culturing MDA-MB-231 breast cancer cells in suspension, in order to mimic the non-adherent growth of aggressive tumors (**Figure 3.1C**), also resulted in decreased SIRT1 expression (**Figure 3.1D**).

Consistent with our previous findings, reduced SIRT1 expression was accompanied by a corresponding decrease in ATP6V1A levels in the mammary tumors (**Figure 3.1B**, middle panel). Moreover, treatment of PYMT mice with the SIRT1 inhibitor, EX-527[8], also resulted in mammary tumors with decreased expression of ATP6V1A (**Figure 3.1E**). To investigate if inhibition of SIRT1 impacts the generation of exosomes *in vivo*, we isolated the exosomes present in serum samples collected from PyMT-positive mice, as well as from control (wild-type) animals. **Figure 3.1F** shows that exosome preparations from PyMT-positive mice are enriched in the exosomal marker CD9[9], while being devoid of any cytosolic contaminants as indicated by the absence of IκBα[10]. Similar to what we observed in our previous studies[5], exosomes collected from the serum of PYMT-mice treated with EX-527 showed a significant enrichment of ubiquitinated proteins, when compared to exosomes collected from the serum of control animals (**Figure 3.1G**).

Next, we determined whether altering SIRT1 activity in PyMT-positive female mice would enhance tumor growth, as well as promote the ability of the tumor cells to colonize in the lungs. Upon the detection of palatable tumors, the mice were administered either vehicle alone or EX-527, bi-weekly for 4 months, at which point they were sacrificed and the primary tumors that formed, and the lungs from the animals, were harvested. Tumors were readily detected in the mammary gland of the vehicle-control treated animals, as expected (**Figure 3.1H**). However, the tumors that

Figure 3.1 SIRT1 downregulation promotes tumor progression *in vivo.*
(A) Scheme illustrating the mouse model (PyMT) and treatment conditions. (B) Western blot analysis of SIRT1 and ATP6V1A levels in PyMT tumors that were collected at different ages of PyMT mouse. β-Actin was used as loading control. (C) Scheme (left) depicting the nonadherent stage in tumor progression. Brightfield image (right) of MDA-MB-231 cells grown in ultra-low attachment conditions. (D) Western blot analysis of SIRT1 and β-Actin in the whole cell lysates (WCL) of MDA-MB-231 cells grown under adherent or nonadherent conditions. (E) Western blot analysis of ATP6V1A and β-Actin levels in PyMT mice that were treated with vehicle or EX- 527 (14 mg/Kg). (F) Western blot analysis of CD9, Flottilin-2, and IKBα levels in tumor extracts and extracellular vesicles collected from mammary tumors and serum respectively. (G) Western blot analysis of ubiquitinated proteins and Flotillin-2 levels in extracellular vesicles collected from the serum of PyMT mice in (E). (H) Total tumor mass (top) and images (bottom) of tumors collected from PyMT mice in (E). (I) Histological images (left) of the lungs of the PyMT mice in (E) and quantification (right) of their metastatic lung nodules.

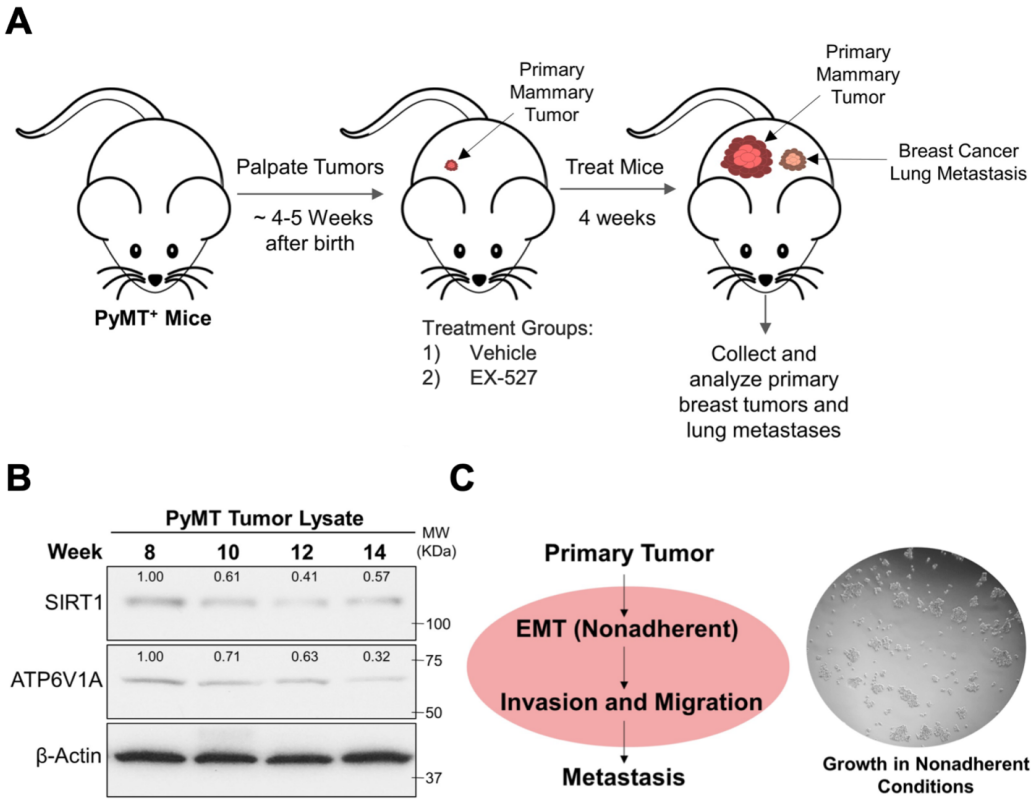
A
Primary Mammary Tumor
Primary Mammary Tumor
Breast Cancer Lung Metastasis
Palpate Tumors
~ 4-5 Weeks after birth
Treat Mice
4 weeks
PyMT+ Mice
Treatment Groups:
1) Vehicle
2) EX-527
Collect and analyze primary breast tumors and lung metastases
B
PyMT Tumor Lysate
Week 8 10 12 14
MW (KDa)
SIRT1
1.00 0.61 0.41 0.57
ATP6V1A
1.00 0.71 0.63 0.32
β-Actin
100
75
50
37
C
Primary Tumor
EMT (Nonadherent)
Invasion and Migration
Metastasis
Growth in Nonadherent Conditions
D
MDA-MB-231 WCL
Adh Non-adh
MW (KDa)
SIRT1
β-Actin
100
37
E
Tumor Lysates
Vehicle EX-527
MW (KDa)
ATP6V1A
1.00 0.33
β-Actin
75
50
37

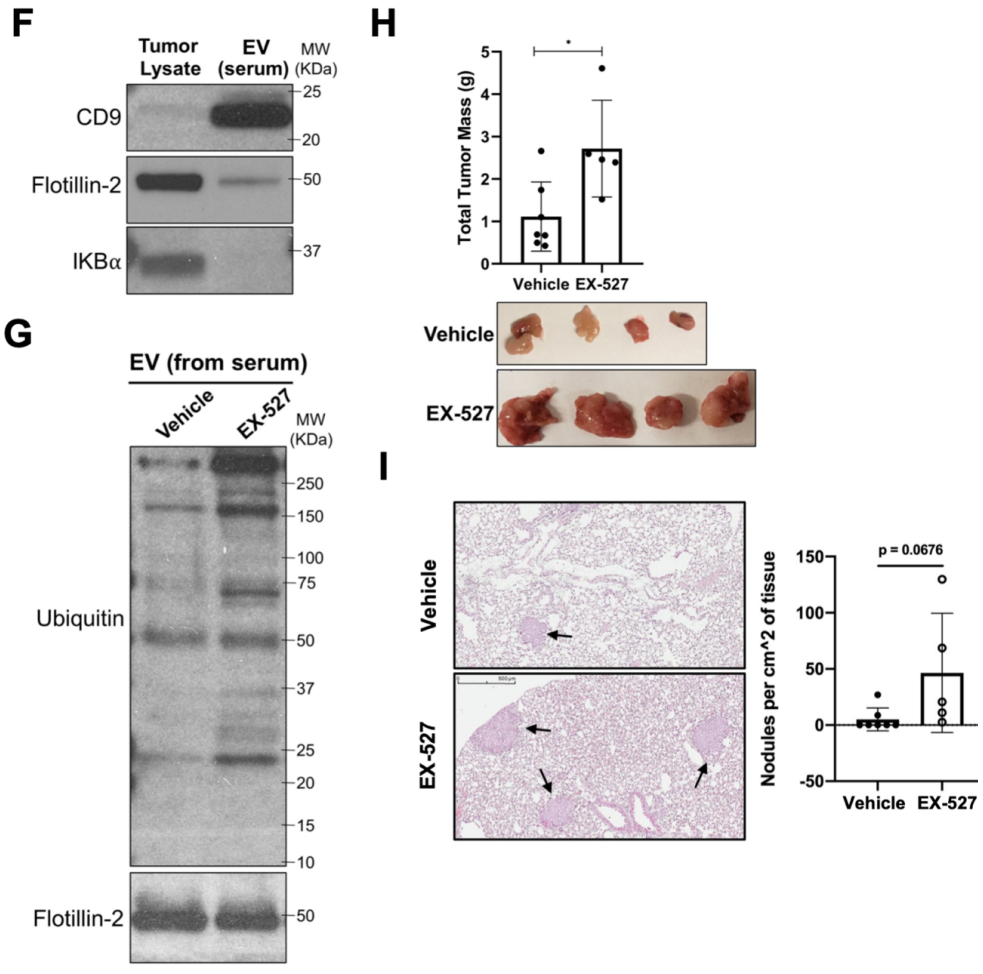
F
Tumor Lysate
EV (serum)
MW (KDa)
CD9
Flotillin-2
IKBα
25
20
50
37
G
EV (from serum)
Vehicle
EX-527
MW (KDa)
Ubiquitin
Flotillin-2
250
150
100
75
50
37
25
20
15
10
50
H
Total Tumor Mass (g)
Vehicle
EX-527
I
Vehicle
EX-527
Nodules per cm^2 of tissue
p = 0.0676

formed in the PyMT mice treated with EX-527 were much larger. The lungs from these same mice were also analyzed for metastatic spread. Inhibiting SIRT1 activity with EX-527 resulted in a significant increase in the number of metastatic nodules detected in PyMT-positive mice, compared to the vehicle-control treated animals (**Figure 3.1I**).

IGF2BP2 Binds to the 3'UTR of ATP6V1A Transcript and Mediates the Effect of SIRT1 Downregulation on ATP6V1A Expression

Given the importance of SIRT1 in regulating lysosomal function to produce a secretome that promotes invasion and metastasis, we set out to better understand the mechanistic basis by which SIRT1 influences the stability of the ATP6V1A transcript. To address this question, we took advantage of our previous finding that a ATP6V1A transcript which lacked its 3' untranslated region (3'UTR) was not degraded under conditions where SIRT1 was depleted from cells, suggesting that the 3'UTR of this transcript mediated its degradation. Therefore, a biotinylated form of the 3'UTR of the ATP6V1A transcript was generated and incubated with extracts collected from SIRT1 knockdown cells (**Figure 3.2A**). The biotinylated 3'UTR construct was precipitated using streptavidin-coated beads, and the proteins that associated with the construct were identified by mass spectrometry. One protein, which bound preferentially to the 3'UTR of ATP6V1A in extracts collected from cells depleted of SIRT1, was the insulin-like growth factor 2 mRNA binding protein 2 (IGF2BP2). Increases in the expression of this protein have indeed been shown to promote the progression of multiple cancer types[11–15] (**Figure 3.2B**). An analysis of the enhanced Crosslinking Immunoprecipitation (eCLIP) data[16] for IGF2BP2 in fact predicted that it would bind preferentially to the 3'UTR of ATP6V1A transcript, compared to its coding region (**Figure 3.2C**). Similar to previous reports, we also noticed that IGF2BP2 have multiple translation initiation sites and thus it appears as multiple bands in SDS-

Figure 3.2 IGF2BP2 binds to the 3'UTR of ATP6V1A transcript and mediates the effect of SIRT1 downregulation on ATP6V1A expression.
(A) Scheme illustrating the strategy used to identify the RBP that binds the 3'UTR of the ATP6V1A transcript. (B) Silver-stains of the eluted proteins from (A), resolved by SDS- PAGE. The region in red was cropped, digested and analyzed with mass spectrometry to determine the identity of the protein corresponding to this region. (C) eCLIP analysis of the binding of IGF2BP2 to the ATP6V1A transcript. (D) Western blot analysis of IGF2BP2 in streptavidin pulldowns of biotinylated probes, containing different segments of the 3'UTR of ATP6V1A transcript, following their incubation with whole cell extracts. (E) RT-qPCR was performed to determine the relative mRNA levels of ATP6V1A co-immunoprecipitated with anti-FLAG antibody in cells expressing FLAG-tagged IGF2BP2 and QKI5. (F) Western blot analysis of ATP6V1A, SIRT1, and IGF2BP2 levels in WCL of sham-shRNA-expressing control, SIRT1 KD, as well as SIRT1 and IGF2BP2 KD cells. (G) RT-qPCR was performed to determine ATP6V1A transcript levels (relative to actin controls) in sham-shRNA-expressing control (CTRL), SIRT1 KD, as well as SIRT1 and IGF2BP2 KD cells.

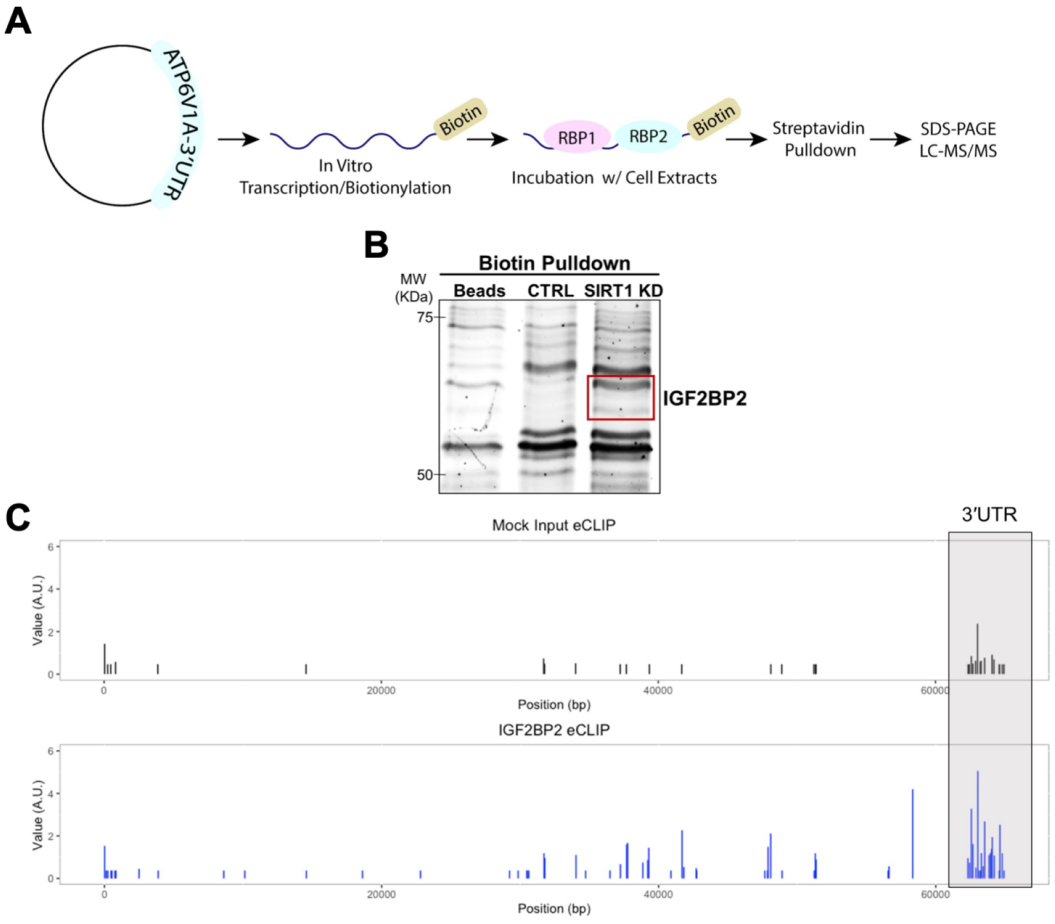
A
ATP6V1A-3'UTR
Biotin
In Vitro
Transcription/Biotionylation
RBP1
RBP2
Biotin
Incubation w/ Cell Extracts
Streptavidin
Pulldown
SDS-PAGE
LC-MS/MS
B
Biotin Pulldown
MW
(KDa)
Beads
CTRL
SIRT1 KD
75
50
IGF2BP2
C
Mock Input eCLIP
3'UTR
Value (A.U.)
Position (bp)
IGF2BP2 eCLIP
Value (A.U.)
Position (bp)

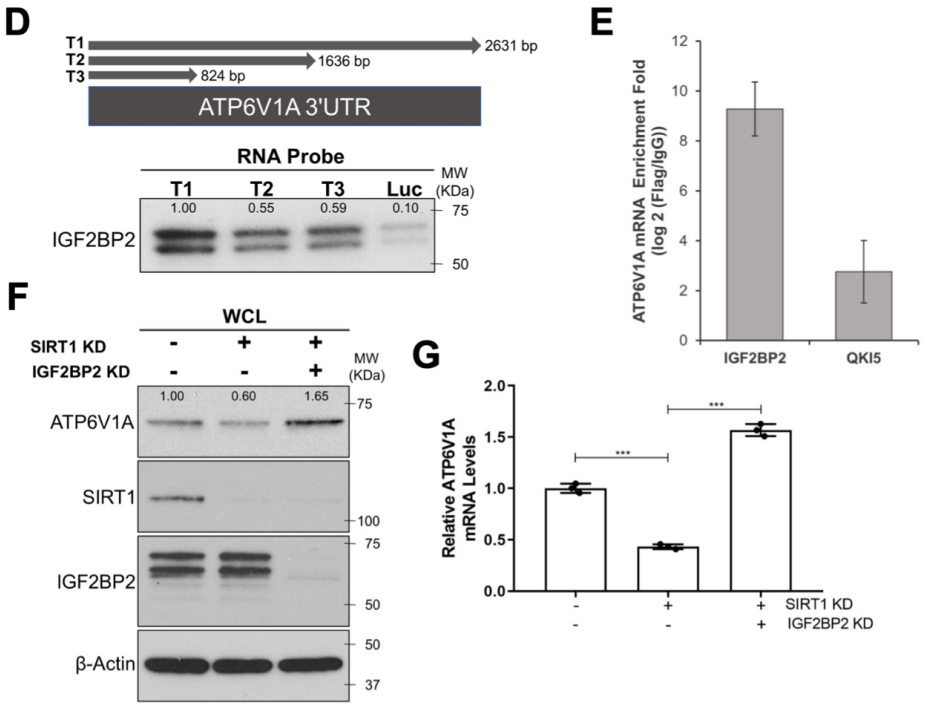
D
T1
T2
T3
2631 bp
1636 bp
824 bp
ATP6V1A 3'UTR
RNA Probe
T1
T2
T3
Luc
MW (KDa)
1.00
0.55
0.59
0.10
75
50
IGF2BP2
E
ATP6V1A mRNA Enrichment Fold (log 2 (Flag/IgG))
12
10
8
6
4
2
0
IGF2BP2
QKI5
F
WCL
SIRT1 KD
IGF2BP2 KD
MW (KDa)
1.00
0.60
1.65
ATP6V1A
SIRT1
IGF2BP2
β-Actin
75
100
75
50
50
37
G
Relative ATP6V1A mRNA Levels
2.0
1.5
1.0
0.5
0.0
***
***
SIRT1 KD
IGF2BP2 KD

PAGE[17]. *In vitro* pull-down assays using various truncations of the ATP6V1A 3'UTR further demonstrated that IGF2BP2 binds with the highest affinity to the full-length 3'UTR construct (2631 bp)(**Figure 3.2D**, T1 construct), although it still exhibited some capability for binding to a construct that consists of only the first 824 bp of the 3'UTR (**Figure 3.2D**, T3 construct). Additionally, when immunoprecipitations using a FLAG antibody were performed on lysates from cells ectopically expressing FLAG-tagged forms of either IGF2BP2 or the RNA binding protein Quaking (QKI5) whose homologue was shown to regulate ATP6V1A (vha-13) expression in *C. elegans*[18], there was a 9-fold enrichment of the ATP6V1A transcript that immunoprecipitated with FLAG-tagged IGF2BP2, compared to FLAG-tagged QKI5 (**Figure 3.2E**).

We examined whether IGF2BP2 has a role in mediating the degradation of the ATP6V1A transcript that accompanies the loss of SIRT1 expression. Control and SIRT1-depleted MDA-MB-231 breast cancer cells were treated with control shRNA or IGF2BP2 shRNA. **Figure 3.2F** shows that IGF2BP2 expression was reduced in these cells by at least 90% (last lane). We found that knocking-down IGF2BP2 in cells lacking SIRT1 fully restored both the protein and transcript levels for ATP6V1A (**Figure 3.2F**, top panel, and **Figure 3.2G**).

IGF2BP2 Knockdown Rescues the Effect of SIRT1 Downregulation

We next sought to investigate whether knocking-down IGF2BP2 could reverse the effects that accompany the knock-down of SIRT1 in cells, namely, the increased release of exosomes enriched in ubiquitinated proteins, as well as the secretion of soluble lysosomal hydrolases (e.g. Cathepsin B). Using density-gradient ultracentrifugation to isolate exosomes from SIRT1-depleted cells (**Figure 3.3A**), we first confirmed that ubiquitinated proteins were indeed enriched in the fraction that contained the canonical exosome marker, CD63[9], as well as the general EV marker,

Figure 3.3 IGF2BP2 knockdown rescues the effect of SIRT1 downregulation. (A) Scheme illustrating the strategy used to isolate exosome pellets based on density gradient centrifugation. (B) Western blot analysis of ubiquitinated proteins, CD63, Flotillin-2, and ubiquitinated histone H2A (UB-H2A) in fractions of exosome pellets collected from SIRT1 depleted cells by density gradient centrifugation. (C) Western blot analysis of ubiquitinated proteins and UB-H2A in exosomes, which were derived from SIRT1 depleted cells, and were left untreated, or treated with trypsin in the presence and absence of Triton-X-100. (D) Western blot analysis of ubiquitinated proteins in exosomes derived from sham- shRNA-expressing control, SIRT1 KD, as well as SIRT1 and IGF2BP2 KD cells. (E) Western blot analysis of Cathepsin B in vesicle-free media (VFM) collected from shRNA-expressing control, SIRT1 KD, as well as SIRT1 and IGF2BP2 KD cells.

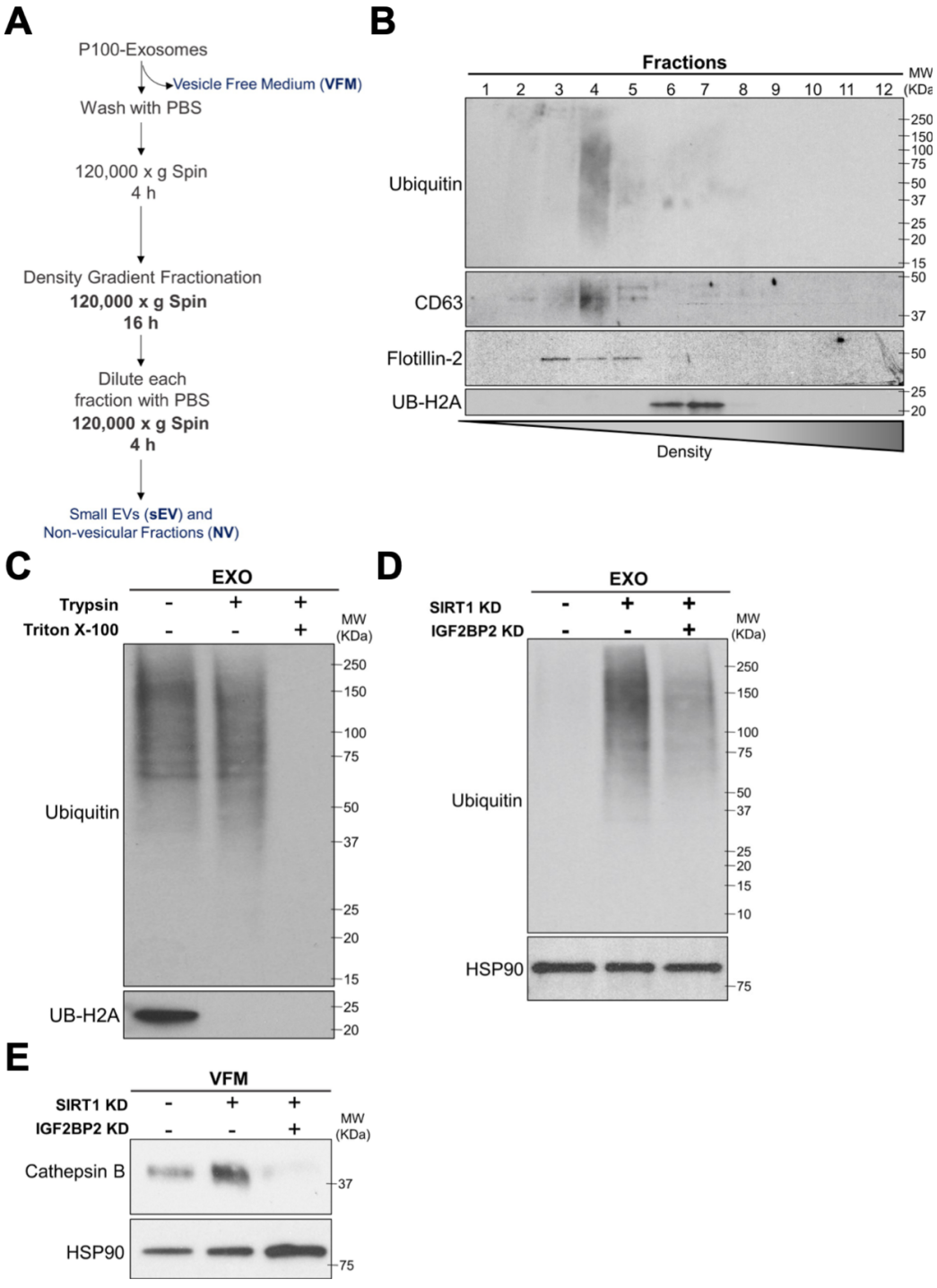
A
P100-Exosomes
Vesicle Free Medium (VFM)
Wash with PBS
120,000 x g Spin
4 h
Density Gradient Fractionation
120,000 x g Spin
16 h
Dilute each
fraction with PBS
120,000 x g Spin
4 h
Small EVs (sEV) and
Non-vesicular Fractions (NV)
B
Fractions
1 2 3 4 5 6 7 8 9 10 11 12
MW (KDa)
Ubiquitin
CD63
Flotillin-2
UB-H2A
Density
C
EXO
Trypsin
Triton X-100
MW (KDa)
Ubiquitin
UB-H2A
D
EXO
SIRT1 KD
IGF2BP2 KD
MW (KDa)
Ubiquitin
HSP90
E
VFM
SIRT1 KD
IGF2BP2 KD
MW (KDa)
Cathepsin B
HSP90

Flotillin-2 (**Figure 3.3B**). Consistent with previous reports[19], which suggest that secreted histones are not associated with exosomes, we also observed that ubiquitinated histones were not detected in the CD63 or Flotillin-2-containing fractions (**Figure 3.3B**). We also found that the ubiquitinated proteins detected in the exosome fractions were protected from protease digestion, whereas the ubiquitinated histones were not (**Figure 3.3C**). Knocking down IGF2BP2 from cells lacking SIRT1 strongly reduced the amount of ubiquitinated proteins detected in the exosomes shed by these cells (**Figure 3.3D**). Likewise, the levels of Cathepsin B secreted in the medium by SIRT1 depleted cells, were reduced back to the control levels (**Figure 3.3E**).

IGF2BP2 is Deacetylated by SIRT1

Because SIRT1 is a lysine deacylase, we examined whether IGF2BP2 was a substrate for SIRT1, such that its acylation would be increased under conditions where SIRT1 expression was reduced. Indeed, when IGF2BP2 was immunoprecipitated from SIRT1 knock-down cells and analyzed by mass spectrometry, lysine residue 530 was identified as a potential acetylation site (**Figure 3.4A**). Western blot analysis performed on the same immunoprecipitated samples, using an antibody that detects acetyl moieties, showed that IGF2BP2 was acetylated to a greater extent in cells where SIRT1 expression was knocked down (**Figure 3.4B**). However, changing lysine 530 to an arginine residue significantly decreased the amount of acetylated FLAG-tagged IGF2BP2 detected in SIRT1 knock down cells (**Figure 3.4B**). In order to further confirm that acetylation of endogenous IGF2BP2 is regulated by SIRT1, immunoprecipitations using an acetyl lysine antibody was performed on cell lysates collected from control and SIRT1 knock-down cells (**Figure 3.4C**, left panel). The results of this experiments showed that more IGF2BP2 was

Figure 3.4 IGF2BP2 is deacetylated by SIRT1.
(A) Mass spectroscopy profile of the acetylated peptide that was identified in proteins immunoprecipitated with an anti-FLAG antibody in cells expressing FLAG-tagged IGF2BP2. This peptide corresponds to the KH4 domain of IGF2BP2. (B) (top) Western blot analysis of acetylated lysine residues, SIRT1, and FLAG-tagged proteins, immunoprecipitated from cells expressing IGF2BP2 Wildtype (WT), or the IGF2BP2 (K530R) mutant, under sham- shRNA expressing control and SIRT1 KD conditions. (bottom) Western blot analysis of SIRT1 in the WCL of the same cells. CNOT1 was used as a loading control. (C) (left) Western blot analysis of (left) acetylated lysine residues and (right) IGF2BP2 from the WCL and the immunoprecipitates obtained with an anti-acetyl lysine antibody. (D) Position of K530 (pink) within the KH4 domain of IGF2BPs (PDB: 2N8M); the GXXG loop is shown in cyan and RNA is shown in orange. (E) RT-qPCR was performed to determine the relative mRNA levels of ATP6V1A co-immunoprecipitated with anti-FLAG antibody from cells expressing FLAG tagged IGF2BP2 Wildtype (WT), IGF2BP2 KH4 domain deleted (ΔKH4), or the IGF2BP2 (K530R) mutant, under sham-shRNA expressing control and SIRT1 KD conditions. Bottom: Western blot analysis of SIRT1 and FLAG-tagged proteins in the same cells.

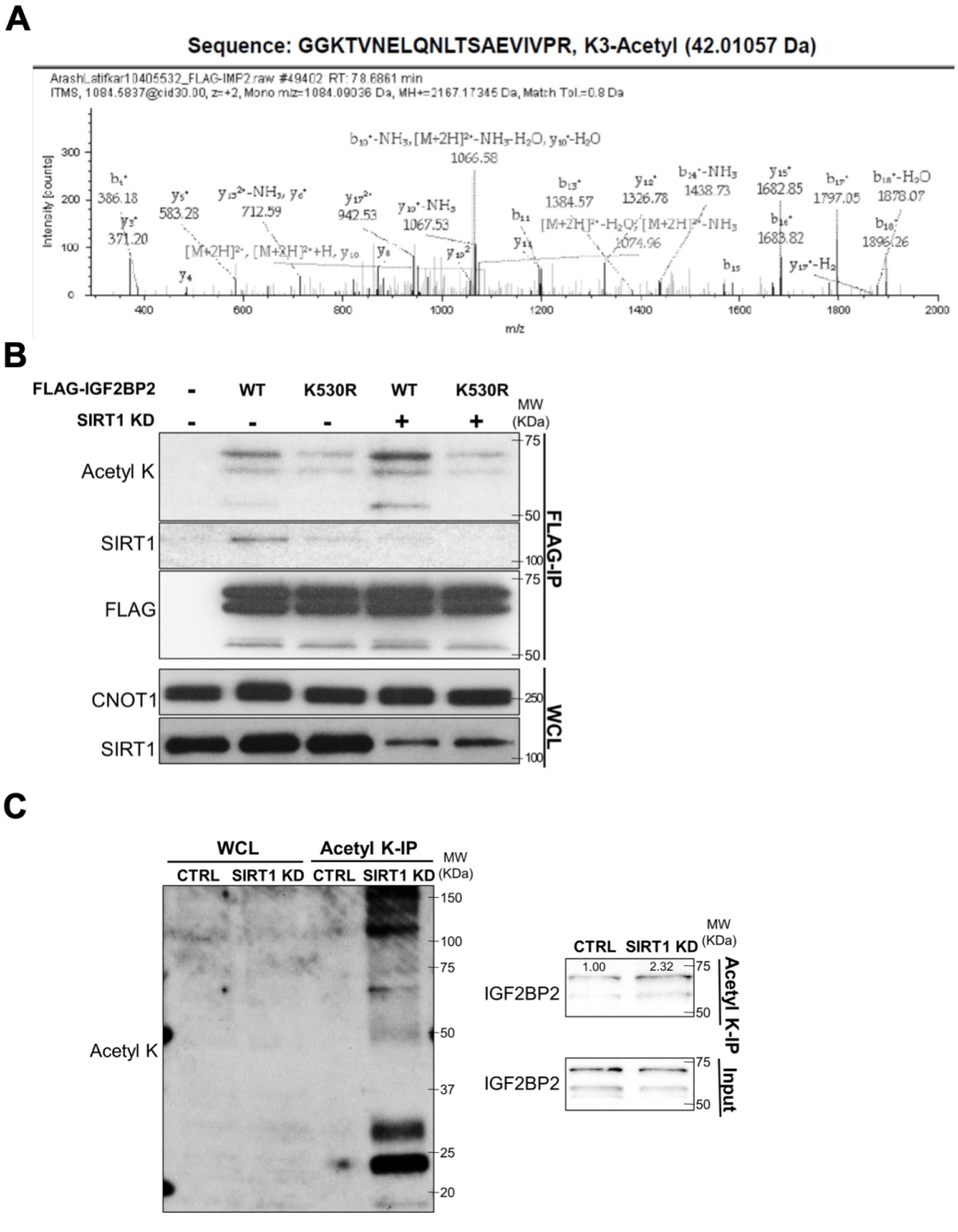
A
Sequence: GGKTVNELQNLTSAEVIVPR, K3-Acetyl (42.01057 Da)
ArashLatifkar10405532_FLAG-IMP2.raw #49402 RT: 78.6861 min
ITMS, 1084.5837@cid30.00, z=+2, Mono m/z=1084.09036 Da, MH+=2167.17345 Da, Match Tol.=0.8 Da
Intensity [counts]
m/z
B
FLAG-IGF2BP2
SIRT1 KD
WT
K530R
MW (KDa)
Acetyl K
SIRT1
FLAG
CNOT1
FLAG-IP
WCL
C
WCL
Acetyl K-IP
CTRL
SIRT1 KD
Acetyl K
IGF2BP2
Acetyl K-IP
Input

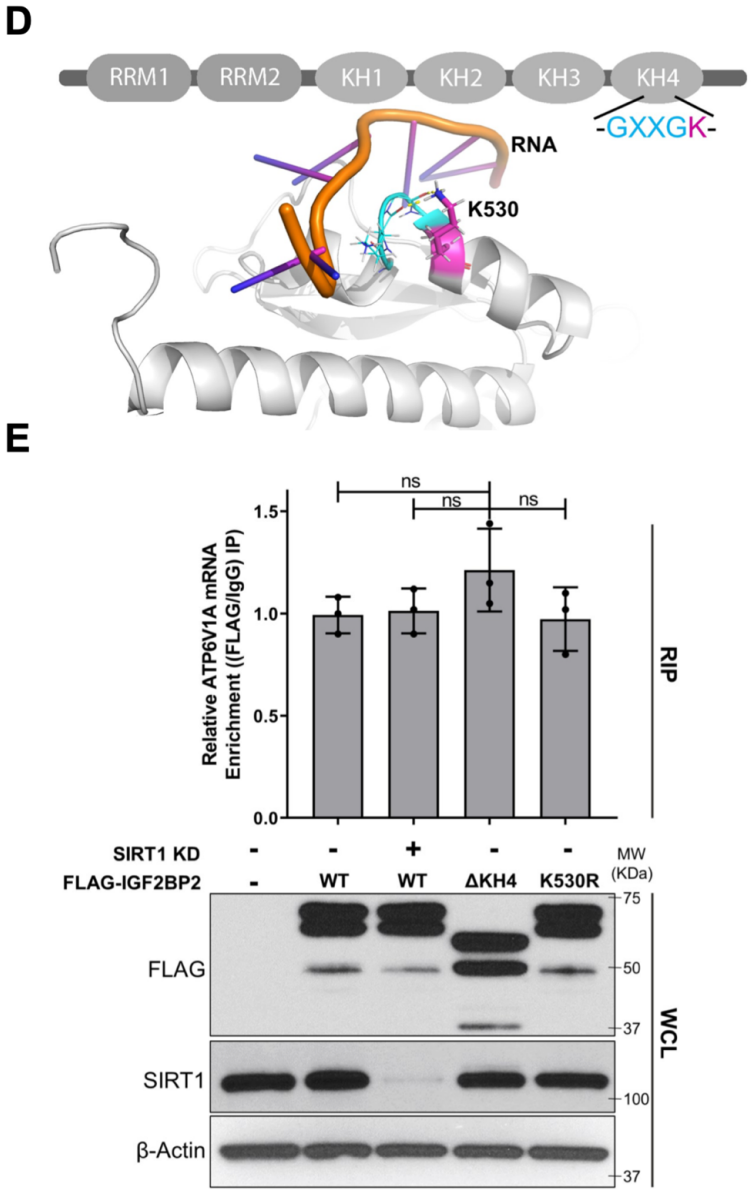
D
RRM1
RRM2
KH1
KH2
KH3
KH4
-GXXGK-
RNA
K530
E
ns
ns
ns
Relative ATP6V1A mRNA Enrichment ((FLAG/IgG) IP)
1.5
1.0
0.5
0.0
RIP
SIRT1 KD
FLAG-IGF2BP2
-
-
+
-
-
-
WT
WT
ΔKH4
K530R
MW (KDa)
FLAG
SIRT1
β-Actin
75
50
37
100
37
WCL

precipitated with this antibody from extracts from SIRT1 depleted cells, compared to control cells (**Figure 3.4C**, right panel).

Lysine 530 is located in the last of six RNA-binding regions on the IGF2BP2 protein, within a domain referred to as KH4[20] (**Figure 3.4D**). Analysis of the X-ray crystal structure of a protein highly related to IGF2BP2, specifically, Zip-code Binding Protein 1 (ZBP1)[21], showed that the analogous lysine residue in ZBP1 immediately follows the canonical RNA binding -GXXG- motif of KH domains and interacts with the -GXXG- loop through the positively charged lysine (**Figure 3.4D**). Thus, we initially suspected that the acetylation of K530 in IGF2BP2 would alter its ability to bind RNA (i.e. the ATP6V1A transcript). RNA immunoprecipitation assays were carried-out to determine how well IGF2BP2, or mutant forms of IGF2BP2 that either cannot be acetylated (IGF2BP2 K530R) or lack the KH4 domain, bound to the ATP6V1A transcript. **Figure 3.4E** shows that the infected cells expressed essentially equivalent amounts of each these constructs, and that they all exhibited a similar capacity for binding the ATP6V1A transcript (**Figure 3.4E**, graph).

XRN2 Binds to Acetylated IGF2BP2 and Degrades ATP6V1A mRNA

These findings suggested that the acetylation of IGF2BP2 may contribute to the destabilization of the ATP6V1A transcript by recruiting another protein(s) that catalyzes RNA degradation. We therefore searched for proteins that co-immunoprecipitated with IGF2BP2 in cells depleted of SIRT1, by mass spectrometry, and identified several potential binding partners that have been reported to play roles in different aspects of RNA processing (**Figure 3.5A**). Among these proteins was the 5'-3' exonuclease 2 (XRN2), whose ability to bind to ectopically expressed IGF2BP2 was enhanced under conditions where SIRT1 was knocked down (**Figure 3.5B**). The same was not true for the Y-box containing protein 1 (YBX1) (**Figure 3.5B**). We then

Figure 3.5 XRN2 binds to acetylated IGF2BP2 and degrades ATP6V1A mRNA.

(A) Table listing the IGF2BP2 interacting proteins that have been previously shown to regulate RNA stability. The proteins are ranked based on their peptide spectrum matches (PSM). (B) Western blot analysis of XRN2, YBX1, and FLAG-tagged proteins in the WCL, and proteins immunoprecipitated with anti-FLAG antibody, from cells expressing FLAG-tagged IGF2BP2 under sham-shRNA expressing control and SIRT1 KD conditions. (C) Western blot analysis (top) and quantification (bottom) of XRN2 co-immunoprecipitated with anti-FLAG antibody from cells expressing FLAG tagged IGF2BP2 Wildtype (WT), IGF2BP2 KH4 domain deleted (ΔKH4), or the IGF2BP2 (K530R) mutant, under sham-shRNA expressing control and SIRT1 KD conditions. (D) RT-qPCR was performed to determine ATP6V1A transcript levels (relative to actin controls) in sham-shRNA- expressing control (CTRL), CNOT1 KD, XRN2 KD, and IGF2BP2 KD cells depleted of SIRT1. (E) Western blot analysis of ATP6V1A, SIRT1, XRN2, and YBX1 in sham-shRNA-expressing control (CTRL), SIRT1 KD, SIRT1 and YBX1 KD, as well as SIRT1 and XRN2 KD cells. (F) Western blot analysis of ubiquitinated proteins in exosomes derived from sham-shRNA-expressing control, SIRT1 KD, as well as SIRT1 and XRN2 KD cells. (G) Nanoparticle tracking analysis (NTA) was performed on the conditioned media collected from an equivalent number of serum-starved sham-shRNA-expressing CTRL, SIRT1 KD, SIRT1 and IGF2BP2 KD, as well as SIRT1 and XRN2 KD cells. (H) Quantification of exosomes generated for each of the conditions in (G). (I) Western blot analysis of Cathepsin B in vesicle-free media (VFM) collected from shRNA-expressing control, SIRT1 KD, as well as SIRT1 and IGF2BP2 KD cells.

A

Protein	# PSMs
YBX1	49
XRN2	31
KHSRP	28
SND1	24
DIS3L2	6
RRP44	4

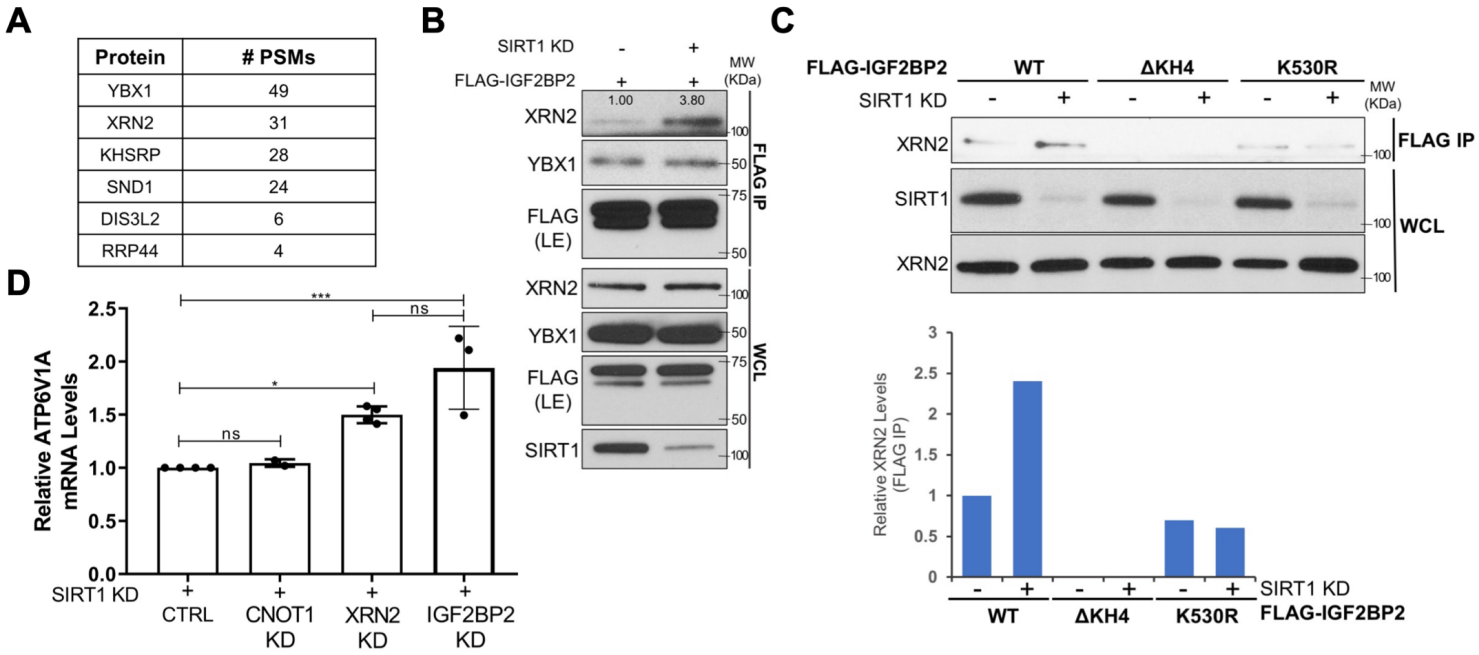

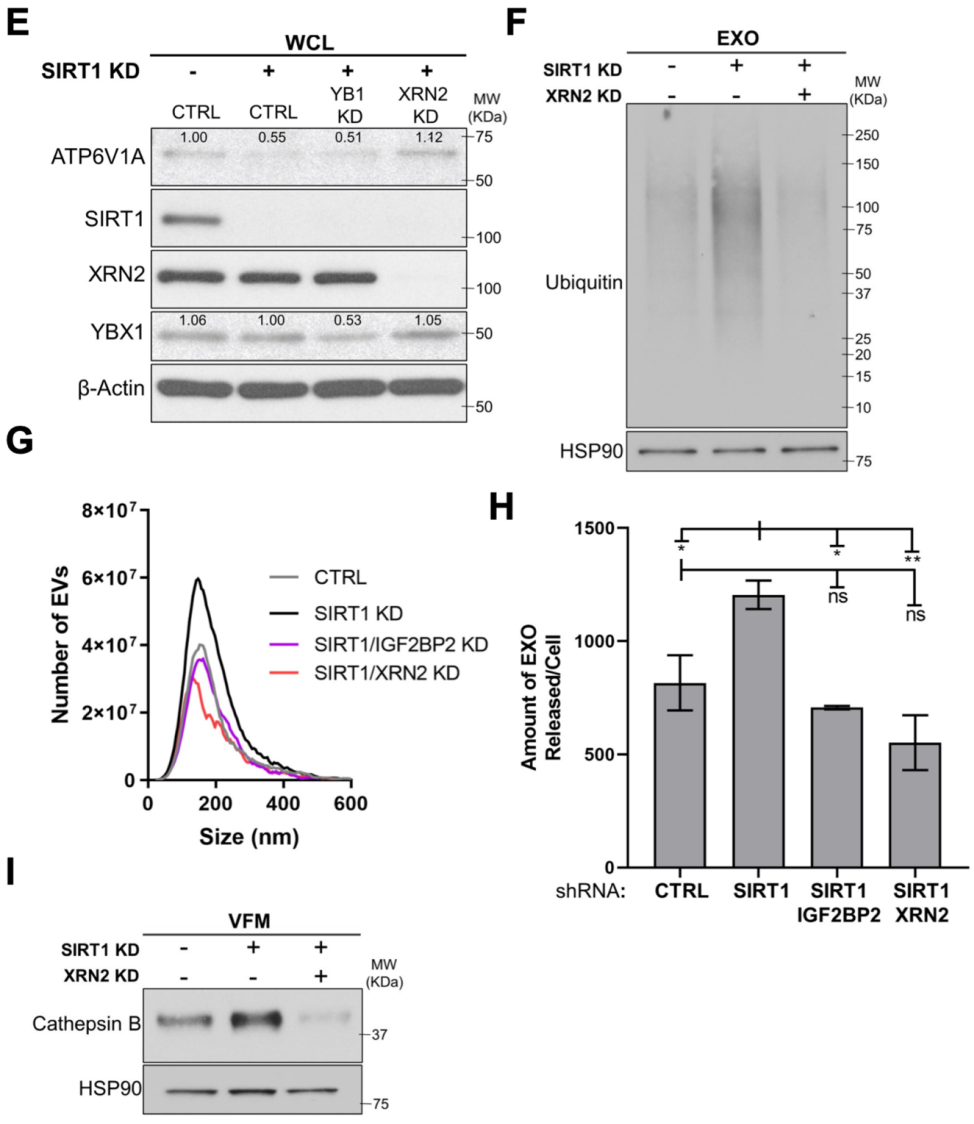
E
WCL
SIRT1 KD
CTRL
CTRL
YB1 KD
XRN2 KD
MW (KDa)
ATP6V1A
1.00
0.55
0.51
1.12
SIRT1
XRN2
YBX1
1.06
1.00
0.53
1.05
β-Actin
F
EXO
SIRT1 KD
XRN2 KD
Ubiquitin
HSP90
G
Number of EVs
Size (nm)
CTRL
SIRT1 KD
SIRT1/IGF2BP2 KD
SIRT1/XRN2 KD
H
Amount of EXO Released/Cell
shRNA:
CTRL
SIRT1
SIRT1 IGF2BP2
SIRT1 XRN2
ns
I
VFM
Cathepsin B
HSP90

determined that the ability of XRN2 to bind IGF2BP2 was impaired when lysine 530 of IGF2BP2 was changed to an arginine residue, as well as when the KH4 domain of IGF2BP2 was deleted (**Figure 3.5C**). As was the case when knocking down IGF2BP2, depleting cells of XRN2 by shRNA, resulted in an increase in both the transcript and protein levels of ATP6V1A in cells lacking SIRT1 (**Figures 3.5D and 3.5E**). These effects were not observed when cells were depleted of CCR4-NOT Transcription Complex Subunit 1 (CNOT1), the cytosolic deadenylating machinery that has been shown to promote mRNA destabilization in certain contexts[22], nor upon knocking down YBX1. Importantly, knocking down XRN2 from SIRT1-depleted cells also resulted in a corresponding decrease in the levels of ubiquitinated proteins in the exosomes (**Figure 3.5F**), as well as reductions in the numbers of exosomes released (**Figures 3.5G and 3.5H**) and in the secreted levels of Cathepsin B (**Figure 3.5I**).

Discussion

Taken together, our findings describe a novel mechanism that explains how the stability of the RNA transcript encoding ATP6V1A is compromised under conditions where SIRT1 levels are low[5]. We have demonstrated that the RNA bindingprotein, IGF2BP2, is a deacetylation substrate for SIRT1, and we have identified lysine 530 as the specific site that is modified by SIRT1. When SIRT1 levels are downregulated, the increased acetylation of IGF2BP2 results in the recruitment of the exonuclease XRN2, thereby promoting the degradation of ATP6V1A transcript (**Figure 3.6**). Although the 5'-3' exonuclease activity of XRN2 requires de-capping of the RNA transcript[23], we have not yet been successful in identifying the de-capping enzyme responsible for promoting XRN2-mediated degradation of the ATP6V1A transcript. We suspect that this has been challenging because of the transient nature of the complex that forms between the de-capping enzyme and the 5' termini of

Figure 3.6 SIRT1 Regulates V-ATPase Expression and Lysosomal Function in Aggressive Breast Cancer.

Model describing how SIRT1 regulates ATP6V1A mRNA stability. In the absence of SIRT1, IGF2BP2 is acetylated at K530 and recruits the exonuclease XRN2. Subsequent decay of ATP6V1A transcript by XRN2 leads to lysosomal impairment, which in turn results in re-routing of multivesicular bodies to the plasma membrane and secretion of their content that can promote the aggressiveness of the tumor microenvironment.

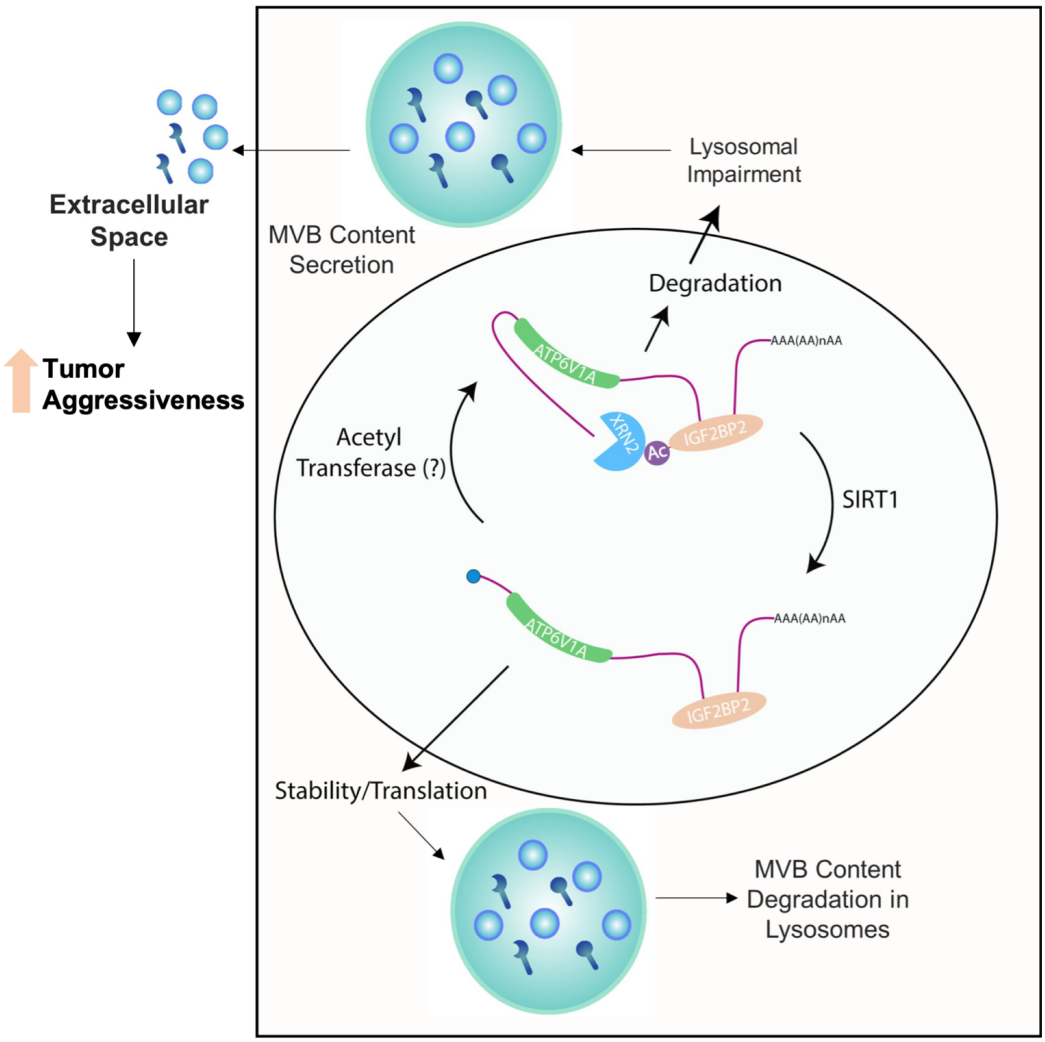
Extracellular Space
Tumor Aggressiveness
MVB Content Secretion
Lysosomal Impairment
Degradation
ATP6V1A
AAA(AA)nAA
XRN2
Ac
IGF2BP2
Acetyl Transferase (?)
SIRT1
ATP6V1A
AAA(AA)nAA
IGF2BP2
Stability/Translation
MVB Content Degradation in Lysosomes

mRNAs. Indeed, XRN1, the cytosolic counterpart of XRN2[24], has similarly been shown to be recruited by the RNA binding protein YTH domain-containing 2 (YTHDC2) to promote the degradation of YTHDC2-bound transcripts. In this study, a specific de-capping enzyme was also not identified[25].

Our data shows that SIRT1 has a previously unappreciated role in regulating mRNA stability. Lysosomal genes have been known to be transcriptionally regulated by transcription factors, such as TFEB. The pathway that we describe here provides the first evidence for the ability of SIRT1 to influence lysosomal activity by affecting the half-life of the RNA transcript encoding a major subunit of the v-ATPase. SIRT1 has been extensively studied in the context of aging and previous studies have shown that the levels of SIRT1 and its co-factor NAD^+ decline as an organism ages, while ectopic expression of SIRT1 in these organisms can extend their lifespan[26–28]. Interestingly, another common phenotype of aging is impaired lysosomal activity[1,29–31] , and homologues of ATP6V1A have been reported to be downregulated in aging yeast[32] and *C. elegans*[33]*.* Thus, the relationship between SIRT1 activity, the expression of ATP6V1A, and thereby lysosomal function, can have important implications in aging and senescence. Notably, a recent study has indicated that reduced levels of SIRT1 in senescent stromal cells negatively impact the expression of ATP6V1A, and the EVs generated by these cells promote the aggressiveness of recipient cancer cells[34]. Therefore, our findings raise the interesting possibility that the inability of SIRT1 to catalyze the deacetylation of its substrate, IGF2BP2, under conditions of SIRT1 downregulation, may give rise to the lysosomal impairment that contribute to aging related phenotypes. Two recent observations further support this possibility: (i) Mice that have lost both copies of IGF2BP2 have longer lifespan[35], and (ii) Mice that have undergone 24 hours of fasting, have significantly reduced levels of IGF2BP2 in their liver[35]. Intriguingly, calorie restriction is often proposed as a strategy

that can contribute to extended lifespan, but the underlying mechanisms for the beneficial aspects of calorie restriction are not clear[36]. These observations would be consistent with our findings showing that downregulation of SIRT1 does not impact ATP6V1A expression when IGF2BP2 is depleted from cells (**Figures 3.2F** and **3.2G**). We predict that future work will shed more light on the implications of post transcriptional regulation of lysosomal function by SIRT1 in other biological contexts, such as aging.

Materials and Methods

Reagent and Resources

The reagent and resources used for the experiments described in this study are listed in Table 1:

Table 1. List of reagents and resources used in this study

REAGENT or RESOURCE	SOURCE	IDENTIFIER
Antibodies		
Anti-SIRT1 antibody	Cell Signaling Technology	2493S; RRID: AB_2188359
Anti-IkBα antibody	Cell Signaling Technology	4812S; RRID: AB_10694416
Anti-β-Actin antibody	Cell Signaling Technology	3700S; RRID: AB_2242334
Anti-Flotillin-2 antibody	Cell Signaling Technology	3436S; RRID: AB_2106572
Anti-Flag antibody	Cell Signaling Technology	8146S; RRID: AB_10950495
Anti-HSP90 antibody	Cell Signaling Technology	4877S; RRID: AB_2233307

Anti-CD63 antibody	Abcam	ab59479; RRID: AB_940915
Anti-ATP6V1A antibody	Abcam	ab137574; RRID: AB_2722516
Anti-IGF2BP2 antibody	Abcam	ab124930; RRID: AB_11131218
Anti-XRN2 antibody	Cell Signaling Technology	13760s; RRID: AB_2798309
Anti-YBX1 antibody	Cell Signaling Technology	4202s; RRID: AB_1950384
Anti-CNOT1 antibody	Cell Signaling Technology	44613s; RRID: AB_2783868
Anti-Acetyl lysine antibody	PTM Biolabs	PTM-102
Anti-Cathepsin B antibody	Cell Signaling Technology	31718S; RRID: AB_2687580
Anti-Ubiquitin antibody	Santa Cruz Biotechnology	sc-8017; RRID: AB_628423
Anti-Ubiquitin antibody	Abcam	ab7780; RRID: AB_306069
Anti-UB H2A antibody	Cell Signaling Technology	8240S; RRID: AB_10891618
Anti-Rabbit IgG-HRP Conjugate antibody	Cell Signaling Technology	7074S; RRID: AB_2099233
Anti-Mouse IgG-HRP Conjugate antibody	Cell Signaling Technology	7076S; RRID: AB_330924

Bacterial and Virus Strains		
E.coli: Stellar Competent Cells	Clonetech	636763
E.coli: One Shot Stbl3 Chemically competent cells	Thermo Fisher	C737303

Chemicals, Peptides, and Recombinant Proteins		
Leupeptin	Sigma	L9783
Aprotinin	Sigma	10236624001
Dithiothreitol (DTT)	Sigma	10197777001
Dimethylsulfoxide (DMSO)	Sigma	D8418
Nicotinamide	Sigma	72340
Sodium butyrate	Sigma	B5887
EX-527	Selleckchem	S1541
Puromycin	Sigma	P9620
DMEM	Gibco	11965-092
RPMI	Gibco	11875-093
DMEM/F12	Gibco	12634-010
Fetal Bovine Serum	Gibco	10437028
Calf Serum	Gibco	16010159
Pen-Strep	Gibco	15140122
Anti-FLAG Magnetic Beads	Sigma	M8823-1ML
Heparin Solution	Stem Cell Technologies	07980
Hydrocortisone	Stem Cell Technologies	07925
PEG-300	Hampton Research	HR2-517
Streptavidin Magnetic Beads	New England Bioenzymes	S1420S

Acetyl-Lysine Affinity Beads	Cytoskeleton, Inc.	AAC04-Beads

Critical Commercial Assays		
Direct-zol RNA Miniprep	Zymo Research	R2051
Direct-zol RNA Microprep	Zymo Research	R2061
InFusion Cloning Kit	Clonetech	638909
Superscript III Reverse Transcriptase	Invitrogen	18080044
HiScribe™ T7 High Yield RNA Synthesis Kit	New England Bioenzymes	937
Pierce™ RNA 3' End Biotinylation Kit	Thermo Fisher	20160
Imprint® RNA Immunoprecipitation Kit	Sigma	RIP-12Rxn
MammoCult™ Human Medium Kit	Stem Cell Technologies	05620

Experimental Models: Cell Lines and Mouse Models		
Human: HEK-293T	ATCC	N/A
Human: MDA-MB-231	ATCC	N/A
Mouse Model: MMTV-PyMT	Provided by Robert Weiss, Cornell University	N/A

Oligonucleotides		
Control shRNA Sequence: CCGGCAACAAGATGAAG AGCACCAACTCGAGTTG	Sigma Mission ShRNA	SHC002

GTGCTCTTCATCTTGTTG

TTTTT

shRNA Targeting Sigma Mission ShRNA TRCN0000218734

Sequence: SIRT1 :

GTACCGGCATGAAGTGC

CTCAGATATTACTCG

AGTAATATCTGAGGCACT

TCATGTTTTTTG

shRNA Targeting Sigma Mission ShRNA TRCN0000255463

Sequence: IGF2BP2 :

CCGGGGTGCCTGCAGCG

GTAATATACTCGAGTATA

TTACCGCTGCAGGCACC

TTTTTG

shRNA Targeting Sigma Mission ShRNA TRCN0000349677

Sequence: XRN2 :

CCGGCCACACATGAACC

GAACTTTACTCGAGTAAA

GTTCGGTTCATGTGTGGT

TTTTG

shRNA Targeting Sigma Mission ShRNA TRCN0000007949

Sequence: YBX1 :

CCGGGACGGCAATGAAG

AAGATAAACTCGAGTTTA

TCTTCTTCATTGCCGTCT TTTT			
shRNA Targeting Sequence: CNOT1 : CCGGCAGCTATTTCCAG CGAATATACTCGAGTATA TTCGCTGGAAATAGCTGT TTTTG	Provided by Andrew Grimson, Cornell University	N/A	
Recombinant DNA			
pLJM1-LAMP1-mRFP-FLAG	Zoncu et al[37], 2011	Addgene #34611	Plasmid
pMD2.G-VSV-G-expressing envelope plasmid	From Didier Trono	Addgene #12259	Plasmid
pCMV delta R8.2-Lentiviral Packaging plasmid	From Didier Trono	Addgene #12263	Plasmid
pLJM1-IGF2BP2-FLAG		This Paper	
Software and Algorithms			
Snapgene Viewer	GSL Biotech	snapgene.com	
ImageJ	NIH	https://imagej.nih.gov/ij/	
Fiji open source image analysis software	Fiji	https://fiji.sc/	

Encode	ENCODE Project Consortium[38], 2012; Davis et al[39], 2018	https://www.encodeproject.org/
Prism	Graphpad	https://www.graphpad.com
Other		
SYBR Green Supermix	Bio-Rad	1725121
Fugene 6 Transfection Reagent	Promega	E2692
Trypsin – Lys-C Mix	Promega	V5073
Sep-Pak C18 Columns	Waters	186000308
0.22 µm Steriflip Filter	Millipore	SEM1M179M6
Amicon Ultra-15 Centrifugal Filter Units – 10 KDa	Millipore	UFC901024
OptiPrep™ Density Gradient Medium	Sigma	D1556-250ML
Ultra-Low Adherent Plate for Suspension Culture	Stem Cell Technolologies	38071
NheI	New England Biolab	R3131S
EcoRI	New England Biolab	R3101S

Experimental Model and Subject Details

Cell Lines. Human embryonic kidney (HEK)-293T and MDA-MB-231 cells were obtained from the ATCC (https://www.atcc.org/). HEK-293T cells were cultured in Dulbecco's Modified Eagle Medium (DMEM) supplemented with 10% calf serum (CS). MDA-MB-231 cells were cultured in Roswell Park Memorial Institute 1640 (RPMI-1640) medium supplemented with 10% fetal bovine serum (FBS). Non-adherent MDA-MB-231 cells were cultured in MammoCult™ Human Medium (Stem

Cell Technologies) supplemented with 4 µg/mL of Heparin Solution (Stem Cell Technologies) and 0.48 µg/mL of hydrocortisone (Stem Cell Technologies). These cells were grown in ultra-low attachment plates (Stem Cell Technologies). All cell lines were maintained at 37°C with 5% CO2.

Cells stably expressing constructs of interest were selected for, and maintained by, supplementing the growth medium with 2mg/mL puromycin.

MMTV-PYMT Mouse Breast Cancer Model. Beginning at 4 weeks of age, MMTV-PyMT transgenic female mice were palpated every other day for mammary tumor development. Upon the detection of tumors, mice were intraperitoneal injected with EX-527 (14 mg/kg, dissolved in a solution containing 70% PEG-300, 5% DMSO and 25% ddH_2O), or vehicle control, every other day for 5 weeks. Mice were monitored daily for health status and weighed every other day. After five weeks of treatment, or if mice met humane endpoint criteria, they were euthanized by CO2 asphyxiation and necropsied. Tumors were weighed, and some portions of the tumors and lungs were snap frozen in liquid nitrogen for protein and RNA extraction, while other portions were fixed with 4% paraformaldehyde for 24 hours and then embedded in paraffin for histopathological analysis.

Method Details

Histological Analysis of the lungs of MMTV-PyMT mice. Paraffin-embedded lungs were cut in 5 µm sections and stained with hematoxylin and eosin (H&E). Slides were digitally scanned using Aperio ScanScope. Five lung sections per mouse were analyzed for metastasis. The number of metastases were quantified using Aperio ImageScope software.

Plasmid Generation, Virus Production, and Cell Infection. The pLJM1-LAMP1-mRFP-FLAG (#34611) construct was purchased from Addgene, and the IGF2BP2 transcript, containing a C-terminal FLAG tag, was cloned into the pLJM1 plasmid using the InFusion Cloning Kit (Clonetech) and following primers:

IGF2BP2-Forward:

CGTCAGATCCGCTAGCATGATGAACAAGCTTTACATCGGG,

IGF2BP2-Reverse:

TCGAGGTCGAGAATTCTCACTTGTCGTCATCGTCTTTGTAGTCACTACCTCCAC CTCCCTTGCTGCGCTGTGAG.

The QKI5 transcript, containing a C terminal FLAG tag, was cloned into the pLJM1 plasmid using InFusion Cloning Kit (Clonetech) and the following primers:

QKI5-Forward:

CGTCAGATCCGCTAGCATGGTCGGGGAAATGGAAACG,

QKI5-Reverse:

TCGAGGTCGAGAATTCTTACTTGTCGTCATCGTCTTTGTAGTCACTACCTCCAC CTCCGTTGCCGGTGGCGGC.

Lenti-viruses were generated by transfecting HEK-293T cells with the shRNA plasmids (Sigma) and the packaging plasmids (#12259 and #12263, Addgene) using Fugene 6 (Promega). The viruses shed into the medium by the cells were harvested 24 and 48 h after transfection. The viruses were then used to infect the target cells using Polybrene (8 μg/mL).

RNA Isolation and Quantitative (q) RT-PCR Analysis. Total RNA was isolated from cells using the Direct-zol RNA Miniprep Kit (Zymo Research), and mRNA transcripts were converted to cDNA using Superscript III Reverse Transcriptase (Invitrogen) and

oligo dT_{20}. The cDNA was then used to determine the expression levels of the indicated transcripts using SYBR Green Supermix (Bio-Rad) and the Applied Biosystems® 7500 Real-Time PCR System with the T method (ABI). The following primers were used for the RT-qPCR analyses are shown in **Table 2.2**.

Table 2.2. List of primers used in this study

PRIMER	SEQUENCE
ATP6V1A-S1-FW	ACATCCCCAGAGGAGTAAACG
ATP6V1A-S1-RW	ACTACCAACCCGTAGGTTTTTG
ATP6V1A-S2-FW	GAGATCCTGTACTTCGCACTGG
ATP6V1A-S2-RW	GGGGATGTAGATGCTTTGGGT
ATP6V1A-S3-FW	GGGTGCAGCCATGTATGAG
ATP6V1A-S3-RW	TGCGAAGTACAGGATCTCCAA

In vitro RNA Transcription and Biotin Pulldown.

A) Preparation of biotinylated RNA probes: Template DNAs were generated by performing PCR using T7 promoter specific primers and cDNA clones of the 3'UTR of the ATP6V1A transcript. Primers for Target RNA probes are as follows:

ATP6V1A-3'UTR containing T7 promoter-Forward:

CTAATACGACTCACTATAGGGAGAAAGCCTTGAAGATTACAACTG,

ATP6V1A-3'UTR Target RNA 1 (T1)-Reverse:

TGTTAATTTAAATCCACTTTTTATTCTTTCACAG,

ATP6V1A-3'UTR Target RNA 2 (T2)-Reverse:

CAGAGCTGTTCTGCAATATGCAGACAC,

ATP6V1A-3'UTR Target RNA 3 (T3)-Reverse:

TGACCAATATGGTGAAACCCCGTTTCTAC,

Luciferase containing T7 promoter-Forward:

CTAATACGACTCACTATAGGGAGAACAATTGCTTTTACAGATGCACATATC,

Luciferase-Reverse:

GAACTGAGATACCTACAGCGTGAGCTATGAG.

In vitro RNA synthesis procedures were carried-out using MEGAscript T7 Transcription Kit (New England Bioenzymes), according to the manufacturers' instructions. The target and luciferase RNA probes were then labeled with Biotin at their 3′ end using Pierce™ RNA 3' End Biotinylation Kit (Thermo Fisher).

B) Preparation of RNA conjugated beads. The magnetic streptavidin beads (New England Bioenzymes, 100 μL per sample) were first washed with binding and wash buffer (5 mM Tris-HCl (pH7.4), and 1 M NaCl), and RNAse inactivated by washing with 400 μL of buffer A (0.1M NaOH and 0.05 M NaCl) twice. To remove the NaOH from the beads, they were washed twice, each time by re-suspending the bead pellets in 400 μL of 0.1 M NaCl solution and collecting them on a magnetic rack. The beads were again washed twice with 300 μL of binding and wash buffer before they were incubated with 100 μL (10-100 pmol) of biotinylated RNA probes for 1 hour at room temperature. The RNA conjugated beads were then collected on a magnetic rack and the supernatants were then discarded. The beads were washed twice, each time with 400 μL of binding and wash buffer followed by rotating the tubes for 5 min at room temperature. The supernatant was discarded after the beads were collected on a magnetic rack and finally, they were resuspended with 50 μL of buffer C (25 mM Tris-HCl (pH 7.4), 150 mM NaCl, 2 mM $MgCl_2$, 1 mM DTT, 1 mM PMSF, 1X protease inhibitor cocktail, and 0.4 U/μl RNase inhibitor) and kept on ice to be later incubation with cellular extracts prepared from the next section.

C) Preparation of cellular extracts and pulldown assays. To prepare cell lysates, MDA-MB-231 cells were grown to 90% confluency in two 15 cm dishes and washed with ice-cold PBS twice before being harvested and pelleted by centrifugation at 200 x g

for 5. The pelleted cells were then resuspended in 2 mL hypotonic buffer (10 mM Tris-HCl (pH 7.4), 10 mM KCl, 2 mM $MgCl_2$, 1 mM DTT, 1 mM PMSF, 1X protease inhibitor cocktail), and transferred to 15 mL Dounce homogenizer and sheared on ice with 20 strokes. The extracts were pelleted again by centrifugation at 3300 x g for 15 min and the resulting supernatant is considered the cytoplasmic lysate, while the pellet (i.e. the nuclei) was resuspended in buffer C supplemented with 0.5% IGEPAL (sigma) and sonicated on ice at level 4 with 10 sec ON/10 sec OFF cycles for 2 minutes. Next, the nuclear debris was pelleted by centrifugation at 16,000 x g for 15 min at 4 °C, and the supernatant collected is considered as the nuclear lysate. The protein concentrations of the cytoplasmic and nuclear lysates were determined using Bradford assay, and they were combined in 1:1 ratio for a total of 750 µg of cellular extracts before being incubated with RNA-conjugated beads for 4 °C with rotation. After 3 h, the beads were collected on a magnetic rack and were washed six times with 1 mL of buffer C containing 40 U RNase inhibitor and 0.25% IGEPAL. The beads were resuspended in 75 µL of buffer C and 25 µL of 4X SDS-PAGE sample buffer, and boiled for 5 min. The samples were next centrifuged at 12,000 x g for 30 sec and the proteins present in the supernatant were resolved by SDS-PAGE and visualized by silver-stain or Western blot.

Mass Spectrometry. Bands on silver-stained gels were analyzed using LC-MS/MS, which was carried out at Proteomic Facility of Institute of Biotechnology at Cornell University.

Exosomes and Vesicle Free Medium Preparation. The conditioned medium collected from 2.0×10^6 serum starved cells was subjected to two consecutive centrifugations at 700 × g to clarify the medium of cells and cell debris. The partially clarified medium

was filtered using a 0.22 μm pore size Steriflip PVDF filter (Millipore). The filter was rinsed two times with 5 mL of Phosphate buffered saline (PBS) to remove any remaining exosome sized EVs (less than 0.22 μm) from the filter. The EVs larger than 0.22 μm retained by the filter were lysed using 250 μL of lysis buffer (25 mM Tris, 100 mM NaCl, 1% Triton X-100, 1 mM EDTA, 1 mM DTT, 1 mM NaVO4, 1 mM β-glycerol phosphate, and 1 μg/ml each aprotinin and leupeptin). The filtrate was then subjected to ultracentrifugation at 100,000 × g for 8 h. The pelleted exosomes were either lysed using 250 μL of lysis buffer, or resuspended in 500 μL of serum free medium for cell-based assays. The supernatant depleted of MVs and exosomes was concentrated using 10 KDa centricons (Amicon). This was considered the vesicle-free medium (VFM). Whole cell lysates (WCL) were prepared by rinsing dishes of cells with PBS, adding 800 μL of lysis buffer, and scraping the cells off the plate. The resulting exosome, and cell lysates were centrifuged at 16,000 x g for 10 min, and then the supernatants were subjected to Western blot analysis.

Density Gradient Fractionation of Exosome Pellet. To further resolve the exosome preparations, the exosome pellets are thoroughly resuspended in 2.4 mL of 36% iodoxanol solution (sigma, diluted from 60% with PBS). Three mL of 30%, 24%, 18%, and 12% iodoxanol solutions are carefully layered on the top of the 36% iodoxanol solution containing exosomes. The resulting gradient was centrifuged at 120,000 × g at 4°C for 16 h. Following centrifugation, twelve 1 mL fractions were carefully collected from the top of gradient column (lowest density), and each fraction was diluted 7-fold in PBS and further centrifuged at 100,000 × g for another 4 hours. The resulting pellet for each fraction was lysed in 50 μL of lysis buffer (25 mM Tris, 100 mM NaCl, 1% Triton X-100, 1 mM EDTA, 1 mM DTT, 1 mM NaVO4, 1 mM β-glycerol phosphate, and 1 μg/ml each aprotinin and leupeptin) and the lysates were centrifuged at 16,000

x g for 10 min. The supernatants were then collected and subjected to Western blot analysis.

Collection of EVs from Serum. Blood samples (~500 µL) collected from wild-type and PYMT-mice, treated as indicated, were centrifuged at 3,000 x g for 10 min at room temperature. The resulting serum was collected, pooled with serum from two other mice, and diluted with 2 mL PBS. This solution was subjected to two consecutive centrifugations at 700 × g to clarify the medium of cells and cell debris. The partially clarified medium was then subjected to ultracentrifugation at 100,000 × g at 4°C for 4 h. The supernatant was discarded, and the pellet was washed in 3 mL PBS and centrifuged again at 100,000 × g at 4°C for another 4 h. The resulting EV pellet was lysed in 250 µL of lysis buffer (25 mM Tris, 100 mM NaCl, 1% Triton X-100, 1 mM EDTA, 1 mM DTT, 1 mM NaVO4, 1 mM β-glycerol phosphate, and 1 µg/ml each aprotinin and leupeptin) and the lysate was centrifuged at 16,000 x g for 10 min. The supernatant was then collected and subjected to Western blot analysis.

Protease Protection Assay for Exosomes. Equivalent amounts of exosomes were resuspended in PBS or PBS containing 1% Triton X-100 in the absence or presence of 50 µg/ml of trypsin for 30 min. The reactions were stopped by the addition of 2× protein sample buffer and boiling for 5 minutes. The lysates were subsequently subjected to Western blot analysis.

Western Blot Analysis. The protein concentrations of tumor, cell, and exosome lysates, as well as of vesicle-free media samples, were determined using the Bradford protein assay. The lysates were normalized by protein concentration, resolved by SDS-PAGE, and the proteins were transferred to PVDF membranes. Membranes

were blocked with 5% bovine serum albumin (Sigma) in TBST (19 mM Tris Base, 2.7 mM KCl, 137 mM NaCl, and 0.5 % Tween-20) for 1 h and the membranes were incubated with the indicated primary antibodies overnight, followed by detection with HRP-conjugated secondary antibodies (Cell Signaling Technology) and exposure to ECL reagent (Pierce).

Nanoparticle Tracking Analysis. The sizes and concentrations of EVs in a given sample were determined using a NanoSight NS300 (Malvern, Cornell NanoScale Science and Technology Facility) as described in Kreger et al[40]. Briefly, the samples were diluted in serum free RPMI-1640 and injected into the beam path to capture movies of EVs as points of diffracted light moving rapidly under Brownian motion. Five 45-s digital videos of each sample were taken and analyzed to determine the concentration and size of the individual EVs based on their movement, and then results were averaged together.

Site-directed Mutagenesis. Mutation of lysine 530 to arginine, as well as deletion of the KH4 domain, in the IGF2BP2 construct containing a C terminal FLAG tag were carried out using the InFusion Cloning Kit (Clonetech) and the following primers:
IGF2BP2-K530R-FW:
AGGTGGCAGGACCGTGAACGAACTGCAGAAC,
IGF2BP2-K530R-RW:
ACGGTCCTGCCACCTTTGCCAATCACCC,
IGF2BP2- ΔKH4-FW:
AAGAGGAAGGAGGTGGAGGTAGTGAC,
IGF2BP2- ΔKH4-RW:
CACCTCCTTCCTCTTTCAGTTTCCCAAAG.

RNA Immunoprecipitation (RIP). RIP analyses were performed using Imprint® RNA Immunoprecipitation Kit (Sigma) according to the manufacturer's instructions. For immunoprecipitation of FLAG tagged protein, 1 µg of anti-FLAG antibody (Cell Signaling Technologies), and 1 µg of isotype control antibody (mouse, Cell Signaling Technologies) were used. Following immunoprecipitation, the RNA was isolated using Direct-zol RNA Microprep Kit (Zymo Research) and analyzed by RT-qPCR.

Immunoprecipitation of FLAG Tagged Proteins. Cells expressing FLAG tagged proteins were harvested when they reach 90-95% confluency, and after two washes with ice-cold PBS, they were lysed using 500 µL of lysis buffer (25 mM Tris, 100 mM NaCl, 1% Triton X-100, 1 mM EDTA, 1 mM DTT, 1 mM NaVO4, 1 mM β-glycerol phosphate, and 1 µg/ml each aprotinin and leupeptin) per 10 cm dish. The protein concentration of cell lysate were determined using Bradford assay, and FLAG tagged proteins were immunoprecipitated from 1 mg of cell lysate using anti-FLAG magnetic beads (sigma) following manufacturer's instruction. Following immunoprecipitation, the beads were resuspended twice, each time in 100 µL of 150 ng/µL of 3X-FLAG peptide (sigma) in TBS buffer (50 mM Tris-Cl (pH 7.5), 150 mM NaCl) and rotated for 30 min. The beads were then collected on a magnetic rack and the resulting supernatants, containing eluted FLAG-tagged proteins, were pooled. For studying the changes in acetylation levels of immunoprecipitated proteins, cell lysates were prepared in lysis buffer that was supplemented with 10 mg/mL of nicotinamide and 10 mg/mL of sodium butyrate to prevent nonselective deacetylation. IGF2BP2 acetylation site and its interacting proteins were analyzed using LC-MS/MS, which was carried out at Proteomic Facility of Institute of Biotechnology at Cornell University.

Immunoprecipitation of Endogenous Acetylated Proteins. Cells growing in two 15 cm dishes were harvested at 90-95% after two washes with ice-cold PBS, they were lysed using 1 mL of lysis buffer (25 mM Tris, 100 mM NaCl, 1% Triton X-100, 1 mM EDTA, 1 mM DTT, 1 mM NaVO4, 1 mM β-glycerol phosphate, and 1 µg/ml each aprotinin and leupeptin) that was supplemented with 10 mg/mL of nicotinamide and 10 mg/mL of sodium butyrate to prevent nonselective deacetylation. To enrich for acetylated peptides, 2.5 mg of cellular lysates were subject to immunoprecipitation using anti-acetyl lysine beads (Cytoskeleton, Inc.) per manufacturer's instruction. Following immunoprecipitation, the beads were resuspended in 30 µL of 2X non-reducing Laemmli buffer (125 mM Tris pH 6.8, 20% glycerol, 4% SDS, and 0.005% Bromophenol blue) and boiled at 95 °C for 5 min. The beads were then pelleted at 3,000 x g for 1 min at 4°C and the supernatant containing acetylated proteins were collected and analyzed using Western blot.

Quantification and Statistical Analysis. Quantitative data are presented as means ± SD. All experiments were independently performed at least three times. Statistical significance was calculated by ANOVA (Tukey's test) for experiments involving comparing more than two conditions, and student's t test for experiments involving comparing two conditions. Error bars represents the mean ± SD. $*p \leq 0.05$, $**p \leq 0.01$, $***p<0.001$, $****p<0.0001$, n.s. = non-significant.

Research Contributions

The author would like to acknowledge the following researchers at Cornell University for their help with this study: Fangyu Wang, for immunoprecipitation experiments and help with isolation of exosomes; Irma Fernandez and James Mullman for experiments involving mouse models.

REFERENCES

1. Folick A, Oakley HD, Yu Y, et al. Lysosomal signaling molecules regulate longevity in Caenorhabditis elegans. *Science*. 2015;**347**:83-86

2. Fraldi A, Klein AD, Medina DL, Settembre C. Brain disorders due to lysosomal dysfunction. *Annu Rev Neurosci*. 2016;**39**:277-295

3. Colacurcio DJ, Nixon RA. Disorders of lysosomal acidification—The emerging role of v-ATPase in aging and neurodegenerative disease. *Ageing Res Rev*. 2016;**32**:75-88

4. Davidson SM, Vander Heiden MG. Critical functions of the lysosome in cancer biology. *Annu Rev Pharmacol Toxicol*. 2017;**57**:481-507

5. Latifkar A, Ling L, Hingorani A, et al. Loss of Sirtuin 1 alters the secretome of breast cancer cells by impairing lysosomal integrity. *Dev Cell*. 2019;**49**:393-408

6. Chi C, Zhu H, Han M, Zhuang Y, Wu X, Xu T. Disruption of lysosome function promotes tumor growth and metastasis in Drosophila. *J Biol Chem*. 2010;**285**:21817-21823

7. Fantozzi A, Christofori G. Mouse models of breast cancer metastasis. *Breast Cancer Res*. 2006;**8**:212

8. Gertz M, Fischer F, Nguyen GTT, et al. Ex-527 inhibits Sirtuins by exploiting their unique NAD+-dependent deacetylation mechanism. *Proc Natl Acad Sci*. 2013;**110**:2772-2781

9. Andreu Z, Yáñez-Mó M. Tetraspanins in extracellular vesicle formation and function. *Front Immunol*. 2014;**5**:422

10. Jacobs MD, Harrison SC. Structure of an IκBα/NF-κB complex. *Cell*. 1998;**95**:749-758

11. Ye S, Song W, Xu X, Zhao X, Yang L. IGF2BP2 promotes colorectal cancer cell proliferation and survival through interfering with RAF-1 degradation by miR-195. *FEBS Lett*. 2016;**590**:1641-1650

12. Barghash A, Golob-Schwarzl N, Helms V, Haybaeck J, Kessler SM. Elevated expression of the IGF2 mRNA binding protein 2 (IGF2BP2/IMP2) is linked to short survival and metastasis in esophageal adenocarcinoma. *Oncotarget*. 2016;**7**:49743-49750

13. Dai N, Ji F, Wright J, Minichiello L, Sadreyev R, Avruch J. IGF2 mRNA binding Protein-2 is a tumor promoter that drives cancer proliferation through its client mRNAs IGF2 and HMGA1. *Elife*. 2017;**6**:e27155

14. Hu X, Peng WX, Zhou H, et al. IGF2BP2 regulates DANCR by serving as an N6-methyladenosine reader. *Cell Death Differ*. 2019. Advance online publication. doi:10.1038/s41418-019-0461-z

15. Li T, Hu PS, Zuo Z, et al. METTL3 facilitates tumor progression via an m6A-IGF2BP2-dependent mechanism in colorectal carcinoma. *Mol Cancer*. 2019;**18**:112

16. Van Nostrand EL, Pratt GA, Shishkin AA, et al. Robust transcriptome-wide discovery of RNA-binding protein binding sites with enhanced CLIP (eCLIP). *Nat Methods*. 2016;**13**:508-514

17. Le HTT, Sorrell AM, Siddle K. Two isoforms of the mRNA binding protein IGF2BP2 are generated by alternative translational initiation. *PLoS One*. 2012;**7**: e33140

18. Bohnert KA, Kenyon C. A lysosomal switch triggers proteostasis renewal in the immortal C. elegans germ lineage. *Nature*. 2017;**551**:629-633

19. Jeppesen DK, Fenix AM, Franklin JL, et al. Reassessment of exosome composition. *Cell*. 2019;**177**:428-445

20. Bell JL, Wächter K, Mühleck B, et al. Insulin-like growth factor 2 mRNA-binding proteins (IGF2BPs): Post-transcriptional drivers of cancer progression? *Cell Mol Life Sci*. 2013;**70**:2657-2675

21. Nicastro G, Candel AM, Uhl M, et al. Mechanism of β-actin mRNA recognition by ZBP1. *Cell Rep*. 2017;**18**:1187-1199

22. Collart MA. The Ccr4-Not complex is a key regulator of eukaryotic gene expression. *Wiley Interdiscip Rev RNA*. 2016;**7**:438-454

23. Brannan K, Kim H, Erickson B, et al. MRNA Decapping Factors and the Exonuclease Xrn2 Function in Widespread Premature Termination of RNA Polymerase II Transcription. *Mol Cell*. 2012;**46**:311-324

24. Nagarajan VK, Jones CI, Newbury SF, Green PJ. XRN 5'→3' exoribonucleases: Structure, mechanisms and functions. *Biochim Biophys Acta - Gene Regul Mech*. 2013;**1829**:590-603

25. Wojtas MN, Pandey RR, Mendel M, Homolka D, Sachidanandam R, Pillai RS. Regulation of m6A Transcripts by the 3'→5' RNA Helicase YTHDC2 Is Essential for a Successful Meiotic Program in the Mammalian Germline. *Mol Cell*. 2017;**68**:374-387

26. Satoh A, Brace CS, Rensing N, et al. Sirt1 extends life span and delays aging in mice through the regulation of Nk2 Homeobox 1 in the DMH and LH. *Cell Metab*. 2013;**18**:416-430

27. Tissenbaum HA, Guarente L. Increased dosage of a sir-2 gene extends lifespan in Caenorhabditis elegans. *Nature*. 2001;**410**:227-230

28. Rogina B, Helfand SL. Sir2 mediates longevity in the fly through a pathway related to calorie restriction. *Proc Natl Acad Sci*. 2004;**101**:15998-16003

29. Carmona-Gutierrez D, Hughes AL, Madeo F, Ruckenstuhl C. The crucial impact of lysosomes in aging and longevity. *Ageing Res Rev*. 2016;**32**:2-12

30. Lawrence RE, Zoncu R. The lysosome as a cellular centre for signalling, metabolism and quality control. *Nat Cell Biol*. 2019;**21**:133-142

31. Leeman DS, Hebestreit K, Ruetz T, et al. Lysosome activation clears aggregates and enhances quiescent neural stem cell activation during aging. *Science*. 2018;**359**:1277-1283

32. Hughes AL, Gottschling DE. An early age increase in vacuolar pH limits mitochondrial function and lifespan in yeast. *Nature*. 2012;**492**:261-265

33. Baxi K, Ghavidel A, Waddell B, Harkness TA, de Carvalho CE. Regulation of lysosomal function by the daf-16 forkhead transcription factor couples reproduction to aging in caenorhabditis elegans. *Genetics*. 2017;**207**:83-101

34. Li S, Jiang J. Senescent stromal cells promote cancer resistance through SIRT1 loss-potentiated overproduction of small extracellular vesicles. *bioRxiv*. doi:10.1101/2020.03.22.002667

35. Dai N, Zhao L, Wrighting D, et al. IGF2BP2/IMP2-deficient mice resist obesity through enhanced translation of Ucp1 mRNA and other mRNAs encoding mitochondrial proteins. *Cell Metab*. 2015;**21**:609-621

36. Redman LM, Smith SR, Burton JH, Martin CK, Il'yasova D, Ravussin E. Metabolic slowing and reduced oxidative damage with sustained caloric restriction support the rate of living and oxidative damage theories of aging. *Cell Metab*. 2018;**27**:805-815

37. Zoncu R, Bar-Peled L, Efeyan A, Wang S, Sancak Y, Sabatini DM. mTORC1 senses lysosomal amino acids through an inside-out mechanism that requires the vacuolar H^+-ATPase. *Science*. 2011;**334**:678-683

38. Consortium EP, Dunham I, Kundaje A, et al. An integrated encyclopedia of DNA elements in the human genome. *Nature*. 2013;**489**:57-74

39. Davis CA, Hitz BC, Sloan CA, et al. The encyclopedia of DNA elements (ENCODE): Data portal update. *Nucleic Acids Res*. 2018;**46**:794-801

40. Kreger B, Johansen E, Cerione R, Antonyak M. The enrichment of Survivin in exosomes from breast cancer cells treated with paclitaxel promotes cell survival and chemoresistance. *Cancers (Basel)*. 2016;**8**:111

CHAPTER 4

Conclusions and Future Directions

Epilogue

Among the most devastating aspects of cancer is the ability of tumor cells to infiltrate the circulation and spread to vital distant organs and tissues, i.e. metastasize. Aggressive metastatic breast cancer is responsible for the deaths of more than 40,000 people per year in the U.S., despite the best efforts of researchers and clinical oncologists. The disappointments in a number of treatment strategies designed to prevent breast tumor growth and metastatic spread highlight the reality that we still have a long way to go toward understanding how aggressive cancer cells get into the circulation and colonize secondary tissues. However, an important development in the field of cancer research could offer exciting new possibilities toward achieving beneficial clinical results against the more aggressive cases of breast cancer. This has to do with the ability of cells to generate a specific class of membrane-enclosed structures, referred to as exosomes. These vesicles appear to function as “satellites of communication”, as they are shed from “donor” cancer cells and can be transferred to and taken-up by “acceptor” cells that reside within the local environment. Exosomes have also been shown to enter the blood stream and affect cells at distant sites. This unique form of intercellular communication can alter the fundamental behavior of acceptor cells in several different ways that contribute to tumorigenesis, and in particular, by changing the cellular architecture at secondary sites so that they become highly receptive to metastatic spread. However, how exosomes are formed and released by aggressive forms of cancer cells, and exactly how they mediate their effects, is still not well understood.

In Chapter 2 of my thesis, I describe a novel mechanism by which breast cancer cells become 'primed' to become highly invasive and metastatic. Specifically, I discovered a novel connection between the reduced expression of the NAD^+-dependent lysine deacylase, SIRT1, in breast cancer cells and the functional impairment of one of the key intracellular organelles (i.e. lysosomes), resulting in the marked increase in the numbers of exosomes containing unique cargo that they release, as well as the secretion of lysosomal hydrolases. This secretome promoted the restructuring of the primary tumor site, such that the cancer cells were able to become invasive and enter the circulation.

In Chapter 3, I further determined the molecular basis by which SIRT1 impacts lysosomal function by showing that it regulates the stability of the transcript encoding one of the major subunits of the V-ATPase, i.e. ATP6V1A. I showed that SIRT1 mediates this effect by catalyzing the deacetylation of lysine residue 530 in the RNA interacting protein Insulin-like growth factor 2 mRNA binding protein 2 (IGF2BP2). Thus, under conditions where cells express sufficient amounts of SIRT1, including normal cell types and low-grade breast cancer cells, IGF2BP2 is properly deacetylated and able to maintain the expression of the ATP6V1A transcript and lysosomal activity. However, when SIRT1 expression levels are downregulated, as is frequently the case in highly aggressive forms of breast cancer, the acetylated form of IGF2BP2 accumulates, and upon binding to the ATP6V1A transcript, it is able to recruit the exonuclease XRN2. This results in the degradation of the ATP6V1A transcript and gives rise to impaired lysosomal function, causing the production of a secretome that promotes aggressive phenotypes (i.e. promote invasion and metastasis).

Here, in this concluding chapter, I will discuss the implications of my dissertation studies, as well as highlight some of the outstanding questions that have emerged from these findings.

SIRT1 Downregulation and Tumor Vulnerabilities

In Chapter 2, I have shown that downregulation of SIRT1 in triple-negative breast cancer produces a secretome that enhances the aggressiveness of the tumor microenvironment. The lysosomal impairment, underlying this phenotype, can have other consequences besides altering the secretome. Some of these outcomes involve the ability of specific macromolecules, which are typically degraded in lysosomes, to remain active under conditions where lysosomal activity is reduced. For example, the transcription factor HIF1α, which is responsible for the upregulation of glycolysis during hypoxia, has been reported to accumulate when cells are treated with bafilomycin-A, a highly potent lysosomal acidification inhibitor[1]. Consistently, we have observed that cells treated with a specific SIRT1 inhibitor, EX-527, are more sensitive to the glycolysis inhibitor 2-deoxyglucose (**Figure 4.1A**).

Because exosomes are lipid-based vesicles, we also predict that enhanced biogenesis of exosomes, in SIRT1 downregulated cells, increases the demand for the biosynthesis of lipids. Interestingly, under conditions where HIF1α is stabilized, glutamine becomes the main carbon source for lipogenic intermediates, such as acetyl-CoA[2]. Over the past decade, glutamine addiction has been proposed to be a vulnerability of cancer cells that rely on high uptake of glutamine[3]. Thus, we anticipate that elevated exosomes secretion, e.g. as a result of SIRT1 downregulation, will create a dependency on glutamine metabolism. To begin to test that idea, I have taken advantage of our laboratory's development of allosteric inhibitors that block the enzyme glutaminase, the first enzyme in the reductive carboxylation route toward

Figure 4.1 Vulnerabilities of SIRT1 downregulated cancer cells.
(A) MDA-MB-231 cells, treated with DMSO or EX-527 (20 μM), were grown in the presence of increasing concentrations of 2-deoxyglucose. The graph shows proliferation at Day 6 for each condition. (B) Reductive carboxylation of glutamine promotes the biosynthesis of lipids.

A

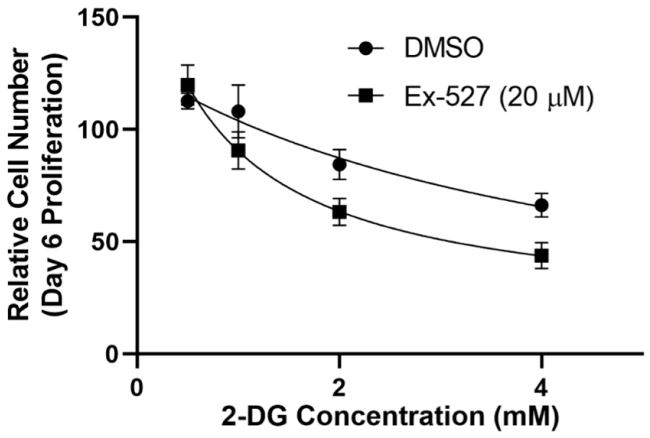
150
100
50
0
Relative Cell Number
(Day 6 Proliferation)
DMSO
Ex-527 (20 μM)
0
2
4
2-DG Concentration (mM)

B

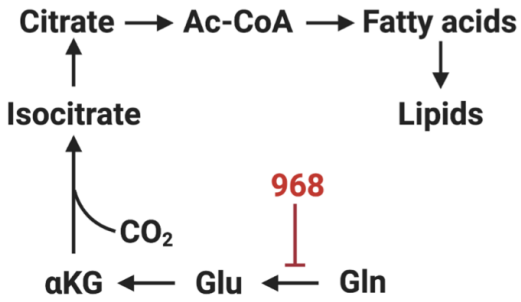
Citrate
Ac-CoA
Fatty acids
Isocitrate
Lipids
968
CO2
αKG
Glu
Gln

production of lipids (**Figure 4.1B**). The synergy between one of the lead compounds for glutaminase inhibition that they identified, **968**[4], and SIRT1 inhibition in impairing the growth of breast tumors will be the subject of future studies.

In the following sections I will discuss the implication of my findings in other biological contexts besides cancer.

Intercellular Communication in Aging and Neurodegeneration

Aging is an irreversible process that is associated with reduced cellular fitness. Lopez *et. al.* described nine hallmarks of aging, which are categorized into primary, antagonistic, and integrative hallmarks[5]. The primary hallmarks include genomic instability, telomere shortening, epigenetic changes, and attenuated proteostasis. To compensate for these changes in fundamental cellular process, cells attempt to adapt by further altering mitochondrial function, senescence, and nutrient signaling. These responses are known as antagonistic hallmarks. The cumulative effects of primary and antagonistic damages during aging ultimately gives rise to integrative hallmarks, such as loss of stem cell populations and altered intercellular communication. The integrative hallmarks of aging are responsible for tissue damage as well as eliciting systemic responses, e.g. inflammation, in the whole organism.

The changes that occur to cells during the aging process predisposes them to neurodegenerative disorders. For example, Parkinson's and Alzheimer's disease patients often show a loss in proteostasis, which leads to the accumulation of proteotoxic aggregates, generally known as Lewy Bodies[6,7]. Similar to malignant transformation, where the spread of tumor cells to vital organs is the primary cause of patient's demise, the detrimental effects associated with neurodegenerative diseases are also thought to increase due to their ability to spread to healthy cells.

One of the earliest indications of this phenomenon came from three independent studies performed in 2008 that showed that healthy neurons grafted into the brains of Parkinson's disease patients became diseased, a process referred to as "non-cell autonomous degeneration"[8–10]. The underlying cause of this effect was due to the transfer of Lewy Bodies from a diseased cell to a nearby non-diseased cell. However, how large protein aggregates could be transferred from one cell to another at that time was unknown, but would require a unique mechanism. A form of cell-cell communication that is potentially capable of transferring protein aggregates between two cells is exosomes. Indeed, multiple studies have now reported that α-synuclein aggregates, which have been implicated in Parkinson's disease, are contained in the exosomes produced by diseased cells[11–13]. Moreover, Emmanouilidou *et. al.* showed that exosomes containing α-synuclein can induce toxicity in recipient neuronal cells[14], suggesting that protein aggregates associated with neurodegenerative disorders can be secreted in exosomes. When these exosomes come in contact with other cells, they are taken up and promote cell death. As a result, inhibiting the secretion of exosomes generated by pathological cells would be a promising therapeutic strategy to delay the progression of neurodegeneration.

Lysosomes as Novel Targets for Neurodegenerative Diseases

Lysosomes were originally discovered by Christian de Duve, as membrane bound sacs that contain enzymes with acid hydrolase activity[15]. de Duve further coined the terms endocytosis and autophagy as processes that are responsible for the delivery of macromolecules to lysosomes for degradation[16]. Thus, it is not unexpected that lysosomes are considered as the primary degradative organelle that clears cells of unwanted materials. Importantly, lysosomal proteolytic activity declines

with aging, and accumulation of β-amyloid and α-synuclein aggregates in Parkinson's and Alzheimer's disease has been attributed to lysosomal dysfunction[17].

One potential mechanism for the reduced lysosomal activity associated with neurodegeneration, as well as cancer, could be due to SIRT1 downregulation. I have already shown that SIRT1 levels are strongly downregulated in highly aggressive forms of breast cancer (see Chapter 1), but SIRT1 levels are similarly decreased in aging and neurogenerative disorders. A good example of this comes from the recent unpublished findings from Drs. Kai Greene and Makoto Endo in the Cerione laboratory. They were investigating the changes that occur in the brains of mice as a result of aging, and found that reductions in the expression levels of SIRT1 were among the most clear and notable changes in these animals. Interestingly, extracellular accumulation of α-synuclein has been linked to reduced expression of SIRT1[18] and activation of SIRT1 has been shown to protect cells in various models of Parkinson's disease[19]. In one notable study, SIRT1 deacetylation of LC3 was suggested to promote the clearance of α-synuclein through autophagy[20]. Our findings regarding SIRT1 regulation of lysosomal function provide another mechanism for how lysosomal impairment caused by SIRT1 downregulation can contribute to the onset of neurodegenerative diseases. The relationship between SIRT1 and lysosomal function and regulation of cellular secretome, which was discussed in Chapter 2, further supports this hypothesis. In this scenario, downregulation of SIRT1 expression as a result of aging would cause a corresponding decrease in lysosomal activity, thereby making neurons more susceptible to accumulation of proteotoxic aggregates.

Thus, increasing the levels of SIRT1 expression and activation, in the context of neurodegenerative disorders, could provide a potential therapeutic strategy by increasing lysosomal activity and promoting the degradation of toxic protein aggregates, as well as reducing the secretion of exosomes that contain them. This

possibility can be tested by investigating the impact of changing the levels of SIRT1 expression in cell-based models of Parkinson's disease. For example, overexpression of α-synuclein in SH-SY5Y cells has commonly been used as a method to model Parkinson's disease[21] and the exosomes generated from these cells have been reported to contain α-synuclein[13]. Given the effect of SIRT1 downregulation on exosome biogenesis, we expect that increasing the expression of SIRT1 in these cells would reduce the secretion of exosomes containing α-synuclein.

Similarly, to study the beneficial effect of SIRT1 activation on the progression of Parkinson's disease, one can take advantage of α-synuclein overexpressing (ASO)-mouse models that are typically used to study Parkinson's *in vivo*[22]. A common method to activate SIRT1 in animals involves administration of NAD^+ precursors, such as NMN, which have been suggested to boost SIRT1 activity[23]. Thus, brain tissue from NMN- and vehicle-treated ASO-mice could be collected and further evaluated for α-synuclein depositions and lysosomal status. Again, we anticipate that the brain of ASO-mice treated with NMN would have less prominent staining for α-synuclein compared with a control vehicle-treated group. Because NAD^+ participates in other enzymatic reactions, brain specific SIRT1 knockout mice can be used to control for SIRT1 independent effects of NMN administration. These questions are currently being addressed by Fangyu Wang, a graduate student who has recently joined the Cerione laboratory. The ultimate goal of these studies would be to develop new approaches to stop or delay the onset of neurodegeneration.

Regulation of Ribonucleoprotein Particles by Post-Translational Modifications

At the heart of dynamic gene expression programs are post-transcriptional processes that regulate messenger RNAs (mRNAs). In these programs, mRNAs associate with RNA-binding proteins (RBPs) to influence their splicing, stability,

localization, and translation into proteins. For the duration of its lifecycle, RNAs encounter numerous proteins, and RNAs often associate with more than one protein at one time, forming complexes that are known as ribonucleoprotein particles (RNPs). One of the earliest observations of RNPs was documented by George Palade when he described the presence of dense particles on the endoplasmic reticulum[24], which are now referred to as ribosomes. Unlike ribosomes, for which the components are very well defined, RNPs that involve mRNA as the RNA constituent are highly dynamic and the protein composition of these particles is constantly undergoing remodeling. For example, with each processing event, such as splicing, nuclear export, and translation, mRNAs encounters encounter distinct machineries. The RNPs are in a sense the molecular determinants of the mRNA fate. Accumulating evidence suggests RNP remodeling is also important for the progression of various diseases, including cancer and neurodegeneration.

One of the commonly employed methods to achieve dynamic RNP assemblies has to do with post-translational modifications (PTMs) of RNA-binding proteins[25]. In this context, writers and erasers of PTMs are critical components of the signaling pathways that regulate RNP remodeling. PTMs can modulate the architecture of RNPs in two ways: (i) Directly disrupting or enhancing the interactions between nucleotide and amino acids, or (ii) recruiting/disallowing proteins or nucleic acids to participate in the RNP complex. An example of the first case involves methylation of the RNA binding domain of the fragile X mental retardation protein (FMRP)[26]. Methylation of arginine residues in this domain has been reported to decrease the ability of FMRP to bind with a subset of FMRP target RNAs that contain G-quadruplexes, thereby reducing their association with polyribosomes[27–29]. My studies (specifically Chapter 3) describe an example for the second scenario, where acetylation of IGF2BP2 results in the recruitment of the exonuclease XRN2 and

degradation of the IGF2BP2-bound ATP6V1A RNA transcript. We suspect that the composition of at least a subset of IGF2BP2 containing RNPs are regulated by the lysine acetylation/deacetylation cycle of IGF2BP2. Although we have shown that the deacetylation of IGF2BP2 is catalyzed by SIRT1, the enzyme responsible for catalyzing the forward reaction, i.e. lysine acetylation, remains to be identified.

Coding of RNA binding proteins with PTMs

DNA binding proteins, i.e. histones, were the first characterized substrates of SIRT1 deacetylation, and it is now well-established that histones undergo unique PTMs, including acetylation, which are responsible for eliciting specific gene expression profiles. The increasing list of PTMs that occur to RNA binding proteins, raises the interesting possibility that "RBP codes" might also represent a distinct set of instructions that shape the post-transcriptional landscape by regulating gene expression (**Figure 4.2**). This hypothesis can be addressed by using recently developed high-throughput technologies for studying RNA-protein interactions (e.g. proximity labeling-based methods coupled with mass spectrometry[30]) and advanced RNA sequencing methods[31]. Specifically, temporal analysis of protein composition of RNPs, together with their PTMs will create a detailed picture of RNP remodeling during the lifetime of specific RNA transcripts. One area that will particularly benefit from these types of studies involves the biology of RNA viruses, such as SARS-CoV-2[32]. Despite extensive knowledge of how these viruses enter and replicate in the cells of their hosts, very little is known about the dynamics of RNPs that consist of host RNA binding proteins and the genomic RNA of the virus. Identification and characterization of these interactions is essential for developing therapeutic strategies that can disrupt viral replication. These outstanding questions will be further explored by the author in his post-doctoral training.

Figure 4.2 Nucleic acid binding proteins code.
Post-translation modifications allow for unique and robust regulation of gene expression in (top) transcriptional, and (bottom) post-transcriptional space.

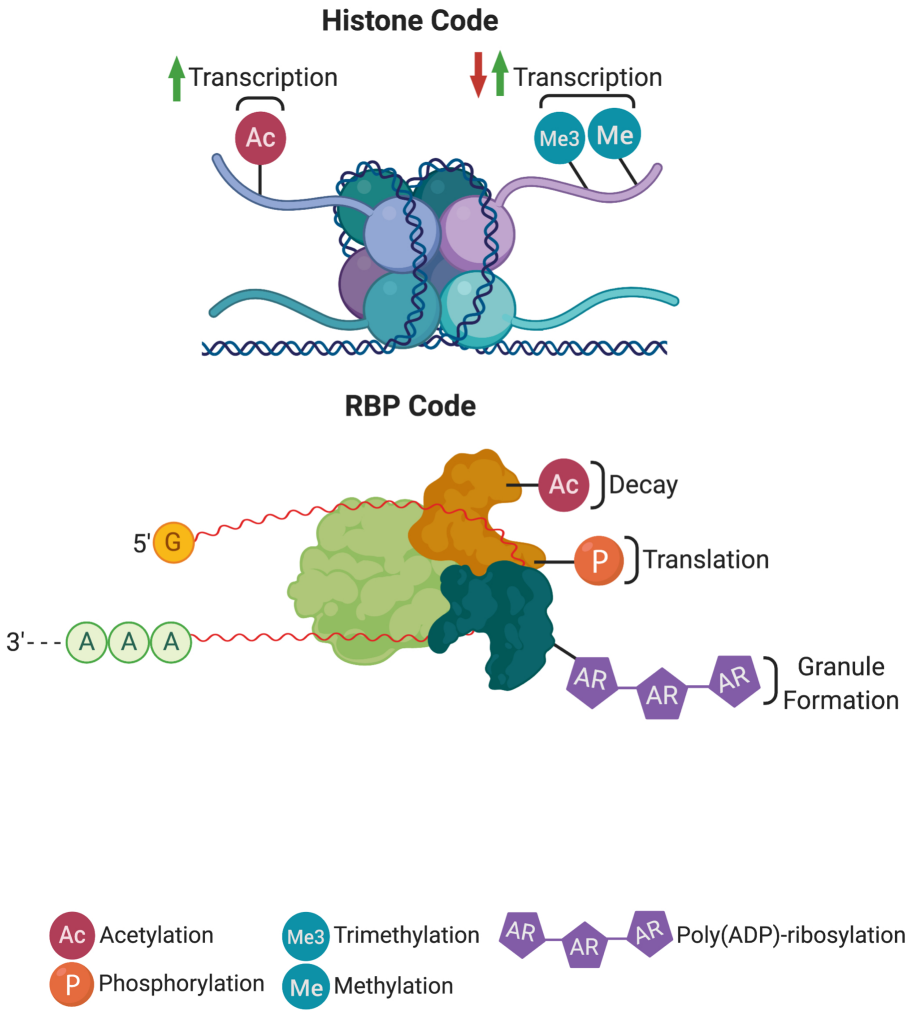
Histone Code
Transcription
Transcription
Ac
Me3
Me
RBP Code
Ac
Decay
5'
G
P
Translation
3'- - -
A
A
A
AR
AR
AR
Granule
Formation
Ac
Acetylation
P
Phosphorylation
Me3
Trimethylation
Me
Methylation
AR
AR
AR
Poly(ADP)-ribosylation

REFERENCES

1. Hubbi ME, Hu H, Kshitiz, Ahmed I, Levchenko A, Semenza GL. Chaperone-mediated autophagy targets hypoxia-inducible factor-1α(HIF- 1α) for lysosomal degradation. *J Biol Chem*. 2013;**288**:10703-10714

2. Anastasiou D, Cantley LC. Breathless cancer cells get fat on glutamine. *Cell Res*. 2012;**22**:443-446

3. Cluntun AA, Lukey MJ, Cerione RA, Locasale JW. Glutamine metabolism in cancer: understanding the heterogeneity. *Trends in Cancer*. 2017;**3**:169-180

4. Wang J Bin, Erickson JW, Fuji R, et al. Targeting mitochondrial glutaminase activity inhibits oncogenic transformation. *Cancer Cell*. 2010;**18**:207-219

5. Adams D, Koike H, Slama M, et al. Ageing as a risk factor for neurodegenerative disease. *Nat Rev Neurol*. 2019;**15**:1-7

6. Wakabayashi K, Tanji K, Mori F, Takahashi H. The Lewy body in Parkinson's disease: Molecules implicated in the formation and degradation of α-synuclein aggregates. *Neuropathology*. 2007;**27**:494-506

7. Metzler-Baddeley C. A review of cognitive impairments in dementia with Lewy bodies relative to Alzheimer's disease and Parkinson's disease with dementia. *Cortex*. 2007;**43**:583-600

8. Kordower JH, Chu Y, Hauser RA, Freeman TB, Olanow CW. Lewy body-like pathology in long-term embryonic nigral transplants in Parkinson's disease. *Nat Med*. 2008;**14**:504-506

9. Li JY, Englund E, Holton JL, et al. Lewy bodies in grafted neurons in subjects with Parkinson's disease suggest host-to-graft disease propagation. *Nat Med*. 2008;**14**:501-503

10. Mendez I, Vĩuela A, Astradsson A, et al. Dopamine neurons implanted into people with Parkinson's disease survive without pathology for 14 years. *Nat Med*. 2008;**14**:507-509

11. Fussi N, Höllerhage M, Chakroun T, et al. Exosomal secretion of α-synuclein as protective mechanism after upstream blockage of macroautophagy. *Cell Death Dis*. 2018;**9**:757

12. Xia Y, Zhang G, Han C, et al. Microglia as modulators of exosomal alpha-synuclein transmission. *Cell Death Dis*. 2019;**10**:174

13. Alvarez-Erviti L, Seow Y, Schapira AH, et al. Lysosomal dysfunction increases exosome-mediated alpha-synuclein release and transmission. *Neurobiol Dis*. 2011;**42**:360-367

14. Emmanouilidou E, Melachroinou K, Roumeliotis T, et al. Cell-produced α-synuclein is secreted in a calcium-dependent manner by exosomes and impacts neuronal survival. *J Neurosci*. 2010;**30**:6838-6851

15. Bowers WE, de Duve C. Lysosomes in lymphoid tissue. II. Intracellular distribution of acid hydrolases. *J Cell Biol*. 1967;**32**:339-348

16. Sabatini DD, Adesnik M. Christian de Duve: Explorer of the cell who discovered new organelles by using a centrifuge. *Proc Natl Acad Sci*. 2013;**110**:13234-13235

17. Fraldi A, Klein AD, Medina DL, Settembre C. Brain Disorders Due to Lysosomal Dysfunction. *Annu Rev Neurosci*. 2016;**39**:277-295

18. Motyl J, Wencel PL, Cieślik M, Strosznajder RP, Strosznajder JB. Alpha-synuclein alters differently gene expression of Sirts, PARPs and other stress response proteins: implications for neurodegenerative disorders. *Mol Neurobiol*. 2017: **55**:727-740

19. Xu J, Jackson CW, Khoury N, Escobar I, Perez-Pinzon MA. Brain SIRT1 mediates metabolic homeostasis and neuroprotection. *Front Endocrinol (Lausanne)*. 2018;**9**:702

20. Guo YJ, Dong SY, Cui XX, et al. Resveratrol alleviates MPTP-induced motor impairments and pathological changes by autophagic degradation of α-synuclein via SIRT1-deacetylated LC3. *Mol Nutr Food Res*. 2016;**60**:2161-2175

21. Xicoy H, Wieringa B, Martens GJM. The SH-SY5Y cell line in Parkinson's disease research: a systematic review. *Mol Neurodegener*. 2017;**12**:1-11

22. Chesselet MF, Richter F, Zhu C, Magen I, Watson MB, Subramaniam SR. A progressive mouse model of parkinson's disease: The Thy1-aSyn ("Line 61") mice. *Neurotherapeutics*. 2012;**9**:297-314

23. Yoshino J, Baur JA, Imai S. NAD+ Intermediates: The biology and therapeutic potential of NMN and NR. *Cell Metab*. 2018;**27**:513-528

24. Palade GE. Studies on the endoplasmic reticulum. II. Simple dispositions in cells in situ. *J Biophys Biochem Cytol*. 1955;**1**:567-582

25. Hofweber M, Dormann D. Friend or foe-Post-translational modifications as regulators of phase separation and RNP granule dynamics. *J Biol Chem*. 2019;**294**:7137-7150

26. Stetler A, Winograd C, Sayegh J, et al. Identification and characterization of the methyl arginines in the fragile X mental retardation protein Fmrp. *Hum Mol Genet*. 2006;**15**:87-96

27. Darnell JC, Jensen KB, Jin P, Brown V, Warren ST, Darnell RB. Fragile X mental retardation protein targets G quartet mRNAs important for neuronal

function. *Cell*. 2001;**107**:489-499

28. Ramos A, Hollingworth D, Pastore A. G-quartet-dependent recognition between the FMRP RGG box and RNA. *Rna*. 2003;**9**:1198-1207

29. Blackwell E, Zhang X, Ceman S. Arginines of the RGG box regulate FMRP association with polyribosomes and mRNA. *Hum Mol Genet*. 2010;**19**:1314-1323

30. Chen CL, Perrimon N. Proximity-dependent labeling methods for proteomic profiling in living cells. *Wiley Interdiscip Rev Dev Biol*. 2017;**6**: e272

31. Ramanathan M, Majzoub K, Rao DS, et al. RNA–protein interaction detection in living cells. *Nat Methods*. 2018;**15**:207-212

32. Beckham CJ, Parker R. P Bodies, stress granules, and viral life cycles. *Cell Host Microbe*. 2008;**3**:206-212